UNIVERSITEIT VAN PRETORIA
UNIVERSITY OF PRETORIA
YUNIBESITHI YA PRETORIA

A COOPERATIVE PREDICTION BASED APPROACH TO SPECTRUM MANAGEMENT IN COGNITIVE RADIO NETWORKS

by

Simon Daniel Barnes

Submitted in partial fulfillment of the requirements for the degree

Philosophiae Doctor (Engineering)

in the

Department of Electrical, Electronic and Computer Engineering
Faculty of Engineering, Built Environment and Information Technology
UNIVERSITY OF PRETORIA

July 2016

© University of Pretoria

UNIVERSITEIT VAN PRETORIA
UNIVERSITY OF PRETORIA
YUNIBESITHI YA PRETORIA

SUMMARY

A COOPERATIVE PREDICTION BASED APPROACH TO SPECTRUM MANAGEMENT IN COGNITIVE RADIO NETWORKS

by

Simon Daniel Barnes

Promoter(s):	Prof. B.T.J. Maharaj
Department:	Electrical, Electronic and Computer Engineering
University:	University of Pretoria
Degree:	Philosophiae Doctor (Engineering)
Keywords:	Cognitive radio, computational complexity, cooperative prediction, cooperative spectrum sensing, detection threshold, energy efficiency, prediction error, spectrum measurements, spectrum occupancy, spectrum sensing, traffic classification

One of the problems facing wireless network planners is a perceived scarcity of spectrum. A technology that addresses this problem is cognitive radio (CR). A critical function of a CR network is spectrum sensing (SS). A secondary user (SU) in a CR network will perform SS to gather information about the radio environment within which it wishes to operate and then make decisions based on that information. While SS by individual SUs is very useful it has been found in the literature that a cooperative approach, where SUs share their individual results, may provide more accurate information about the radio environment. It has also been shown that it is beneficial for SUs to be able to make proactive decisions about spectrum resource allocation. To be able to make these proactive decisions, a SU will need to be able to make predictions about the future behaviour of other users of the same spectrum.

This research project was divided into two parts. Firstly, a measurement campaign was performed to characterise spectrum scarcity in the South African context. Detailed information, about the occupancy of various commercially utilised South African frequency bands, was collected from spectrum measurement campaigns carried at the Hatfield campus of the University of Pretoria and at Pinmill Farm in Johannesburg. These bands included the television

© University of Pretoria

broadcast and mobile cellular bands. On average, the television broadcast bands were found to be underutilised highlighting the existence of a number of opportunities for television white space devices. However, the mobile cellular bands were found to be much more heavily occupied, particularly for the bands around 900 MHz, suggesting that mobile operators are currently in need of additional spectrum resources.

The second part of this thesis followed a more theoretical approach and was based on the need for proactive decision making in CR networks. A single SU prediction method, of relatively cheap computational complexity, was proposed and tested under various traffic conditions. The premise that collaboration between SUs may improve the accuracy of single SU traffic predictions was then explored. Pre-fusion and post-fusion approaches to cooperative prediction were compared with the single SU prediction scenario. The prediction error for the cooperative approaches was found to be lower than for the single SU case, especially for the pre-fusion scenario. For example, for a signal-to-noise ratio of 8 dB and individual forecast probability of 0.9, the pre-fusion prediction error was found to be approximately 2% compared with 26% for single SU prediction error. The cost of this improvement, however, was added algorithm complexity.

It was then demonstrated that primary user traffic prediction could be used to improve the energy consumption associated with cooperative SS in a CR network. Combined with an optimal scheduling algorithm, this approach was shown to prolong the lifetime of a group of twenty cooperating SUs by 21.2 time samples for a uniformly distributed group of SUs when predictions were made ten time samples into the future.

© University of Pretoria

OPSOMMING

'N KOÖPERATIEWE VOORSPELLING BENADERING VAN DIE SPECTRUM BESTUUR IN KOGNITIEWE RADIO NETWERKE

deur

Simon Daniel Barnes

Promotor(s):	Prof. B.T.J. Maharaj
Departement:	Elektriese, Elektroniese en Rekenaar-Ingenieurswese
Universiteit:	Universiteit van Pretoria
Graad:	Philosophiae Doctor (Ingenieurswese)
Sleutelwoorde:	Energie-doeltreffendheid, kognitiewe radio, koöperatiewe voorspelling, koöperatiewe spektrum sensing, opsporing drumpel, rekenkundige kompleksiteit, spektrum metings, spektrum besetting, spektrum sensing, verkeer klassifikasie, voorspellings fout

Een van die probleme wat draadlose netwerk beplanners in die gesig staar is 'n vermeende skaarsheid van die radio frekwensie spektrum. 'n Tegnologie wat hierdie probleem aanspreek is 'n kognitiewe radio (KR). A kritiese funksie van 'n KR netwerk is spektrum sensing (SS). 'n Sekondêre gebruiker (SG) in 'n KR netwerk sal SS gebruik om inligting oor die radio omgewing waarbinne dit wil werk in te samel en dan dit gebruik om besluite te neem wat gebaseer is op hierdie inligting. Terwyl SS deur individuele SGs baie nuttig is, is daar gevind in die literatuur dat samewerking tussen SGs, waar hulle hul individuele resultate deel, kan meer akkurate inligting oor die radio omgewing voorsien. Dit het ook getoon dat dit voordelig is vir SGs om proaktiewe besluite te neem oor die toekenning van spektrum hulpbronne. Om hierdie proaktiewe besluite te neem, sal 'n SG in staat moet wees om voorspellings te maak oor die toekomstige gedrag van ander gebruikers van dieselfde spektrum.

Hierdie navorsing is in twee dele verdeel. Eerstens is 'n meting veldtog uitgevoer om spektrum skaarsheid in die Suid-Afrikaanse konteks te karakteriseer. Gedetailleerde inligting, oor die besetting van verskeie kommersieel gebruikte Suid-Afrikaanse frekwensiebande, is van spektrum meet veldtogte by die Hatfield-kampus van die Universiteit van Pretoria en by Pinmill

© University of Pretoria

Farm in Johannesburg ingesamel. Hierdie frekwensiebande ingesluit die televisie-uitsending en mobiele sellulêre bande. Op die gemiddelde is die televisie-uitsending bande onderbenut gevind, vat die bestaan van 'n aantal geleenthede vir televisiewitspasietoestelle beklemtoon. Maar dit is gevind dat die mobiele sellulêre bande baie meer swaar beset is, veral vir die bande om 900 MHz, wat daarop dui dat die mobiele operateurs tans in die behoefte van addisionele spektrum hulpbronne is.

Die tweede deel van hierdie tesis is 'n meer teoretiese benadering wat gebaseer is op die behoefte vir proaktiewe besluitneming in KR netwerke. 'n Enkele SG voorspelling metode van relatief goedkoop rekenkundige kompleksiteit is voorgestel en getoets onder verskillende tipe verkeer. Die veronderstelling dat samewerking tussen SGs die akkuraatheid van 'n enkele SG voorspellings kan verbeter is toe ondersoek. Voorsamesmelting en nasamesmelting benaderings tot koöperatiewe voorspelling is vergelyk met die enkele SG voorspellings skema. Die voorspelling fout vir die koöperatiewe benaderings is laer as vir die enkele GS geval bevind, veral vir die voorsamesmelting skema. Byvoorbeeld, vir 'n sein-tot-ruis-verhouding van 8 dB en individuele voorspelling waarskynlikheid van 0.9, is die voorsamesmelting voorspelling fout ongeveer 2% gevind in vergelyking met 'n 26% enkel SG voorspellings fout. Die koste van hierdie verbetering was egter bygevoege algoritme kompleksiteit.

Dit is dan bewys dat primêre gebruiker verkeer voorspelling gebruik kan word om die energieverbruik wat verband hou met koöperatiewe spektrum sensing in 'n KR netwerk te verbeter. Gekombineer met 'n optimale skeduleringsalgoritme is hierdie benadering getoon om die leeftyd van 'n groep van twintig eenvormig verspreide SGs te verleng deur 21.2 tyd monsters toe voorspellings van tien tyd monsters in die toekoms gemaak is.

© University of Pretoria

This thesis is dedicated to:

- *Our creator, through whom all things are possible.*
- *Tarryn and Liam, my motivation and inspiration.*
- *My parents, for their support and good advice.*

It is better to be vaguely right than exactly wrong - Carveth Read (1848–1931).

© University of Pretoria

ACKNOWLEDGEMENTS

I would like to thank the following people and organisations for their assistance in making this work possible:

- My supervisor, Prof B.T.J. Maharaj, for his provision and guidance.
- Prof A.S. Alfa, University of Manitoba, Canada, for his insight and technical advice.
- The Sentech Chair in Broadband Wireless Multimedia Communication (BWMC) at the University of Pretoria, the National Research Foundation (NRF) and the Independent Communications Authority of South Africa (ICASA) for their financial support.
- All of my colleagues at the Sentech BWMC, especially Dr K. Dhuness, Mr P.R. Botha, Mr P.A. Jansen van Vuuren, Mr M.J. Prinsloo and Dr D.J. Louw.
- The Computing Clusters of the University of Pretoria's Department of Electrical, Electronic and Computer Engineering, maintained by Mr H. Grobler.
- My wife, Mrs T. Barnes, for her enduring love, support and inspiration throughout my postgraduate studies.
- My parents Prof L.A. Barnes and Mrs J.G. Barnes for their guidance, wisdom, encouragement and language expertise.
- Mr G.D. Frost for his unwavering support and motivation.

© University of Pretoria

LIST OF ABBREVIATIONS

AI	Artificial intelligence
ANN	Artificial neural networks
BS	Base Station
CA	Carrier aggregation
CFA	Cooperative forecasting algorithm
CPE	Cooperative prediction error
CO	Channel occupancy
CSS	Cooperative spectrum sensing
CR	Cognitive radio
CRN	Cognitive radio network
D2D	Device-to-device
DMT	Digital mobile television
DSA	Dynamic spectrum access
DTT	Digital terrestrial television
DVB-H	Digital video broadcasting - hand held
DVB-T2	Digital video broadcasting - second generation
ED	Energy detection
EE	Energy efficiency
FC	Fusion centre
FCC	Federal communications commission
GLSDB	Geo-location spectrum database
GPS	Global positioning system
GSM	Global system for mobile communications
HMM	Hidden Markov model
ICASA	Independent communications authority of South Africa
IE	Implicit enumeration
IEEE	Institute of electrical and electronics engineers
ITU	International telecommunication union
ITU-R	International telecommunication union radiocommunication sector
LNA	Low noise amplifier
LSA	Licensed shared access

© University of Pretoria

LTE	Long term evolution
λG	Lambda greedy
MC	Markov chain
MIMO	Multiple-input-multiple-output
MLP	Multilayer perceptron
MMB	Millimetre-wave broadband
MNF	Maximum normal fit
MP	Menlo park
MSE	Mean squared error
NLMS	Normalised least mean square
NOF	No-fusion prediction
OW	Occupancy window
PDF	Probability density function
PE	Prediction error
PMF	Probability mass function
POF	Post-fusion prediction
PRF	Pre-fusion prediction
PSD	Power spectral density
PU	Primary user
QoS	Quality of service
ROHT	Recursive one-sided hypothesis test
RLS	Recursive least squares
RND	Random prediction
SA	Spectral availability
SNR	Signal-to-noise ratio
SO	Spectral occupancy
SOF	Spectral opportunity forecasting
SS	Spectrum sensing
SU	Secondary user
SVM	Support vector machines
TV	Television
TVWS	Television white spaces
UHF	Ultra-high frequency
VHF	Very-high frequency
WSD	White space device

© University of Pretoria

TABLE OF CONTENTS

© University of Pretoria

© University of Pretoria

© University of Pretoria

© University of Pretoria

CHAPTER 1

INTRODUCTION

1.1 BACKGROUND AND MOTIVATION

Mobile broadband communications are an important driver of social and economic development around the world. The global proliferation of wireless communication devices has already lead to unprecedented volumes of mobile traffic [1] and recent trends suggest that this ever increasing demand for mobile broadband services may soon outstrip available spectrum resources [2, 3]. Rapidly increasing numbers of mobile devices, competing for spectrum at ever increasing date rates, are primarily responsible for this prediction. Regulatory bodies and enterprises, such as the federal communications commission (FCC), Cisco Systems and the international telecommunication union radiocommunication sector (ITU-R), have predicted that wireless network planners and mobile operators will soon face a spectrum crunch [3]. A study released by Cisco Systems indicated that global mobile data traffic more than doubled in the year 2011 and has predicted an 18-fold increase by the year 2016 [4]. While a report by the ITU-R on future spectrum requirements has predicted at least a 25-fold increase with a possible maximum 100-fold increase in mobile traffic by the year 2020 [5], illustrated in Figure 1.1. Data-hungry technologies such as tablet computers, smart phones, machine-to-machine (M2M) communications, mobile video, media rich social networking, portable gaming consoles, cloud computing services and the proposed concept of the internet of things have been listed as the main drivers of this phenomenon [1, 4].

The deployment of fourth generation (4G) networks has allowed for significant increases in the speeds at which these devices are able to operate. The well know Shannon

© University of Pretoria

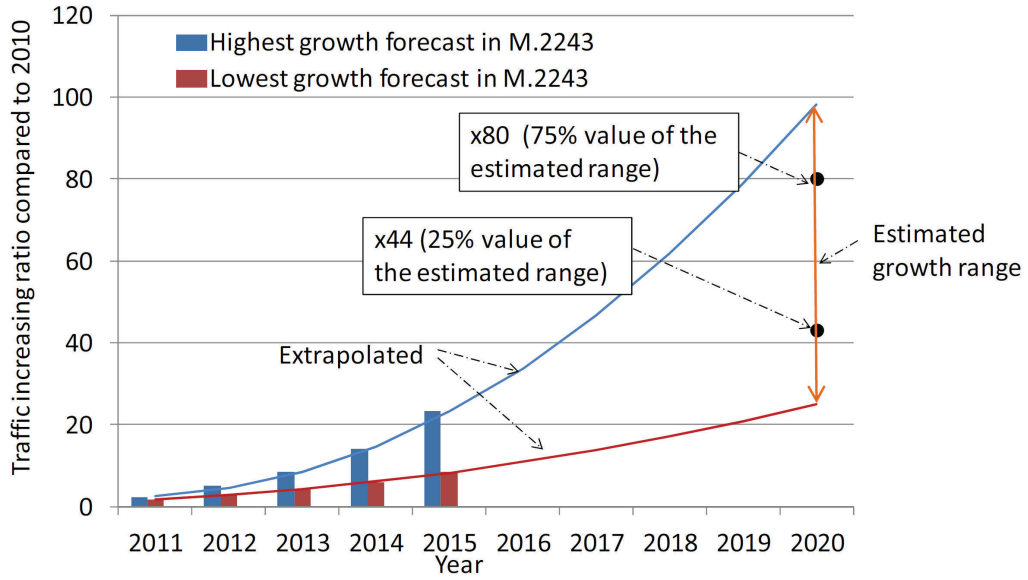

Figure 1.1: ITU-R mobile traffic forecasts up to the year 2020 [5].

channel capacity theorem states that [6],

$$C = B \log_2 (1 + SNR), \tag{1.1}$$

where C refers to the channel capacity, B bandwidth and SNR is the signal-to-noise ratio. Equation (1.1) indicates that either SNR or B needs to be increased to support this increase in capacity. Since it is not always practical to increase SNR, future increases in channel capacity will heavily rely on an increase in B, which places greater demands on the amount of spectrum that is required. A look at the bandwidth requirements of mobile telecommunications technologies over the past few decades, as shown in Table 1.1, reinforces this concept.

Generation	Technology	Bandwidth
1G	AMPS	25 – 30 KHz
2G	GSM	200 KHz
3G	WCDMA	5 MHz
4G	LTE	1.4 – 20 MHz
4G	LTE-A	1.4 – 100 MHz

Table 1.1: Mobile telecommunication technology channel bandwidths.

© University of Pretoria

UNIVERSITEIT VAN PRETORIA
UNIVERSITY OF PRETORIA
YUNIBESITHI YA PRETORIA

The channel bandwidths employed have clearly increased at each successive wireless network generation, with support for up to a 100 MHz of aggregated spectrum proposed for long term evolution advanced (LTE-A) [7]. However, the spectral efficiency of 4G networks is already approaching the theoretical channel capacity limit. Spectrum is a scarce resource that clearly needs to be managed in an efficient manner if future spectrum demands are to be met.

While the impending spectrum crunch is being driven by rapidly increasing mobile data traffic and data speeds, a major underlying reason for the spectrum crunch, has to do with static legacy spectrum allocation policies. Cognitive radio networks (CRN) have been proposed as a potential approach at making more efficient usage of existing spectrum by moving away from a static to a dynamic approach to the allocation of spectrum resources [8, 9, 10].

Secondary users (SU) within a CRN need to be aware of each other and of the primary users (PU) within the network. Due to the effects of shadowing and multipath fading in urban environments, the spectrum sensing process may suffer from various problems, including the hidden node problem. This process may thus benefit from a cooperative approach to gathering information about the behaviour of other users of the spectrum. Furthermore, there are usually power and time constraints that are placed on the spectrum sensing process. Combining prediction with cooperative sensing to produce a cooperative prediction process may hold significant benefits for the dynamic assignment process and the overall performance of the network.

1.2 OBJECTIVES

The main objectives of this thesis are summarised as follows:

- To quantify the actual usage of commercially utilised spectrum within the South African context. Specifically the television broadcast and mobile cellular bands.

- To investigate the feasibility of spectrum sensing and geo-location spectrum database based decision making by comparing actual measured data to a locally available spectrum database.

- To develop a method whereby PU spectrum occupancy may be predicted with low

© University of Pretoria

UNIVERSITEIT VAN PRETORIA
UNIVERSITY OF PRETORIA
YUNIBESITHI YA PRETORIA

complexity for different types of PU traffic patterns.

- To investigate the trade-offs between complexity and accuracy when predicting spectrum occupancy for different types of PU traffic patterns.

- To develop a method whereby spectrum occupancy may be predicted in a cooperative manner and to investigate how this could be optimally achieved.

- To investigate the trade-offs between cooperative prediction gain and overhead.

- To investigate how cooperation in a CRN can be implemented in a power efficient manner and how PU traffic prediction may contribute to this.

1.3 CONTRIBUTION AND OUTPUTS

1.3.1 Research contribution

The main research contributions of this thesis are summarised as follows:

- A novel noise threshold detection technique, known as the maximum normal fit method, was presented [1]. This technique separates the noise and signal components of a received signal based on its statistical properties.

- An extensive spectrum occupancy measurement campaign was conducted to characterise the current usage of the TV broadcast and mobile cellular bands. The maximum normal fit method was employed to calculate spectrum occupancy.

- A computationally simple approach to predicting PU traffic, called the occupancy window method, was proposed and compared with certain other methods from the literature, under various different traffic conditions.

- The concept of cooperative prediction for cognitive radio networks was discussed

[1] The author would like to thank Mr P.A. Jansen van Vuuren and Mr M.J. Prinsloo for there contributions to this technique.

© University of Pretoria

UNIVERSITEIT VAN PRETORIA
UNIVERSITY OF PRETORIA
YUNIBESITHI YA PRETORIA

and investigated. An optimal cooperative forecasting problem was formulated and a heuristic for solving the problem was proposed.

- The application of traffic forecasting was combined with optimal scheduling to provide a novel approach to improving the spectrum sensing related energy efficiency of cooperating SUs within cognitive radio network.

1.3.2 Publications

The following publications emanated from the research activities undertaken by the author during this research project.

1.3.2.1 Journal publications

The following articles were either published in or submitted to accredited peer-reviewed journals:

1. S.D. Barnes, P.A. Jansen van Vuuren and B.T. Maharaj, "Spectrum occupancy investigation: Measurements in South Africa," *Measurement*, vol. 46, no. 9, pp. 3098–3112, Nov. 2013.

2. S.D. Barnes, B.T. Maharaj and A.S. Alfa, "Cooperative prediction in cognitive radio networks," *Wireless Personal Communications*, vol. 89, no. 4, pp. 1177–1202, Aug. 2016.

3. S.D. Barnes, P.R. Botha and B.T. Maharaj, "Spectral occupation of TV broadcast bands: Measurement and analysis," *Measurement*, vol. 93, pp. 272–277, Nov. 2016.

1.3.2.2 International conference proceedings

The following papers were presented at and published in the peer reviewed proceedings of an international conference:

1. S.D. Barnes and B.T. Maharaj, "Collaborative spectral opportunity forecasting for cognitive radio," *Proceedings of IEEE AFRICON Conference*, Addis Ababa, Ethiopia,

© University of Pretoria

UNIVERSITEIT VAN PRETORIA
UNIVERSITY OF PRETORIA
YUNIBESITHI YA PRETORIA

Sept. 2015, pp. 1-6.

2. S.D. Barnes, B.T. Maharaj and A.S. Alfa, "Spectrum opportunity forecasting for energy efficient sensing in cognitive radio networks," *Proceedings of the 2nd IEEE International Symposium on Telecommunication Technologies*, Langkawi, Malaysia, Nov. 2014, pp. 128-132.

3. S.D. Barnes and B.T. Maharaj, "A comparison of spectrum occupancy in the South African 900 MHz GSM cellular bands," *Proceedings of IEEE AFRICON Conference*, Port Louis, Mauritius, Sept. 2013, pp. 1-5.

4. R.R. Thomas, S.D. Barnes and B.T. Maharaj, "TOA Location estimation based on cognitive radio channel occupancy prediction," *Proceedings of the IEEE Wireless and Mobile Communications Conference*, Barcelona, Spain, Oct. 2012, pp. 733-738.

1.3.2.3 National conference proceedings

The following papers were presented at and published in the peer reviewed proceedings of a local South African conference:

1. S.D. Barnes and B.T. Maharaj, "An occupancy window approach to primary user traffic modelling for cognitive radio," *Proceedings of the Southern African Telecommunications Networks and Applications Conference*, Stellenbosch, South Africa, Sept. 2013, pp. 395-399.

2. S.D. Barnes, K. Dhuness, R.R. Thomas and B.T. Maharaj, "Proactive dynamic spectrum access based on energy detection," *Proceedings of the Southern African Telecommunications Networks and Applications Conference*, George, South Africa, Sept. 2012.

1.3.2.4 Invited conference presentations

The following invited paper was presented at a local South African conference:

1. S.D. Barnes and B.T. Maharaj, "Spectrum occupancy and modelling: A South African case study," *South African IEEE Joint AP/MTT/EMC Chapter Conference*, Pretoria,

© University of Pretoria

UNIVERSITEIT VAN PRETORIA
UNIVERSITY OF PRETORIA
YUNIBESITHI YA PRETORIA

South Africa, May 2014.

1.4 THESIS OUTLINE

This thesis has been organised into seven Chapters. A flow chart is provided in Figure 1.2 that summarises both the topics covered and contributions made in this thesis. This diagram also indicates how each of the topics are related and fit together.

A review of the literature pertaining to spectrum efficiency and cognitive radio networks is provided in Chapter 2. This chapter provides background knowledge to support the work presented in the chapters that make up the rest of the thesis.

The current state of spectrum usage in various South African commercial bands has been investigated in Chapter 3. The results of a spectrum measurement campaign, encompassing various commercially utilised bands, are described and the case for dynamic spectrum access in South Africa is presented. These results provide motivation for the need to investigate technologies that can make efficient usage of current spectrum resources and lay the contextual foundation for the chapters that follow in this thesis.

PU traffic modelling and forecasting, for individual SUs, is discussed in Chapter 4. The occupancy window prediction method is presented and its performance is compared with other prediction methods for various traffic conditions.

Cooperation amongst SUs, for the purposes of detection and collaborative PU traffic forecasting, is investigated in Chapter 5. An optimal solution to collaborative PU traffic forecasting is sought where a balance between prediction accuracy and complexity can be achieved.

The effect that forecasting has on the energy efficiency of collaborating SUs is investigated in Chapter 6. Spectral opportunity forecasting, for proactive spectrum access, has been shown to help reduce the energy consumption of cognitive radio networks.

Finally, the topics covered by this research project are summarised and conclusions drawn in Chapter 7. Recommendations for possible future research are also discussed.

© University of Pretoria

UNIVERSITEIT VAN PRETORIA
UNIVERSITY OF PRETORIA
YUNIBESITHI YA PRETORIA

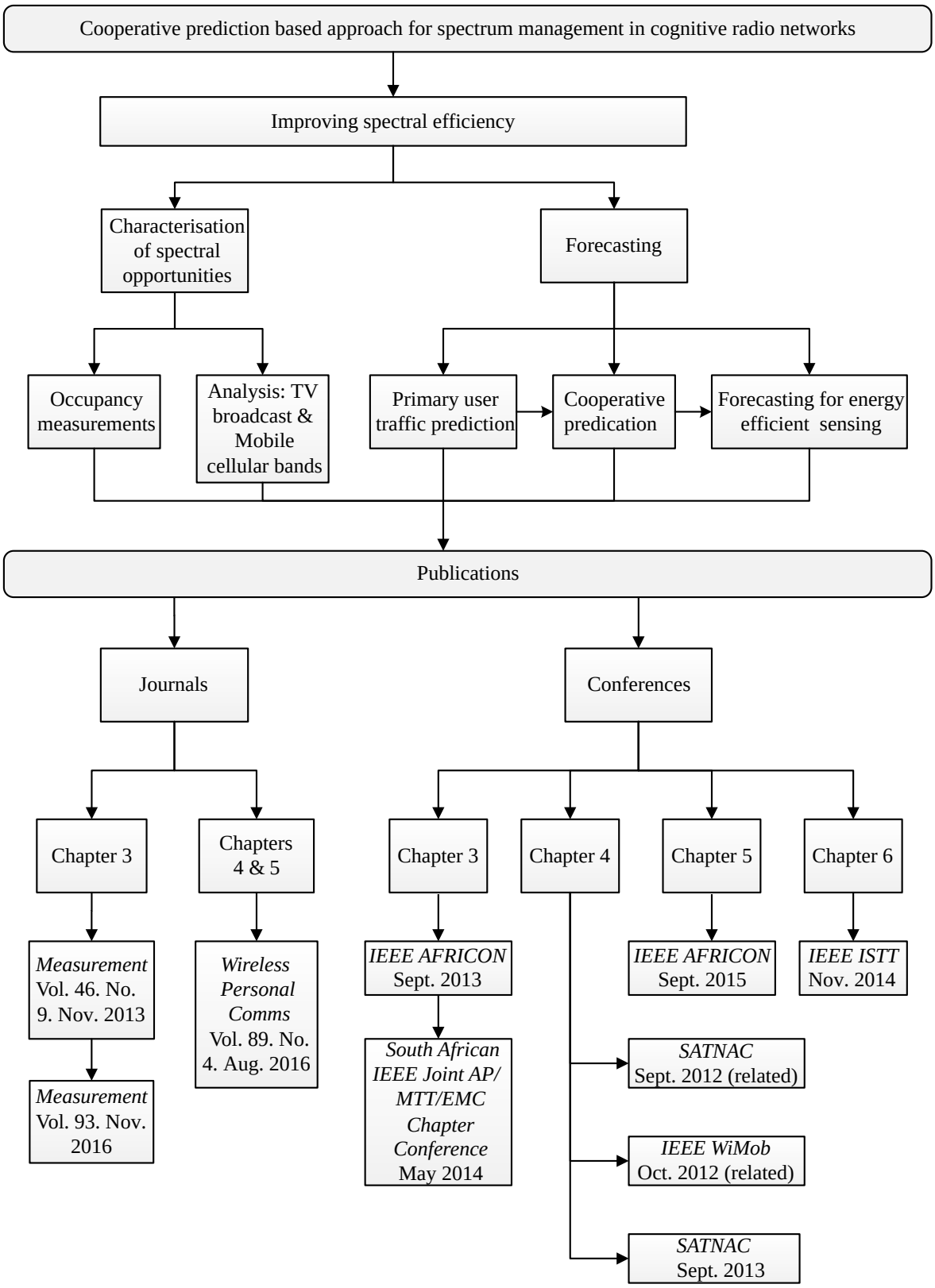

Figure 1.2: Thesis flow chart providing an overview of the topics covered and contributions made.

© University of Pretoria

CHAPTER 2

BACKGROUND: IMPROVING SPECTRAL EFFICIENCY

2.1 INTRODUCTION

Given predictions about exponential increases in the demand for spectrum [1], coupled with the fact that it is a limited natural resource, future technologies will need to balance spectrum efficiency with interference-free communication so as to ensure that the spectrum needs of future wireless networks can be met. Various approaches to achieving this balance have been proposed in the literature [9, 11], some of which will be explored in this chapter.

The chapter begins with a discussion on spectral efficiency, the electromagnetic spectrum and a selection of technologies that have been earmarked for improving spectral efficiency in future wireless networks. A brief overview on spectrum usage studies both in South Africa and around the world, together with a brief look at the South African spectrum regulatory environment, is also presented. One of the technologies earmarked for improving spectral efficiency, known as cognitive radio [8, 12], is then discussed in greater detail with a strong focus on spectrum sensing. Which is a critical process whereby information is gathered about the radio environment and the behaviour of other users of the spectrum. The focus on spectrum sensing then continues as an overview of the cooperative spectrum sensing (CSS) concept, aimed at improving spectrum sensing accuracy through cooperation and sharing amongst cognitive radios (CR), is presented. The chapter is concluded by a discussion on how the behaviour of other users of the spectrum can be modelled and predicted so as to facilitate proactive decision making within cognitive radio networks.

© University of Pretoria

UNIVERSITEIT VAN PRETORIA
UNIVERSITY OF PRETORIA
YUNIBESITHI YA PRETORIA

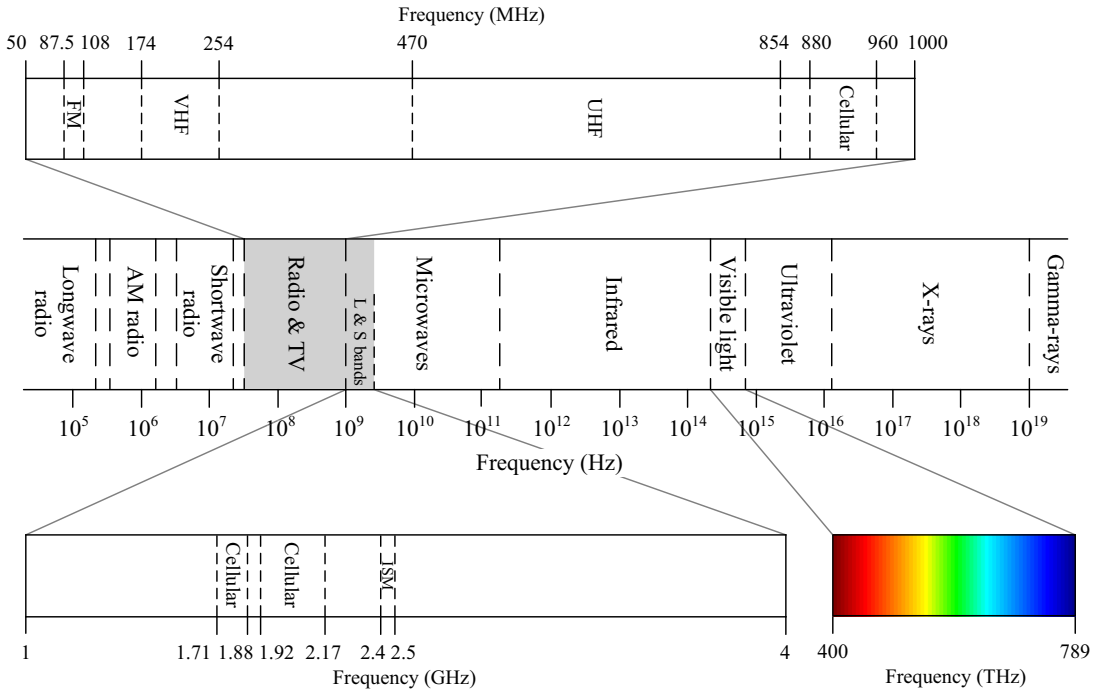

Figure 2.1: The electromagnetic spectrum. Adapted from [13], with permission (Copyright © 2005, John Wiley and Sons, Inc.).

2.2 SPECTRAL EFFICIENCY

The mobile traffic forecast illustrated in Figure 1.1, means that demand for spectrum in certain bands is rapidly increasing and will continue to do so into the future. A segment of the electromagnetic spectrum is presented in Figure 2.1. For convenience, the spectrum has been organised into general divisions roughly based on application and general propagation characteristics [13]. The divisions shown range from the bands used for long range radio through the visible spectrum and right up to X and Gamma-rays.

The regions that are currently of interest for broadband wireless communication, the bands where the demand for spectrum is rapidly growing, are shaded in grey. These are the bands traditionally assigned to television (TV) and radio applications as well as parts of the L and S microwave bands. The radio and TV bands, shown at the top of the figure, fall within the

© University of Pretoria

UNIVERSITEIT VAN PRETORIA
UNIVERSITY OF PRETORIA
YUNIBESITHI YA PRETORIA

region from 50 MHz up to 1000 MHz and are traditionally shared by broadcast radio and TV services as well as cellular communication networks. The L and S bands lie within the region from 1000 MHz up to 4000 MHz, as shown at the bottom left hand side of Figure 2.1. Parts of these bands are also used for cellular communications as well as for unlicensed services such as Wi-Fi and blue tooth in the industrial, scientific and medical bands.

As the demand for mobile and wireless connectivity grows within the shaded bands, so does the amount of spectrum required to support it. Regulatory bodies and researchers around the world are thus considering new and better approaches to making use of this scarce resource. In this section, various technologies and approaches, that have been considered for improving spectral efficiency in future generation wireless networks, are discussed.

2.2.1 Fifth generation network technologies

It has been predicted that the evolution from fourth generation to fifth generation mobile networks will most likely lead to massive increases in capacity, data rates and device connectivity, as well as reduced latency and improved energy efficiency (EE) [11]. However, this will require large amounts of spectrum. Existing spectrum allocations will thus need to be used in a more efficient manner. Some of the core technologies proposed for this purpose include licensed shared access (LSA), dynamic spectrum access (DSA), carrier aggregation (CA), device-to-device (D2D) communication and millimetre-wave broadband (MMB).

2.2.1.1 Licensed shared access

Licensed shared access allows for a particular class of user, most likely a cellular operator, to access spectrum that has already been allocated to an incumbent on a quasi-static basis. A license is provided that allows this user exclusive access to the spectrum during the time for which this license is valid. The agreement that the incumbent has with the LSA user may span a period of several years and since the incumbent user forfeits its right to the spectrum during this time, the LSA user can guarantee a certain level of quality of service (QoS) to its customers [14]. The concept of LSA is currently under study in the 2.3 to 2.4 GHz frequency band [15].

The LSA scheme may be useful to mobile operators as they could make use of such an

© University of Pretoria

UNIVERSITEIT VAN PRETORIA
UNIVERSITY OF PRETORIA
YUNIBESITHI YA PRETORIA

agreement to improve their capacity during peak usage times where the incumbent is willing to lease spectrum to the mobile operator in a specific geographic area. The mobile operator benefits since it does not need a license for the entire country and the incumbent has the potential to gain revenue from spectrum that it might not be using at that specific time and geographical location. In a similar way, devices that would form part of the internet of things could also make use of LSA spectrum, since there spectrum usage may be erratic with large intervals between transmissions.

This is a short to medium term solution to the spectrum scarcity problem and it is envisioned that it will evolve into a more dynamic form of spectrum sharing in the future, where the lease time becomes shorter and shorter, until it actually meets the requirements for full dynamic spectrum access.

2.2.1.2 Dynamic spectrum access

A further step towards spectrally efficient communication, dynamic spectrum access, is a technology that builds on the LSA concept by allowing users opportunistic access to under-utilised spectrum [16, 17]. Central to the concept of DSA is a technology known as CR. A CR is a radio with learning capabilities and thus independently able to obtain knowledge of its radio environment [8]. It uses this knowledge to dynamically switch between channels that are unused so as to temporarily make use of spectrum that would otherwise have simply remained idle and thus gone to 'waste'. Such an approach has the potential to significantly increase spectral efficiency. Global interest in Cognitive Radio technologies has thus grown significantly in recent years. CR will be discussed in much greater detail in Section 2.3.

2.2.1.3 Carrier aggregation

Carrier aggregation (CA) is a technique that allows operators to combine several possibly non-contiguous blocks of spectrum into a single data stream with a wider bandwidth. This allows for underutilised spectrum to be more efficiently utilised and is the key to achieving higher data rates in long term evolution advanced (LTE-A) networks, since it allows for the use of bandwidths that are wider than 20 MHz. The three main ways in which carriers may be combined are: Contiguous intra-band, non-contiguous intra-band and inter-band CA [18].

© University of Pretoria

UNIVERSITEIT VAN PRETORIA
UNIVERSITY OF PRETORIA
YUNIBESITHI YA PRETORIA

An advanced form of CA allows for the combination of carriers from different bands, e.g. Wi-Fi can be combined with LTE and 3G services, so as to greatly improve the data rate of the link. An example of such a system is the SpiderRadio, developed at the Stevens Institute of Technology [19], which is a software driven CR prototype that can be used to aggregate multiple data services based on the concept of bandwidth aggregation. The SpiderRadio can sense radio spectrum, detect PUs and perform dynamic spectrum access. Using dynamic spectrum management (of cost, required performance, access of policies, etc.), the SpiderRadio simultaneously takes advantage of multiple broadband services by aggregating multiple low data rate services, to obtain a high data rate connection. For example, data services (including Wi-Fi, 2G, 3G, 4G and fixed line services) could be aggregated to obtain a higher combined throughput and link quality than either of the individual services.

2.2.1.4 Device-to-device communication

The idea behind D2D communication is that wireless devices, operating within the same cell, can make use of intra-cell communication protocols to communicate directly with each other. This technology can be employed to take some of the load away from the base station (BS) by offloading tasks to the users that it serves. D2D communication thus has the potential to improve network performance and decrease end to end delays by allowing direct communication between devices over multiple, re-usable operating channels.

The potential benefits of D2D include improved power efficiency, network capacity, data throughput and spectrum utilisation. However, practical challenges surrounding self-coexistence between neighbouring cells, resource allocation and intra-cell multi-hop communication will need to be overcome. Also questions surrounding how best to share spectrum amongst devices (orthogonal or opportunistic access), over what range devices should operate and whether an underlay or an overlay approach should be adopted, must be answered. D2D devices will thus need to posses additional functionality so as to be able communicate directly with each another [20].

2.2.1.5 mmWave communication

Another technology that could help to alleviate the spectrum crunch is millimetre-wave broadband, where spectrum in the microwave region between 3 – 300 GHz can be used to comple-

© University of Pretoria

UNIVERSITEIT VAN PRETORIA
UNIVERSITY OF PRETORIA
YUNIBESITHI YA PRETORIA

ment the traditional wireless communication bands below 3 GHz [21]. The region from 28 – 38 GHz has been considered as eligible for MMB since both atmospheric absorption (less than 0.1 dB/km) and specific attenuation due to rainfall are lower than at higher frequencies [22, 23]. Atmospheric absorption losses in the region between 70 – 100 GHz and 125 – 160 GHz are also acceptable (less than 1 dB/km).

Since MMB has access to large amounts of bandwidth, it holds the potential for high data rate communications (in the order of 1 Gb/s) that could potentially be used to provide much greater capacity in both back-haul links as well as from the BS to the user. However, while spectrum scarcity is not a problem for MMB there are a number of challenges related to operating at higher frequencies. These may include poor penetration through most solid materials, high attenuation due to foliage and in the presence of heavy rain fall, higher atmospheric absorption in certain bands (e.g. 15 dB/km in the oxygen absorption band at 60 GHz) as well as various antenna and RF design challenges due to smaller wave lengths.

Initially this technology may be limited to the use of narrowly focused beam widths in point-to-point back-haul networks or for communication over relatively short distances, due to the nature of the environment that MMB devices would be operating in. However, the smaller wave lengths of these bands allows for new spatial processing and polarisation techniques such as massive multiple-input-multiple-output (MIMO) [24, 25] and adaptive beam-forming [26]. The adoption of these techniques, together with other advances such as the use of small cells, cooperative MIMO, relay stations and other interference mitigation techniques, could make MMB a viable option for the alleviation of congested spectrum.

2.2.2 Television white spaces

Using the white spaces in the bands traditionally assigned for TV broadcasting has been proposed as a way to more efficiently make use of this spectrum. White space devices (WSD) can exploit opportunities that exist due to spectral holes in the very-high frequency (VHF) bands (30-300 MHz) and also in the ultra-high frequency (UHF) bands (300-1000 MHZ) [27]. These spectral holes are gaps in the TV transmissions. Spectrum in this frequency range is highly desirable due to its high penetration and favourable propagation characteristics. This technology is commonly referred to as TV white space (TVWS).

© University of Pretoria

UNIVERSITEIT VAN PRETORIA
UNIVERSITY OF PRETORIA
YUNIBESITHI YA PRETORIA

Some regulators, e.g. the federal communications commission and the Office of Communications, are moving towards regulation that will allow for the license exempt usage of the TV bands. TVWS technology is an attractive solution for rural broadband networks since TVWS spectrum is generally readily available in the rural areas and lends itself well to signal propagation over large distances. Standards that support rural broadband communications over TVWS include the Institute for Electrical and Electronics Engineers 802.22 (IEEE 802.22), IEEE 802.11af (also known as Super Wi-Fi) and the European computer manufacturers association-392 standards.

WSDs can use spectrum sensing (SS) to detect free channels, however, SS is not always accurate and in many locations may suffer from the so called hidden node problem (where SS may be inaccurate due to among others things shadowing and fading). The geo-location spectrum database (GLSDB) has been proposed to helps WSD devices to overcome this problem [28]. A GLSDB is a geographical database of TV transmitter propagation curves that allow WSD to detect spectrum holes without performing spectrum sensing. WSD can access a GLSDB to obtain information about the location and geographically relevant transmitter power of the incumbent users of the spectrum. To make the GLSDB accurate, a combination of TV broadcast planning parameters, measurement campaigns and propagation models should be taken into account.

Some of the operators that currently provide free GLSDB services include companies such as Google [29] and Microsoft. However, paid GLSDB services are provided by companies such as Fair Spectrum, Key Bridge, Spectrumbridge and Telcordia. In South Africa a free GLSDB, that uses the international telecommunications union radiocommunication sector (ITU-R) P.1546-4 and federal communications commission curves propagation models (grade-B and grade-C), is provided by the Meraka Institute of the Council for Scientific and Industrial Research (CSIR). A screen shot of the database, where free channels at the University of Pretoria are shown in green, is provided in Figure 2.2 [30].

A number of TVWS trials have been performed around the world. The most prominent trials include: The Cape Town white space trial in South Africa, the Kenya white space project, the advanced internet regions consortium and University of west Virginia trial in the USA, a white space project on the Isle of Bute in Scotland, a telemedicine over TVWS project in the Philippines and a white spaces pilot project in Singapore.

© University of Pretoria

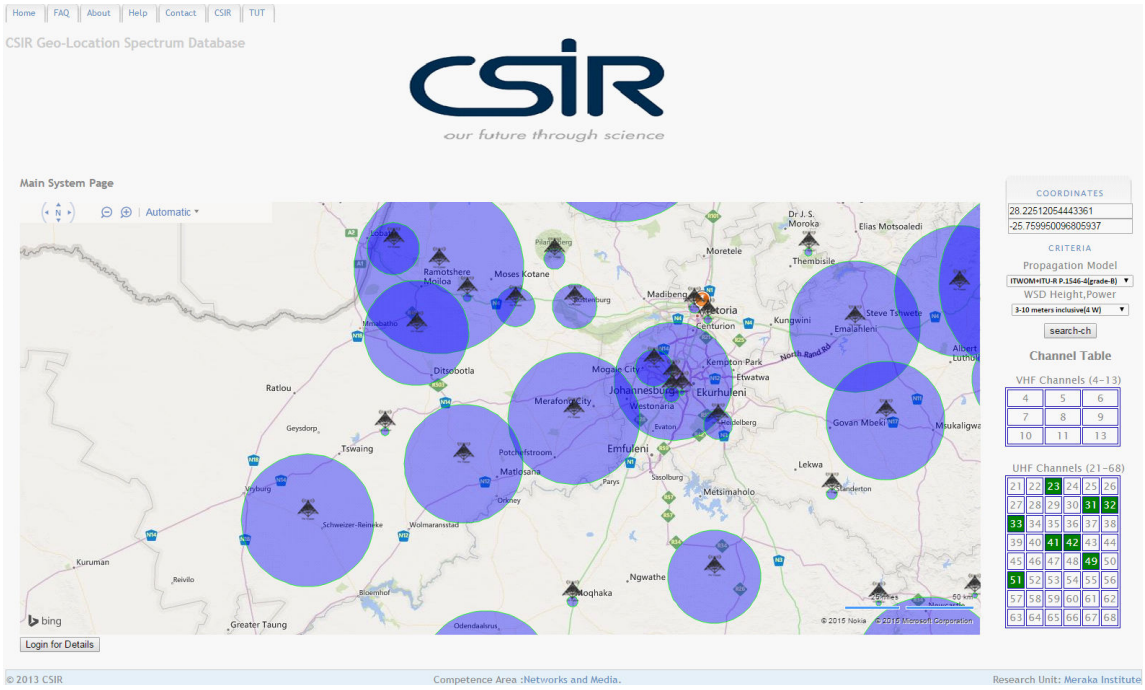

Figure 2.2: A screen shot of the CSIR GLSB. Free channels are highlighted in green [30].

2.2.3 Characterising spectrum occupancy

To gain a better perspective of the needs of future wireless networks, it is necessary to determine how much spectrum is currently being used and where congestion is currently the highest. The best way to do this is to actually take measurements of the spectrum in the bands of interest to these networks. These measurements can then be used by regulatory bodies as a basis for future planning. Measurement campaigns that have been conducted are briefly listed below. The general conclusion drawn from most of these campaigns was that outdated spectrum assignments and regulatory policies have led to a situation where spectrum appears to be scarce, but in actual fact is underutilised due to inefficiency.

2.2.3.1 Local measurement campaigns

A few of measurement campaigns have been conducted to gain insight into the actual usage of spectrum in South Africa, most notably a TVWS trial performed in Cape Town by the Meraka Institute of the CSIR in collaboration with the independent communications authority of South Africa (ICASA) [31, 32]. This trial helped to identify un-unused spectrum in the TV broadcast bands in the Cape Town suburb of Tygerberg and has lead to further work on

© University of Pretoria

UNIVERSITEIT VAN PRETORIA
UNIVERSITY OF PRETORIA
YUNIBESITHI YA PRETORIA

developing a TVWS GLSDB for South Africa [30]. However, in the South African context, knowledge about actual measured spectral occupancy is limited. As a step toward better spectral awareness in South Africa, a detailed measurement campaign of all of the bands listed in Table 2.2, will thus be presented in Chapter 3 of this thesis.

2.2.3.2 International measurements campaigns

A number of comprehensive measurement campaigns have been performed around the world that cover more than just the bands used for TV broadcast and mobile broadband. These included measurement campaigns carried out in various parts of the USA (New York City, Chicago, Washington, DC, Greenbank, WV) by both universities and other organisations such as the Shared Spectrum Company [33, 34, 35, 36, 37]. In general spectrum usage was found to be high in certain bands, e.g. the mobile cellular bands, yet many of the bands were actually found to be underutilised. Measurements conducted in other countries include campaigns carried out in Auckland, New Zealand [38], Barcelona, Spain [39], Aachen, Germany [40, 41], Maastricht, The Netherlands [42, 41] and Dublin, Ireland [43].

The results obtained from these measurement campaigns are summarised in Table 2.1. A comparison is made against the average occupancy of the bands reportedly used for mobile cellular communications as well as those used for television broadcasting. The values presented in Table 2.1 represent the average occupancy of the bandwidth allocated for either mobile broadband communication or broadcast television (both VHF and UHF bands) at each measurement location. The bands allocated for cellular communication around the 800/900 MHz region are denoted Mobile A and those around the 1800/1900 MHz region, Mobile B.

Certain observations can be made from Table 2.1. Firstly, that the broadcast TV bands are

Table 2.1: A comparison of measured spectral utilisation at various international locations.

Band	New York	Chicago	Virginia	Barcelona	Dublin
TV	35.93	52.40	30.54	82.08	36.36
Mobile A	46.30	54.70	42.53	51.30	0.70
Mobile B	33.80	42.90	19.70	29.41	36.80

© University of Pretoria

UNIVERSITEIT VAN PRETORIA
UNIVERSITY OF PRETORIA
YUNIBESITHI YA PRETORIA

underutilised at all of the locations, except for Barcelona, Spain. Secondly, mobile A tends to be more heavily utilised than mobile B, with the exception of Dublin, Ireland where mobile A does not seem to be in use at that particular measurement location.

It must be noted that it is difficult to obtain an exact comparison of occupancy, since there are differences in the regulatory policy surrounding frequency planning, the number of TV stations operating at each location and the exact bandwidths set aside for mobile communication for each country. Also, the thresholds used to detect band usage have not always been clearly defined. However, there is clearly spectrum that is still available in the TV and cellular bands, which could be exploited by other technologies.

2.2.4 Spectrum regulation

National regulatory bodies are usually tasked with allocating spectrum. In South Africa this falls under the ICASA. They are an independent regulatory body which is also a member of both the African Telecommunications Union and the International Telecommunications Union (ITU).

The bands that are allocated for mobile telephony and mobile broadband services are currently most at risk of spectral congestion. Current allocation for these services is limited to the bands from 880 MHz to 960 MHz, 1710 MHz to 1880 MHz, 1920 MHz to 2170 MHz and 2305 MHz to 2483.5 MHz (LTE) [44]. At the same time, however, other bands are not actually being fully utilised. An example of this is the bands currently assigned for television (TV) broadcast, where outdated spectrum planning for analogue TV has lead to inefficient usage of these bands. Since South Africa falls within Region one of the ITU), TV broadcast services are currently allocated for spectrum between 174 MHz to 254 MHz (band III), 470 MHz to 582 MHz (band IV) and 582 MHz to 854 MHz (band V) [44]. These allocations are summarised in Table 2.2.

Future wireless networks will require regulators to balance spectrum efficiency with interference free communication so that the spectrum needs of future wireless broadband networks can be met. This will require appropriate licensing models for users of the spectrum as well as monitoring of the spectrum to ascertain what the actual usage is. As a step in this direction the Conférence Européenne des Administrations des Postes et des Télécommunications

© University of Pretoria

UNIVERSITEIT VAN PRETORIA
UNIVERSITY OF PRETORIA
YUNIBESITHI YA PRETORIA

Table 2.2: Band allocations for TV broadcast and mobile telephony in South Africa.

Band	**Frequency (MHz)**
Band III	174 - 254
Band IV	470 - 582
Band V	582 - 854
GSM 900	880 - 960
GSM 1800	1710 - 1880
WCDMA	1920 - 2170
LTE	2305 - 2483.5

has proposed various spectrum sharing methods. These methods include the following three license regimes: Spectrum trading licenses, individual usage licenses and general cognitive radio equipment licenses [45].

2.3 COGNITIVE RADIO

The term cognition refers to the mental processes of knowing and making decisions through awareness, perception, reasoning, judgement and intuition. It is the process whereby input stimuli are processed so as to generate an output, and although this process is traditionally associated with human intelligence, it may be extended to the realm of artificial intelligence (AI) [46]. In this section an AI extension that is applicable to wireless communication networks, known as CR, will be discussed.

2.3.1 Definition

A CR is a radio that interacts with its radio environment by observing the activity of other users in that environment and then, based on those observations, makes decisions about which frequencies to occupy, at which geographical location and also when to occupy them. A CR has the ability to continuously and automatically adapt its operating parameters to its operational environment. Essentially, a CR is a radio with AI [8]. The concept of CR is based on the concept of a software defined radio, which is a radio whose operating parameters

© University of Pretoria

UNIVERSITEIT VAN PRETORIA
UNIVERSITY OF PRETORIA
YUNIBESITHI YA PRETORIA

can be dynamically programmed in a software environment [47].

The following definitions provide a more extended explanation of the CR concept:

- ***Dr Joseph Mitola (founder of CR)***: "A really smart radio that would be self-, RF- and user-aware, and that would include language technology and machine vision along with a lot of high-fidelity knowledge of the radio environment" [8].

- ***Institute for electrical and electronic engineers (IEEE) 1900.1***: "A type of radio in which communication systems are aware of their environment and internal state and can make decisions about their radio operating behaviour based on that information and predefined objectives" [17].

- ***International telecommunications union radio communication sector (ITU-R)***: "A radio system employing technology that allows the system to obtain knowledge of its operational and geographical environment, established policies and its internal state; to dynamically and autonomously adjust its operational parameters and protocols according to its obtained knowledge in order to achieve predefined objectives; and to learn from the results obtained" [48].

2.3.2 Primary functions

Traditionally, fixed portions of spectrum have been allocated to primary users (PU) of the spectrum. This has lead to a situation where regions exist in space, time and frequency that are un-utilised by the PUs, either momentarily or for protracted periods of time. These space-time-frequency regions are referred to as spectrum holes [12]. In a cognitive radio network (CRN), secondary users (SU) are allowed to exploit these holes by dynamically transitioning from hole-to-hole as dictated by PU behaviour [9]. An illustration of this concept is provide in Figure 2.3. The grey blocks represent portions of used spectrum for four different frequency channels over a period of time, while the spaces between them represent spectrum holes. A SU of this spectral region would need to adapt to the environment by following the arrows from the bottom left to the bottom right hand portion of the diagram. This is the DSA process referred to in the previous section.

It very important that a CR does not interfere with other users of the same spectrum. To

© University of Pretoria

UNIVERSITEIT VAN PRETORIA
UNIVERSITY OF PRETORIA
YUNIBESITHI YA PRETORIA

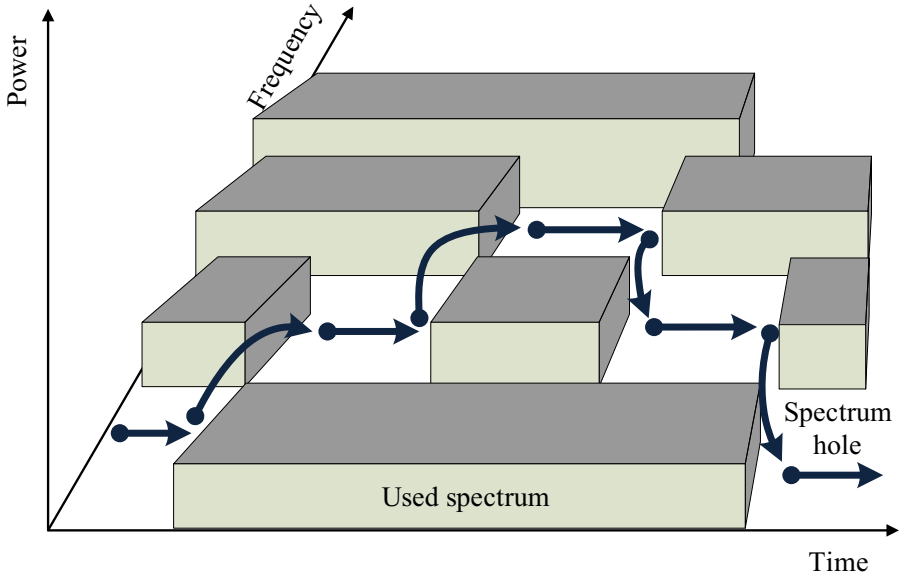

Figure 2.3: Illustration of the spectrum hole concept. Adapted from [49], with permission.

help it do this, a CR device needs to fulfil the following requirements,

- Have knowledge of who the spectrum users are and what protection criteria are required.
- Be able to detect PU field strength and system type (e.g. analogue or digital transmission)
- Be capable of intelligently detecting and avoiding incumbent spectrum users.

These requirements may in turn be met by following a cognitive cycle. This cycle is illustrated in Figure 2.4 and is primarily a repetition of the following steps,

- ***Sensing***: A real time wide-band spectrum monitoring process where information about the radio environment is gathered.
- ***Analysis***: The inference of the occurrence of spectrum holes and the presence of PUs from the information gathered during spectrum sensing.
- ***Decision***: The course of action to be followed is determined by taking user requirements and the current radio environment into account.
- ***Action***: The transition to new operating parameters including fair sharing of spectrum among coexisting SUs.
- ***Learning***: The retention of knowledge about the current cycle that can be used to assist with decision making in future cycles.

© University of Pretoria

UNIVERSITEIT VAN PRETORIA
UNIVERSITY OF PRETORIA
YUNIBESITHI YA PRETORIA

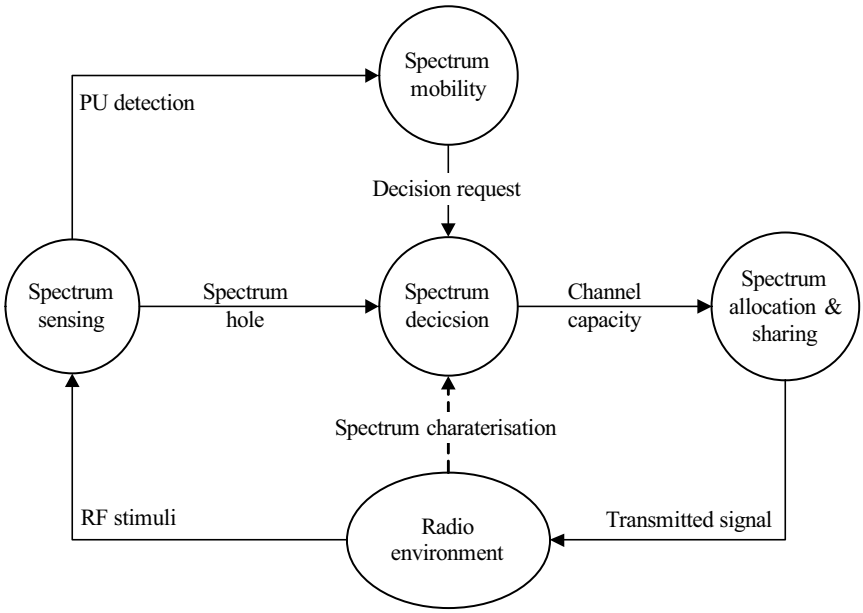

Figure 2.4: Illustration of the cognitive radio cycle. Adapted from [49], with permission.

2.3.3 Spectrum sensing

A SU needs to be able to detect both the presence of spectrum holes and other spectrum users, before it may operate in a CR network. It uses information gathered during SS to this. SS is therefore one of the most important components of a CR system since knowledge about the radio environment must be obtained before SU communication may commence.

2.3.3.1 Sensing techniques

A number of methods including matched filtering, waveform-based sensing, radio identification, cyclostationary feature detection, energy detection and cooperative sensing have been proposed in the literature [50, 51]. A comparison between the accuracy and complexity of some of the most prominent techniques is shown in Figure 2.5. A brief description now follows:

- ***Matched filter detection***: The SU receiver needs to have pre-existing knowledge of the PU's signalling features and be able to demodulate the actual PU signal. This is the most accurate technique for detecting a PU [52]. However, it suffers from impractical levels of receiver complexity [53].

© University of Pretoria

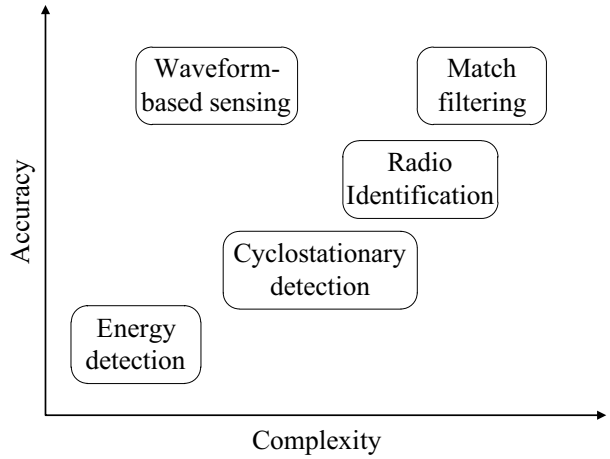

Figure 2.5: Comparison between SS techniques illustrating a trade-off between accuracy and complexity. Adapted from [50], with permission (Copyright © 2009, IEEE).

- ***Waveform-based sensing***: Waveform-based sensing can be employed when PU waveform patterns are known to the SU. These patterns may be correlated with the measured signals to establish the presence of the PU. Waveform-based detection methods possess the advantage of having short sensing times, but may suffer from synchronisation issues [50].
- ***Radio identification based sensing***: Through the continual search for transmission modes before and during communication, transmission technology can be used to detect PUs. Feature extraction is used to select the most probable technology from parameters such as the centre frequency, channel bandwidth and amount of energy detected as well as other statistical information about the measured signal [50].
- ***Cyclostationary feature detection***: The presence of a PU is detected using cyclically varying features of the PU signal, e.g. mean and autocorrelation. This is achieved by analysing the cyclic spectral density function of a received signal, since it can differentiate between noise and the PU signal. Several techniques have been proposed in the literature [54, 55, 56, 57].
- ***Energy detection***: Energy detection (ED) is the least complex, but also the least accurate technique, and requires no prior information about the PU signal. The received signal is pre-filtered by a band pass filter, squared and then integrated over an interval of time so as to measure the amount of energy contained within the received waveform [58].

© University of Pretoria

UNIVERSITEIT VAN PRETORIA
UNIVERSITY OF PRETORIA
YUNIBESITHI YA PRETORIA

Even though ED is the least accurate SS technique it is the most popular approach, due to its low computational complexity and relative ease of implementation. For the rest of this thesis, further reference to SS will be assumed to follow the ED technique.

2.3.3.2 Sensing accuracy

The result of the SS process can be described by the binary hypothesis that a channel that is unoccupied is given by H_0 and that a channel that is occupied by H_1, such that,

$$\begin{aligned} H_0 : r(n) &= w(n), \\ H_1 : r(n) &= s(n) + w(n), \end{aligned} \tag{2.1}$$

where $r(n)$ is the signal measured during SS, $s(n)$ is the actual transmitted signal and $w(n)$ denotes additive white Gaussian noise. Thus, in the absence of the PU, $s(n) = 0$. Alternatively $|s(n)| > 0$ when the PU is present. Using ED, let the absolute energy measured for $r(n)$ be denoted by E, then a binary occupancy decision D can be made by comparing E to a noise threshold λ, such that,

$$D = \begin{cases} 1, & E > \lambda \\ 0. & \text{otherwise} \end{cases} \tag{2.2}$$

Since SS is crucial to the performance of a CRN. It is necessary to do so in an accurate manner. The probability of detection P_d, the probability of miss-detection P_{md} and the probability of false alarm P_f are measures that can be used to characterise SS performance. These measures may be defined as follows [50],

$$P_d = Pr\{E > \lambda | H_1\}, \tag{2.3}$$

$$P_{md} = Pr\{E < \lambda | H_1\}, \tag{2.4}$$

where $P_{md} = 1 - P_d$ is the probability of mis-detection (the probability of detecting the band to be free when it is actually occupied) and P_f is the probability of false alarm (the probability that the channel is found to be occupied when it is in fact not), given as,

$$P_f = Pr\{E > \lambda | H_0\}. \tag{2.5}$$

When performing SS it is desirable for P_{md} and P_f to be minimised and for P_d to be maximised.

© University of Pretoria

UNIVERSITEIT VAN PRETORIA
UNIVERSITY OF PRETORIA
YUNIBESITHI YA PRETORIA

A collaborative approach to SS has been shown to improve SS accuracy [50, 59, 60], particularly under channel conditions where fading, shadowing and noise uncertainty, are prevalent [61]. In this approach SUs share information about their individual SS results so that a combined SS result can be obtained. Space, time and frequency diversity can also be exploited to further improve cooperative SS performance [62].

Since multiple cooperating sensing nodes are employed, the concept of a cooperative probability of detection Q_d and a cooperative probability of false alarm Q_f has been proposed in the literature [63]. Assuming the use of the k-out-of-N fusion rule (a commonly employed hard decision fusion rule, fusion rules are briefly discussed in Section 2.4.3), these probabilities may be defined as,

$$Q_d = Pr\left\{\sum_{i=1}^{N} D_i \geq k|H_1\right\}, \tag{2.6}$$

$$Q_f = Pr\left\{\sum_{i=1}^{N} D_i \geq k|H_0\right\}. \tag{2.7}$$

Considering the extreme cases of the k-out-of-N rule leads to the OR rule [64], when $k = 1$, where (2.6) and (2.7) become,

$$Q_d = 1 - \prod_{i=1}^{N}(1 - P_{d,i}), \tag{2.8}$$

$$Q_f = 1 - \prod_{i=1}^{N}(1 - P_{f,i}), \tag{2.9}$$

and the AND rule [64], when $k = N$, where (2.6) and (2.7) respectively become,

$$Q_d = \prod_{i=1}^{N} P_{d,i}, \tag{2.10}$$

$$Q_f = \prod_{i=1}^{N} P_{f,i}. \tag{2.11}$$

2.4 COOPERATIVE SPECTRUM SENSING

As already mentioned in the previous section, the SS process may not always be accurate and in reality there are a number of problems associated with this process. Inaccuracy in the SS process may occur when a SU makes a decision about the occupancy of a particular band while not actually being in a position to accurately measure the status of that band.

© University of Pretoria

UNIVERSITEIT VAN PRETORIA
UNIVERSITY OF PRETORIA
YUNIBESITHI YA PRETORIA

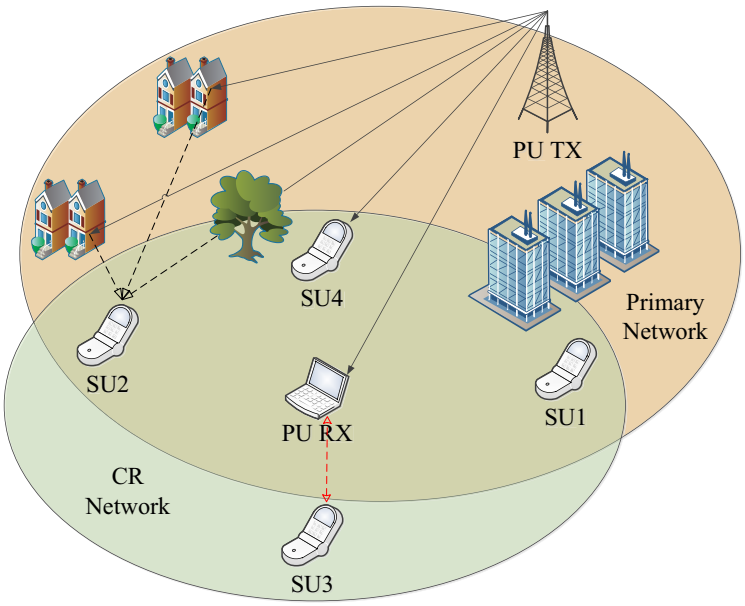

Figure 2.6: Multi SU CR scenario illustrating some of the problems associated with SS. Adapted from [65], with permission.

This may be due to the effects of the hidden node problem, shadowing, multipath fading and receiver uncertainty [10].

A typical CR scenario, where these problems are highlighted, is illustrated in Figure 2.6. Firstly, the signal transmitted by the PU transmitter is hidden from SU1 due to shadowing from the high-rise buildings that lie between them. SU1 is thus a hidden node. Secondly, multiple attenuated versions of the signal that have been reflected or scattered off nearby buildings and vegetation, arrive at SU2 making the correct detection of the PU signal difficult to achieve. Thirdly, while situated within the secondary CR network, SU3 lies just outside of the range of the PU transmitter and thus suffers from receiver uncertainty since it cannot detect the PU. The problem with receiver uncertainty is that SU3 transmissions could interfere with the PU receiver. Fortunately SU4 has a direct line of sight with the transmitter and should be able to accurately detect the presence of the PU. There is thus clearly a need for cooperation amongst the SUs. Cooperative SS makes use of spatial diversity amongst SUs within a CRN to overcome the sensing deficiencies of individual users. This means that SU4 could potentially share its SS results with the other users, thus allowing them to improve their individual SS results.

© University of Pretoria

UNIVERSITEIT VAN PRETORIA
UNIVERSITY OF PRETORIA
YUNIBESITHI YA PRETORIA

2.4.1 Objectives and essential elements

Given a group of cooperating SUs exposed to diverse channel conditions, the essence behind the idea of cooperative sensing may be summarised by the following three questions [66]:

- How can individual CR users cooperate with each other?
- How much can be gained by cooperating as opposed to acting alone?
- What is the cost/overhead associated with following this approach?

These questions should be considered within the context of the following objectives [65]:

- To avoid harmful interference to PUs.
- To exploit spectrum holes so as to improve CRN throughput and QoS.
- To enhance spectrum sensing performance.
- To exploit spatial diversity.
- To provide greater sensing accuracy by making combined decisions.

While cooperative SS can be summarised as a process where individual users try to detect the presence of a PU and then share their results so that they can be fused together to obtain a cooperative spectrum decision, it is also comprised of a number of other essential elements. These elements are crucial to the success of the process and can affect cooperative SS accuracy. These essential elements are as follows [65, 63]:

- ***A cooperation model***: SUs are allowed to share information among themselves, e.g. Parallel fusion or game theoretic models.
- ***A sensing technique***: Individual SUs gather data about their radio environment, e.g. ED or cyclostationary detection.
- ***A statistical hypothesis***: Individual SUs test for the presence of the PU, e.g. binary hypothesis, composite hypothesis or sequential testing,
- ***Control and reporting channels***: SS results are shared or fed to a fusion centre (FC) using these channels. They should be reliable, efficient and tolerant of fading and bandwidth limitations.
- ***A data fusion process***: Data is combined to make a cooperative decision about the presence of the PU.
- ***An optimal user selection process***: Cooperating SUs are selected so as to maximise

© University of Pretoria

UNIVERSITEIT VAN PRETORIA
UNIVERSITY OF PRETORIA
YUNIBESITHI YA PRETORIA

cooperative gains while minimising losses, e.g. a centralised or cluster-based approach.

- ***A radio environment knowledge base***: This is used to facilitate the cooperation process using information about signal strength, geographical location and PU activity models, e.g. the TVWS GLSDB discussed earlier in this chapter.
- ***System synchronisation***: Communication between all of the cooperating nodes is necessary to ensure that SU transmissions do not interfere with the SS process.
- ***A suitable geographical spread***: Diversity between the cooperating nodes is important since it improves SS accuracy by minimising the effect of the hidden node problem.

2.4.2 Approach

Traditionally there are two main ways in which cooperative SS sensing is carried out, as illustrated in Figure 2.7 [65]:

- ***A centralised approach***: A master node within the network acts as a FS and collects all sensing information from the other nodes. Cooperating nodes report their results via a control channel to the FC. The FC then makes a decision about which channels are available.
- ***A distributed approach***: Individual nodes have a higher degree of autonomy and no single node has the power to control the network, i.e. there is no FC. The cooperating nodes share their sensing results with each other which they use, together with their own information, to make a unified decision. This approach is based on a distributed

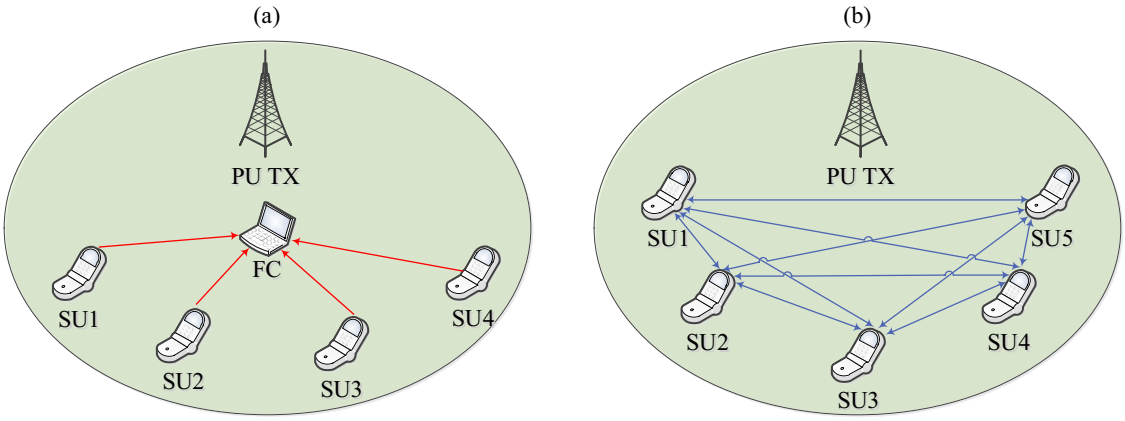

Figure 2.7: Different approaches to CSS: (a) centralised and (b) distributed. Adapted from [65], with permission.

© University of Pretoria

UNIVERSITEIT VAN PRETORIA
UNIVERSITY OF PRETORIA
YUNIBESITHI YA PRETORIA

algorithm and iterated so as to reach a unanimous cooperative decision.

As a variation, a relay-assisted approach has also been proposed in the literature [65]. The relay-assisted approach makes decisions using relay channels that allow the data to be forwarded by multi-hop techniques. SUs with strong report channels are used as relay channels for SUs with weak reporting channels. In this way strong channels can be exploited while weak channels are ignored. This approach can be used in either a distributed or a centralized fashion.

2.4.3 Decision making

When making a cooperative decision, two main approaches are generally followed for combining or fusing reported SS results:

- ***Soft decision***: Either the complete test statistic or the entire sample of original sensing data, from each SU, is used to make a decision. No local processing is performed by individual SUs, but rather at the FC. Techniques such as maximal ratio combining, equal gain combining and optimal combining could be employed for this purpose [67]. Quantised versions of the original sample are sometimes also used to improve computational cost [68].
- ***Hard decision***: A single bit decision from each SU is used to make the cooperative decision [65]. In this case linear fusion rules such as the *AND*, *OR* and majority rules, which are derived from the k-out-of-N rules, are commonly applied. The OR rule, when $k = 1$, is best for large numbers of cooperating SUs, while the AND rule, when $k = N$, is better when there are fewer cooperating SUs. Various schemes, such as reinforcement learning and Q-Learning have been proposed in the literature to improve the performance of hard decision fusion [69, 70].

It has been shown in the literature that soft decision fusion generally outperforms hard decision fusion [71, 72]. However, the hard decision fusion approach is much less complex to implement. A compromise between these two approaches was presented in [73], where a ternary decision process was proposed that still outperforms the binary decision making process.

© University of Pretoria

UNIVERSITEIT VAN PRETORIA
UNIVERSITY OF PRETORIA
YUNIBESITHI YA PRETORIA

2.4.4 Cooperative sensing gains and costs

There are undeniable benefits to performing cooperative SS, however, these benefits also come at a cost. Any cooperative SS scheme needs to consider both and also how to find the best compromise between them.

2.4.4.1 Gains

The performance improvement associated with cooperative SS is referred to as cooperative gain [65, 69]. In a CRN, cooperative gain is mainly experienced as an improvement in the accuracy of PU signal detection, i.e. higher values for P_d and lower values for P_f. The detection of weak signals becomes far more likely, since cooperation can help to address the problems associated with multipath fading, shadowing and receiver uncertainly by effectively relaxing the receiver sensitivity requirements of individual SUs. Cooperative SS also leads to increased SU agility since cooperation allows for more and better channel switching options, given that the SUs now have a more complete picture of the actual channel conditions within which they intent to operate.

2.4.4.2 Costs

The cost of cooperation, also know as cooperative overhead, is a limiting factor of cooperative SS. The following is a list of the most common problems associated with cooperative SS:

- ***Time delays***: The process of detecting the PU signal can lead to various delays, especially if the reporting process is not synchronised. The SS process is inherently time consuming since every spectrum sample uses up time that could otherwise have been spent transmitting or receiving data. Also, the more samples taken, the greater the SS accuracy. Having to report results to a FC also takes time that would not be needed in a non-cooperative SS scheme [74].
- ***Energy efficiency***: Energy consumption can become a issue in cooperative SS schemes, since both the processes of local sensing as well as reporting require additional energy. If there are a large number of cooperating SUs, EE can be significantly affected. EE can be improved either by reducing the amount of reporting needed or by optimising which SUs actually need to perform local sensing [64, 75].

© University of Pretoria

UNIVERSITEIT VAN PRETORIA
UNIVERSITY OF PRETORIA
YUNIBESITHI YA PRETORIA

- ***Spatial correlation and mobility***: Nodes experiencing shadowing or receiver uncertainty, that are situated too close to each other, can influence each others' SS results. This leads to something known as spatially correlated fading, which can degrade cooperative SS performance [76]. Mobility amongst SUs could also lead to spatial correlation as individual SUs could move closer together, however, it could also improve spatio temporal diversity [77].
- ***Security***: Cooperation may also lead to a number of security issues since incorrect reporting of local SS results could influence the cooperative decision. This could happen by accident when a SU malfunctions, or it could be a consequence of deliberate falsification, e.g. malicious SUs could report false information so as to selfishly gain access to spectrum and further their own agendas [78].

2.5 WHITE SPACE PREDICTION

While critical to a CRN, the SS process has certain drawbacks. One of the main drawbacks is that the time spent performing SS subtracts from the time available for actual data transmission. Also, SS can increase the power consumption of the SS device [64]. However, if accurate predictions about future PU activity can be made, then some of the time spent on SS could potentially be replaced by predictions [12]. Furthermore, accurate prediction of future PU behaviour allows for proactive decision making, which has been shown to improve the channel selection process [79, 80].

Predicting future channel occupancy first requires SUs to gather information about PU traffic patterns. Statistical models can then be generated from this information and used to predict PU behaviour. These models can be classified according to three major groups: AI based models, linear models and statistical and moving average based models. In this section, a number of techniques for modelling and predicting PU traffic patterns are presented.

2.5.1 Artificial intelligence

Since predicting PU behaviour can be a complex process, the use of various AI techniques has been proposed in the literature. In [81] and [82, 83], Neural networks were proposed. The use of support vector machines (SVM) was suggested in [84] and a number schemes involving various forms of both Markov chains (MC) and hidden Markov models (HMM) have also

© University of Pretoria

UNIVERSITEIT VAN PRETORIA
UNIVERSITY OF PRETORIA
YUNIBESITHI YA PRETORIA

been proposed [85, 86, 87, 88, 89, 90, 91, 92, 93].

2.5.1.1 Neural networks

Artificial neural networks (ANN) have been proposed for channel status prediction in CRNs since, unlike other statistical methods, they do not rely on a-priori information about the underlying statistical distributions of PU behaviour [82]. An ANN is an adaptive and non linear model which allows for the mapping of input data to output data via an interconnected network of artificial neurons. These neurons make use of mathematical or computational models to process information.

In [82, 83], a multilayer perceptron (MLP) feed-forward ANN is used for future state prediction. The input data is made up of historical observations of PU behaviour and the outputs of the model are the future predicted states.

An MLP is made up of multiple layers which include an input layer, an output layer and multiple hidden layers in-between. Each layer consists of a group of artificial neurons or nodes. Nodes from different layers are connected to each other via adaptive weights. With the exception of the input nodes, each node calculates a weighted sum of all of its inputs and then passes that sum through a nonlinear activation function $\Gamma(.)$ (a hyperbolic tangent is often used). Let the output of node $n_j, \quad 1 \leq j \leq N^l$ from layer l be denoted as y_j^l, the output of node $n_i, \quad 1 \leq i \leq N^{l-1}$ from layer $l-1$ be denoted as y_i^{l-1} and the connection weight between these two nodes be denoted as w_{ij}^{l-1}, then the weighted sum of all the inputs to the current node may be calculated as,

$$v_j^l = \sum_i^{N^l} y_i^{l-1} w_{ij}^{l-1}. \tag{2.12}$$

The output of the current node may be calculated as,

$$y_j^l = \Gamma\left(v_j^l\right). \tag{2.13}$$

If a hyperbolic tangent is used for $\Gamma(.)$ in (2.13), then the output y_j^l becomes,

$$y_j^l = \frac{1 - \exp\left(-v_i^l\right)}{1 + \exp\left(-v_i^l\right)}. \tag{2.14}$$

A simple example of a second order MLP is depicted in Figure 2.8, where there are two input neurons in the input layer, four neurons in the only hidden layer and a single neuron in the

© University of Pretoria

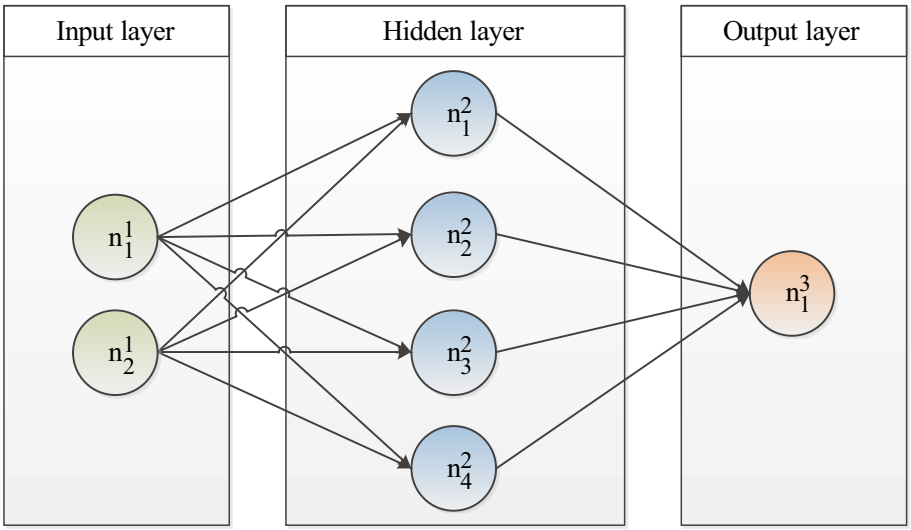

Figure 2.8: Basic example of a feed-forward ANN. Adapted from [94], with permission.

output layer (the network order is equal to the number of neurons in the input layer).

One the major problems associated with ANN is the training process of the model. In [82, 83] a method known as the backpropagation algorithm was utilised. The algorithm attempts to minimise the mean square error $\mathbf{E}$ of the output of the MLP network over successive iterations of the MLP. It does this by adjusting the weight parameters w_{ij}^l until the output of the MLP approximately matches the desired value. The parameters are updated as follows,

$$\mathbf{w}_t = \mathbf{w}_{t-1} + \Delta \mathbf{w}_t, \tag{2.15}$$

with $\mathbf{w}_t$ the weight parameter at at time t. The change in weight function may be described as follows,

$$\Delta \mathbf{w}_t = -\eta \frac{\partial \boldsymbol{E}}{\partial \boldsymbol{w}_t} + \beta \Delta \boldsymbol{w}_{t-1}. \tag{2.16}$$

where η and β are constants for the learning rate and momentum. They can be chosen from the following ranges, $\eta \in \{0, 1\}$ and $\beta \in \{0.5, 0.9\}$.

2.5.1.2 Support vector regression

In [84], support vector regression is combined with empirical mode decomposition to perform spectrum series prediction. Support vector regression makes use of SVMs to perform regression estimation that is based on the principle of structural risk minimisation.

© University of Pretoria

A function $f(x)$ needs to be found that deviates from y_i by no more than ϵ, given a set of training data $\{(x_i, y_i)\}_{i=1}^{N}$, with $x_i \in \Re$ an input value of the space of input patterns X and $y_i \in \Re$ its corresponding target value. In the linear case $f(x)$ may be expressed as,

$$f(x) = \langle w, x \rangle + b. \quad w \in X, b \in \Re \tag{2.17}$$

The term $\langle w, x \rangle$ refers to the dot product, where w is the regression vector and b is a bias term. Flatness in (2.17) is desired which can be achieved by minimising the norm $\|w\|^2 = \langle w, w \rangle$. This leads to a convex optimisation problem, which can be expressed as follows [95],

$$\min_{w,\zeta_i,\zeta_i^*} L = \frac{1}{2}\|w\|^2 + C\sum_{i=1}^{N}(\xi_i + \xi_i^*) \tag{2.18}$$

$$s.t. \begin{cases} y_i - \langle wx_i \rangle - b \leq \epsilon + \xi_i \\ \langle wx_i \rangle + b - y_i \leq \epsilon + \xi_i^* \\ \xi_i, \xi_i^* \geq 0 \end{cases} \tag{2.19}$$

where ξ_i, ξ_i^* are slack variables that allow for a certain amount of error in the optimisation problem, thus helping to alleviate problems that would otherwise be associated with infeasible constraints. The constant term C can be adjusted for a trade-off between how much deviation above ϵ would be tolerated and the flatness of the function $f(x)$. The linear function $f(x)$ is illustrated in Figure 2.9.

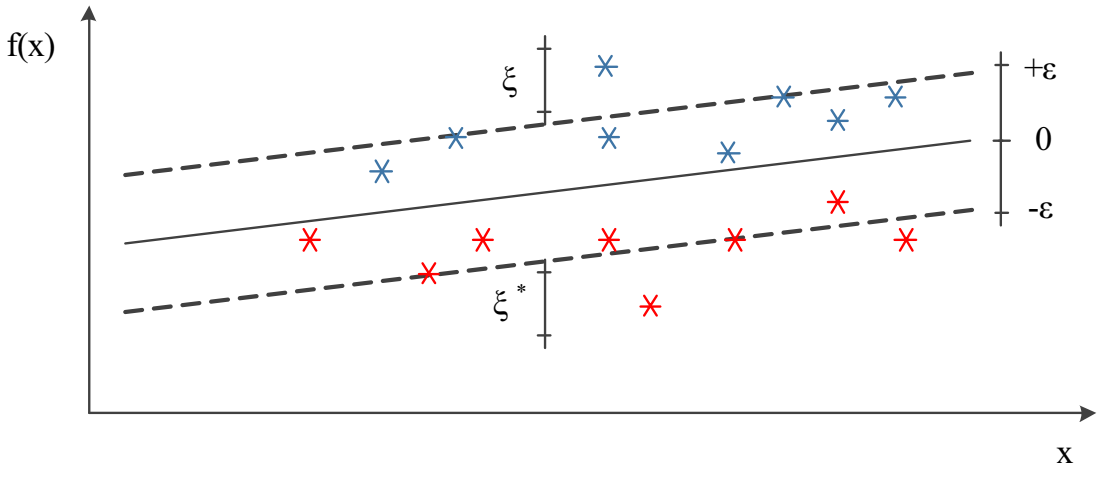

Figure 2.9: Graphical depiction of a generic linear SVM function. Adapted from [96], with permission.

© University of Pretoria

UNIVERSITEIT VAN PRETORIA
UNIVERSITY OF PRETORIA
YUNIBESITHI YA PRETORIA

2.5.1.3 Markov modelling

A number of techniques for modelling channel occupancy, employing MC and HMMs, have been suggested in the literature [85, 86, 87, 88, 89, 90, 91, 92, 93, 97]. If the occupancy status of a channel can be described by a sequence of binary states, then a simple two-state MC may be utilised to model the presence of a PU on that channel. The one state represents an OFF period (no PU present) and the other state represents an ON period (PU present) [92]. It is assumed that there is a statitical relationship between the PU's current occupancy state, its previous state its future state. A simple two-state MC is illustrated in Figure 2.10.

Let the probability of changing from an OFF state to an ON state be denoted by f and the probability of changing from an ON state back to an OFF state be denoted by b then, assuming that the state at time t is denoted by q_t, the state transition matrix P may be defined as follows,

$$\boldsymbol{P} = \begin{pmatrix} 1-f & f \\ b & 1-b \end{pmatrix}. \tag{2.20}$$

In (2.20), f is described by,

$$f = P\left(q_t = ON | q_{t-1} = OFF\right), \tag{2.21}$$

and b is described by,

$$b = P\left(q_t = OFF | q_{t-1} = ON\right), \tag{2.22}$$

Estimates for the values of f and b are obtained by counting the number of transitions between the ON and OFF states that occur during a observation interval. Based on the

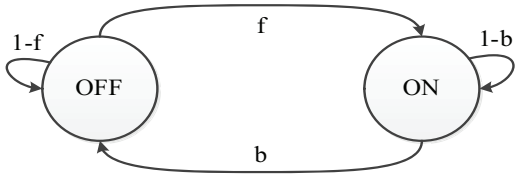

Figure 2.10: A two-state ON-OFF Markov chain. Adapted from [98], with permission (Copyright © 2008, IEEE).

© University of Pretoria

UNIVERSITEIT VAN PRETORIA
UNIVERSITY OF PRETORIA
YUNIBESITHI YA PRETORIA

estimates for f and b, the MC can then be used to predict a sequence of future states $y_m(n+k) = \{y_0, y_1, \ldots, y_{k-1}\}$, where k is the number of future samples predicted.

Since errors occur in the SS process, the MC approach can easily be extended to using a HMM. A HMM was employed in [85]. In this case each PU state also had an error state e associated with it, which represents the probability of predicting a PU state incorrectly.

2.5.2 Linear models

Various linear approaches to PU traffic modelling have been proposed in the literature, due to their relative simplicity. These include methods based on correlation [99, 100], auto and linear regression [101, 102, 103, 99] and least squares [104, 105, 106].

2.5.2.1 Binary time series

Linear regression techniques were employed to predict spectrum opportunities in [101]. A binary time series B_t with a time index t, where the presence of a PU is indicated as $B_t = 1$ and its absence as $B_t = 0$, was used to model PU channel occupancy. The probability of a successful prediction was then expressed as the sigmoid function transformation of the following expression,

$$\mu_t = \sum_{k=1}^{d} \beta_k B_{t-k}, \tag{2.23}$$

with the model parameters given by β. A linear regression was performed on past observations, with $\boldsymbol{S}$ representing the band of interest to a CR, and the probability of success was evaluated by logit transformation, such that,

$$P\left(S_{it} = 1 | S_{t-1}, S_{t-2}, \cdots, S_{t-p}\right) = \frac{1}{1 + e^{-\boldsymbol{M}}}, \tag{2.24}$$

where $\boldsymbol{M}$ is an auto regression function,

$$\boldsymbol{M} = a_0 + \sum_{j=1}^{d} (\boldsymbol{A}_j \boldsymbol{S}_{t-j}) + \boldsymbol{n}, \tag{2.25}$$

with offset a_0, coefficient matrices $\boldsymbol{A}_j$, historical observations $\boldsymbol{S}_{t-j}$ and error vector $\boldsymbol{n}$.

2.5.2.2 Correlation and linear regression

A method based on correlation among spectrum status of channel observations was proposed in [99]. This method begins by calculating the Pearson correlation coefficient ρ of a set of

© University of Pretoria

UNIVERSITEIT VAN PRETORIA
UNIVERSITY OF PRETORIA
YUNIBESITHI YA PRETORIA

historical channel observations, which is given as,

$$\rho_{X,Y} = \frac{cov(X,Z)}{\sigma_X \sigma_Z}. \tag{2.26}$$

Historical observations are denoted by $\boldsymbol{X} = \{x_1, x_2, \ldots, x_p\}$ and the index vector by $\boldsymbol{Z} = \{1, 2, \ldots, p\}$. If this coefficient is found to be above a certain threshold δ_C, then the status of the most recent observation is used as the predicted value. However if the coefficient falls below the threshold, then the majority result of the historical observation window is selected.

A linear regression based prediction scheme is also proposed, in [99], where future points are calculated using linear regression if $\rho > \delta_C$. Assuming that there a linear relationship between historical data $\boldsymbol{X} = \{x_{i1}, x_{i2}, \ldots, x_{ip}\}_{i=1}^{n}$ and the predicted data $\boldsymbol{y} = \{y_1, y_2, \ldots, y_n\}$, such that,

$$\boldsymbol{y} = \boldsymbol{X}\boldsymbol{\beta} + \epsilon. \tag{2.27}$$

where $\boldsymbol{\beta} = \{\beta_1, \beta_2, \ldots, \beta_p\}$ are the regression coefficients and ϵ is an error term.

2.5.2.3 Auto regression

Auto regressive models have been proposed for channel and spectrum hole prediction in CRN [102, 107]. A second order auto regressive model, together with a Kalman filter predictor, was employed in [102]. However, in [107], a particle filter predictor was shown to be more accurate than the Kalman filter used in [102].

A discrete-time random process $X(k)$, can be modelled according to the following expression,

$$X(k) = -\sum_{j=1}^{p} \phi_j x\,(k-j) + \omega_k. \tag{2.28}$$

The order of the process is given by p, ω_k is the observed noise value at the k^{th} instant and ϕ_j represents the parameters of the model. The autocorrelation matrix R_{xx} for $X(k)$ is given as,

$$R_{xx}[k] = \begin{cases} -\sum_{m=1}^{p} \phi_m x\,(k-m) \\ -\sum_{m=1}^{p} \phi_m x\,(-m) \end{cases} \tag{2.29}$$

The parameters $\boldsymbol{\Phi} = [\phi_1, \phi_2, \ldots, \phi_p]$ can be calculated using Yule-Walker equations. For an

© University of Pretoria

UNIVERSITEIT VAN PRETORIA
UNIVERSITY OF PRETORIA
YUNIBESITHI YA PRETORIA

AR-2 model, this may be done as follows,

$$\begin{aligned}\phi_1 &= \frac{\rho_1(1-\rho_2)}{1-\rho_1^2},\\ \phi_2 &= \frac{\rho_2-\rho_1^2}{1-\rho_1^2}\end{aligned} \tag{2.30}$$

where $\rho_1 = \rho_{xx}(L\Delta t)$, $\rho_2 = \rho_{xx}(2L\Delta t)$ and the sampling interval is denoted by L.

2.5.2.4 Normalised least mean square algorithm

In the literature, the normalised least mean square algorithm (NLMS) linear predictor has been proposed for predicting video traffic in real-time multimedia applications [104, 105]. In this paper the application of the NLMS error linear predictor to the prediction of PU traffic is investigated (illustrated in Figure 2.11).

The NLMS method is rooted in adaptive filter theory [108]. Given an input vector $\boldsymbol{X}(n)$ of length p symbols, such that,

$$\boldsymbol{X}(n) = [x(n), x(n-1), \ldots, x(n-p+1)]^T, \tag{2.31}$$

and a set of prediction filter coefficients $\boldsymbol{W}$, given as,

$$\boldsymbol{W} = [w(0), w(1), \ldots, w(p-1)]^T, \tag{2.32}$$

then the output of a k-step, pth-order linear predictor $y_s(n+k)$ may be described by the

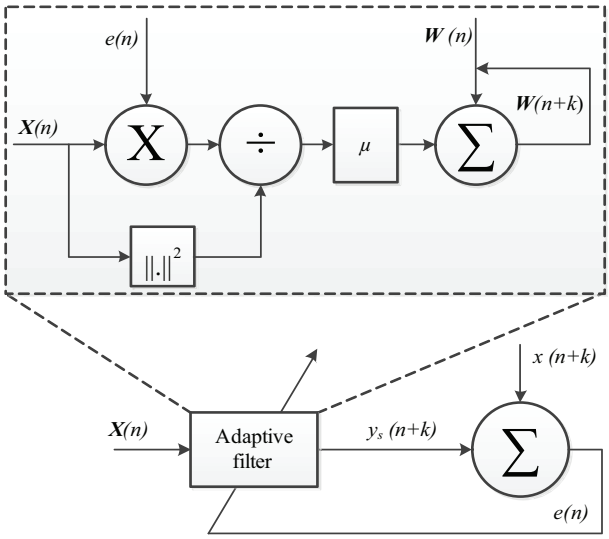

Figure 2.11: The normalised least mean square error linear predictor.

© University of Pretoria

UNIVERSITEIT VAN PRETORIA
UNIVERSITY OF PRETORIA
YUNIBESITHI YA PRETORIA

following expression,

$$y_s(n+k) = \sum_{l=0}^{p-1} w(l)x(n-l). \tag{2.33}$$

The algorithm commences by estimating an initial value for $\boldsymbol{W}(0)$. For each new data point thereafter, $\boldsymbol{W}(n)$ is updated according to the following expression,

$$\boldsymbol{W}(n+1) = \boldsymbol{W}(n) + \frac{\mu e(n)\boldsymbol{X}(n)}{\|\boldsymbol{X}(n)\|^2}, \tag{2.34}$$

where $\|\boldsymbol{X}(n)\|^2 = \boldsymbol{X}(n)^T\boldsymbol{X}(n)$ and μ is a constant known as the step size. Changing μ leads to a trade-off between convergence rate and filter coefficient fluctuation (larger values for μ mean faster convergence but increased filter coefficient fluctuation). The error $e(n)$ is calculated as follows,

$$e(n) = x(n+k) - y_s(n+k), \tag{2.35}$$

where $x(n+k)$ is the actual data sequence and $y_s(n+k)$ is the predicted sequence.

2.5.2.5 Recursive least squares algorithm

To assist proactive network management in wireless networks a traffic prediction method, known as the recursive least squares (RLS) algorithm, has been proposed [106]. This method is also rooted in adaptive filter theory and is a computationally efficient approach to quickly predicting network traffic. No statistical assumptions are needed for the data being observed and near future traffic load is predicted using recent observations. Future traffic load $y\,(n)$ may be estimated as,

$$y\,(n) = w^T\,(n-1)\,u\,(n)\,, \tag{2.36}$$

where $w\,(n)$ is a set of weighting factors and $u\,(n)$ represents a corresponding set of n recent traffic observations. If the true traffic load is denoted $d\,(n)$ then prediction error $e\,(n)$ is given as,

$$e\,(n) = d\,(n) - y\,(n)\,. \tag{2.37}$$

Using an exponential weighting factor λ, this approach attempts to minimise the mean square prediction error by minimising the cost function $J\,(n)$, as follows,

$$\min \quad J\,(n) = \sum_{i=1}^{n} \lambda^{n-i}\,[e\,(i)]^2\,. \tag{2.38}$$

© University of Pretoria

UNIVERSITEIT VAN PRETORIA
UNIVERSITY OF PRETORIA
YUNIBESITHI YA PRETORIA

To obtain the minimum value for Equation (2.38), the weight factor $w(n)$ was calculated using the following expression,

$$w(n) = w(n-1) + K(n)\, e(n), \tag{2.39}$$

where the gain vector $K(n)$ was derived as,

$$K(n) = \frac{\lambda^{-1} P(n-1)\, u(n)}{1 + \lambda^{-1} u^T(n)\, P(n-1)\, u(n)} \tag{2.40}$$

and the cross correlation $P(n)$ between the actual traffic load and the observed signal, is calculated as,

$$P(n) = \sum_{i=1}^{n} u(i)\, d(i). \tag{2.41}$$

2.5.3 Statistical and moving average approaches

Channel occupancy is usually not a random process, since it is driven by human behavioural patterns. Various PU modelling techniques that assume non-random PU activity patterns, that are non-AI based, can be found in the literature [109, 99, 102, 103]. In this subsection a statistical method based on the exponential distribution [110, 79] as well as a simple nearest neighbour approach to prediction [90, 111], are briefly discussed.

2.5.3.1 Alternative exponential approach

The most prominent statistical approach models PU activity, for a set of channels $q = 1, 2 \ldots, \vartheta$, as a Poisson process with arrival rate λ_q. It is assumed that only one PU occupies a channel during time interval t_ψ. The probability that a PU enters this band k times during this interval, is thus given as [110],

$$f(k, \lambda_q) = \frac{{\lambda_q}^k e^{-\lambda_q}}{k!}, \quad q = 1, 2 \ldots, \vartheta. \tag{2.42}$$

Channel occupancy is modelled as an independently exponentially distributed process. The following probability density function is used to describe a PU channel q, with an ON occupancy duration of length $t_{ON}(q)$ and a mean ON duration $1/\lambda_{t_{ON}(q)}$,

$$f(t_{ON}(q), \lambda_q) = \begin{cases} \lambda_q e^{-\lambda_q t_{ON}(q)}, & t_{ON}(q) \geq 0 \\ 0, & t_{ON}(q) < 0. \end{cases} \tag{2.43}$$

© University of Pretoria

UNIVERSITEIT VAN PRETORIA
UNIVERSITY OF PRETORIA
YUNIBESITHI YA PRETORIA

Similarly, the probability density function for a PU channel q with an OFF duration of length $t_{OFF}(q)$ and a mean OFF duration $1/\lambda_{t_{OFF}(q)}$, is given as,

$$f\left(t_{OFF}\left(q\right),\lambda_q\right) = \begin{cases} \lambda_q e^{-\lambda_q t_{OFF}(q)}, & t_{OFF}\left(q\right) \geq 0 \\ 0, & t_{OFF}\left(q\right) < 0. \end{cases} \tag{2.44}$$

2.5.3.2 Nearest neighbours

A simple single-SU predictor, named the 1-nearest neighbour (1-NN), was utilised in [90, 111]. In this approach the current channel status q_t is used to predict future channel status $q_t + x$, as follows,

$$q_t + x = q_t, \tag{2.45}$$

where x is the number of future slots predicted. Channel occupancy status is calculated by comparing the observed signal to a threshold value.

2.5.4 Cooperative prediction

As discussed in Section 2.4, CSS presents a potential solution to the hidden node problem [62]. A natural progression from CSS is to perform PU traffic prediction in a cooperative manner.

This concept was introduced in [111], where both a soft and a hard combining rule were employed to combine the independent predictions of multiple cooperating SUs. The k-out-of-N rule, applied to the prediction of a single future state, was assumed for the hard decision. However, for the soft combining rule, the likelihood probabilities for each predicted state were combined to obtain accumulated probabilities for both the *idle* and *busy* PU states. For the ith cooperating SU, given the likelihood probabilities for an idle state $P_{0,i}$ and for a busy state $P_{1,i}$, this soft combining rule is given as,

$$\sum_{i=1}^{N} \frac{P_{0,i} - P_{1,i}}{P_{0,i} + P_{1,i}} \gtrless_{busy}^{idle} 0. \tag{2.46}$$

The CSS concept was taken further in [112] to incorporate a coalition game theory based approach to CSS. In this case the cooperative miss prediction Ψ_m and cooperative prediction

© University of Pretoria

UNIVERSITEIT VAN PRETORIA
UNIVERSITY OF PRETORIA
YUNIBESITHI YA PRETORIA

false alarm Ψ_f were given as,

$$\Psi_m(S_k^i) = \prod_{j \in S_k^i} [\psi_{mji}(1 - P_{ej\hat{a}}) + (1 - \psi_{mji})P_{ej\hat{a}}], \tag{2.47}$$

$$\Psi_f(S_k^i) = 1 - \prod_{j \in S_k^i} [(1 - \psi_{fji})(1 - P_{ej\hat{a}}) + \psi_{fji}P_{ej\hat{a}}], \tag{2.48}$$

where ψ_{mji} and ψ_{fji} are the local cooperative miss prediction and cooperative prediction false alarm probabilities of each cooperating SU in the set of SUs $j \in S_k^i$, $\hat{a}$ is the coalition leader and $P_{ej\hat{a}}$ is the probability of a transmission error occurring between SU j and $\hat{a}$.

In both cases, a prediction accuracy improvement was found for CSS over individual SS. The concept of CSS will be further investigated in Chapter 5.

2.6 CONCLUSION

This chapter provided an overview of the literature pertaining to spectral efficiency in future wireless networks. Rapid growth in mobile data traffic and its associated spectrum demands has been predicted. To meet this demand spectrum will need to be used in a more efficient manner in the future. Technologies that are envisioned to play a leading role in improving spectrum efficiency were discussed in this chapter, with a strong focus on CR. The concepts of SS, CSS and channel state prediction in CRN were also explored. The remaining chapters in this thesis are derived from the concepts discussed in this chapter.

© University of Pretoria

CHAPTER 3

SPECTRUM OCCUPANCY AND EFFICIENCY: A SOUTH AFRICAN PERSPECTIVE

3.1 INTRODUCTION

As mentioned in Section 2.2.3, various measurement campaigns have been undertaken around the world to characterise the actual usage of currently utilised commercial spectrum [33, 38, 39, 34, 35, 36, 37, 40, 42, 41, 12, 31, 32]. These measurements can help regulators to gain a better perspective on the spectral needs of future wireless networks. In South Africa, a general lack of knowledge about actual spectral utilisation validates the need for such measurement campaigns in the local context. The work presented in this chapter sought to fill this gap by gathering spectrum occupancy information for various commercially relevant bands in the South African context. It also aims to provide motivation for the need to investigate technologies that can make more efficient usage of current spectrum resources and lay the contextual foundation for the chapters that follow in this thesis.

A modular spectrum measurement system, developed as part of the authors previous work [12], was employed to gather information about the actual spectrum occupancy of the television (TV) broadcast and mobile cellular bands. A technique for differentiating between the information and noise bearing components of a measured signal, described as the maximum normal fit (MNF) method, was developed to calculate the spectrum occupancy of these bands. Measurement data was collected from various locations at the University of Pretoria as well as at Pinmill Farm Office Park in Johannesburg. The findings of these measurement campaigns suggest that a number of TV white space (TVWS) opportunities, that could be

© University of Pretoria

UNIVERSITEIT VAN PRETORIA
UNIVERSITY OF PRETORIA
YUNIBESITHI YA PRETORIA

exploited by spectrally efficient future wireless technologies, currently exist in the TV bands (this should increase after the proposed analogue TV switch off in 2015 [113]), but that the mobile cellular bands are currently heavily utilised.

The rest of this chapter is organised as follows: Calculating spectral occupancy using the MNF method is described in Section 3.2, the spectrum measurement system is summarised in Section 3.3 and details pertaining to each measurement campaign are provide in Section 3.4. Spectrum measurement results for the TV broadcast bands are presented in Section 3.5 and for the mobile cellular bands in Section 3.6. The chapter is concluded in Section 3.8. Parts of this chapter were published in [114], [115] and [116].

3.2 CALCULATING SPECTRUM OCCUPANCY

To calculate spectrum occupancy it is necessary to distinguish between the information and noise bearing components of a measured signal. In this section, a method is thus described for calculating the detection threshold λ needed to test the binary hypothesis from Section 2.3.3.2.

3.2.1 Maximum normal fit method

A threshold detection method, known as the recursive one-sided hypothesis test (ROHT), has been proposed in the literature [117]. This method makes the assumption that the probability density function (PDF) of the noise component of a received signal $r(x)$, as given in Equation (2.1), will always follow a Gaussian distribution. In this section, a new approach, called the MNF method, is presented as an evolution of the ROHT method. The MNF method follows a 'best-fit' approach for calculating the noise threshold, as opposed to the 'recursive-removal' approach followed by the ROHT method [117] and also does not require that the PDF of the signal component of Equation (2.1) be specifically defined. For the MNF method, the detection threshold is computed as the point of intersection between fitted estimates for the PDFs of the signal and noise components of the measured signal.

An algorithmic description of the MNF method is provided in Algorithm 1. The MNF method begins by calculating a histogram m_i from the discrete samples of measured power $r(x)$ that are acquired during the spectrum sensing (SS) process. The histogram, where k is the number

© University of Pretoria

Algorithm 1 Maximum normal fit method

$\hat{\sigma} = 10$

$\hat{\alpha} = 10$

Given $r(x)$ ▷ power in dBm

Compute histogram $j = \sum_{i=1}^{k} m_i$ ▷ from $r(x)$ with number of bins k and observations j

$H(x) = \{m_1, m_2, \ldots, m_k\}$

Smooth $H(x)$ ▷ moving average filter with a span of 9

$h(x) = \frac{d}{dx} H(x)$

Solve $h(x) = 0$

$\beta_N = \min(x)$

$\hat{\mu}_N = H(\beta_N)$

$f_{R_N}(x) = \{H(1), H(2), \ldots, H(\beta_N), H(\beta_N - 1), H(\beta_N - 2), \ldots, H(1)\}$

$[f_N(x)] = \text{EstimateDistribution}(\hat{\mu}_N, \hat{\sigma}, \hat{\alpha}, f_{R_N}(x))$

$f_{R_S}(x) = H(x) - f_N(x)$

$\hat{\mu}_S = \max\{f_{R_S}(x)\}$

$[f_S(x)] = \text{EstimateDistribution}(\hat{\mu}_S, \hat{\sigma}, \hat{\alpha}, f_{R_S}(x))$

Solve $f_N(x) - f_S(x) = 0$

$$\lambda = \begin{cases} x, & \hat{\mu}_N \leq x \leq \hat{\mu}_S \\ \max(x), & \text{otherwise} \end{cases}$$

function EstimateDistribution($\hat{\mu}$, $\hat{\sigma}$, $\hat{\alpha}$, $f_R(x)$)

    $\epsilon = 1 \times 10^{-3}$

    $ii = 20 \times 10^3$

    while $\Delta \geq \epsilon$ AND $ii \geq 0$ **do**

        $f(x) = \frac{\hat{\alpha}}{\sqrt{(2\pi\hat{\sigma}^2)}} e^{-\frac{1}{2}\left(\frac{x-\hat{\mu}}{\hat{\sigma}}\right)^2}$

        $\Delta = \frac{1}{2\beta_N - 1} \sum_{x=1}^{2\beta_N - 1} \{f_R(x) - f(x)\}^2$

        $\hat{\sigma} = \hat{\sigma} + \mathcal{U}(0,1) - c_s$

        $\hat{\alpha} = \hat{\alpha} + \mathcal{U}(0,1) - c_a$

        $ii = ii - 1$

    end while

    return $f(x)$

end function

© University of Pretoria

of bins and j is the total number of observations, adheres to the condition that $j = \sum_{i=1}^{k} m_i$. This histogram is essentially a probability mass function (PMF) of $r(x)$ and its continuous time counterpart thus represents its PDF, $f_R(x)$.

In order to calculate a noise detection threshold, the MNF method seeks to identify and separate the portion of the histogram that belongs to the noise component of $r(x)$. To do this the mean of the noise component needs to be identified. A vector $H(x) = \{m_1, m_2, \ldots, m_k\}$ is thus populated, from the PMF of $r(x)$, and smoothed using a moving average filter. The derivative $h(x) = \frac{d}{dx}H(x)$ is then calculated and the roots of $h(x)$ are solved for. The first root, i.e. the root with the smallest value, is then assumed to represent the index $x = \beta_N$ at which the mean $\hat{\mu}_N$ of the noise component occurs. The mean can then be calculated as $\hat{\mu}_N = H(\beta_N)$. This information is used to estimate the PMF of the noise component $f_{R_N}(x)$. The first half of $f_{R_N}(x)$ is obtained by using all the samples of $H(x)$ from the lowest sample up to the sample containing β_N, while the second half is obtained by mirroring the first half as follows,

$$f_{R_N}(x) = \{H(1), H(2), \ldots, H(\beta_N), H(\beta_N - 1), H(\beta_N - 2), \ldots, H(1)\} \tag{3.1}$$

The MNF algorithm then tries to generate a function $f_N(x)$ that closely resembles $f_{R_N}(x)$. If the assumption is made that $f_{R_N}(x)$ follows a Gaussian distribution, since it represents noise, then $f_N(x)$ is generated using an amplitude scaled Gaussian distribution, as described by the following expression,

$$f_N(x) = \frac{\hat{\alpha}}{\sqrt{(2\pi\hat{\sigma}^2)}} e^{-\frac{1}{2}\left(\frac{x-\hat{\mu}_N}{\hat{\sigma}}\right)^2}. \tag{3.2}$$

Initially, random guesses are made for the standard deviation $\hat{\sigma}$ and amplitude scaling factor $\hat{\alpha}$ (chosen within arbitrary selected minimum bounds). At each iteration, the mean squared error (MSE) Δ between $f_N(x)$ and $f_{R_N}(x)$ is calculated as follows,

$$\Delta = \frac{1}{2\beta_N - 1} \sum_{x=1}^{2\beta_N - 1} \{f_{R_N}(x) - f_N(x)\}^2. \tag{3.3}$$

If Δ is not sufficiently small then $\hat{\sigma}$ and $\hat{\alpha}$ are modified according to the following expressions,

$$\hat{\sigma} = \hat{\sigma} + \mathcal{U}(0, 1) - c_s, \tag{3.4}$$

$$\hat{\alpha} = \hat{\alpha} + \mathcal{U}(0, 1) - c_a, \tag{3.5}$$

© University of Pretoria

UNIVERSITEIT VAN PRETORIA
UNIVERSITY OF PRETORIA
YUNIBESITHI YA PRETORIA

where c_s and c_a are constants (e.g. $c_s = c_a = 0.5$) and $\mathcal{U}(0,1)$ represents a uniformly distributed random number between zero and one. This process is continued until the maximum number of iterations is exceeded (denoted by ii in Algorithm 1) or Δ becomes sufficiently small, such that $\Delta < \epsilon$, where ϵ represents an arbitrary small value, e.g. $\epsilon = 10^{-3}$. The convergence time and accuracy of the algorithm are influenced by the values chosen for ϵ, c_s and c_a. At this point, the most recently calculated values for $\hat{\sigma}$ and $\hat{\alpha}$, together with $\hat{\mu}_N$, are taken to be the standard deviation, amplitude scaling factor and mean of the final estimate for the noise distribution curve respectively.

The next step is to isolated the signal component $f_{R_S}(x)$ from $H(x)$ by subtracting the noise distribution estimate $f_N(x)$ from $H(x)$ as follows,

$$f_{R_S}(x) = H(x) - f_N(x). \tag{3.6}$$

A function $f_S(x)$, that can be matched to $f_{R_S}(x)$, is then generated. An estimate for the mean $\hat{\mu}_S$ is obtained by identifying the maximum value of $f_{R_S}(x)$. Therefore, $\hat{\mu}_S = \max\{f_{R_S}(x)\} = f_{R_S}(\beta_S)$, where $x = \beta_S$ is the index at which this point occurs. The same iterative procedure that was followed to obtain $f_N(x)$ is then followed to calculate $f_S(x)$, by substituting $\hat{\mu}_S$ into Equation 3.2 as well as $f_S(x)$, $f_{R_S}(x)$ and β_S into Equation 3.3.

The detection threshold λ can then be computed from the roots of the intersection of $f_N(x)$ and $f_S(x)$ by solving the following expression,

$$f_N(x) - f_S(x) = 0. \tag{3.7}$$

The root that falls between $\hat{\mu}_N$ and $\hat{\mu}_S$ is chosen as the detection threshold, however, if no such solution exists then the largest root is chosen. Therefore,

$$\lambda = \begin{cases} x, & \hat{\mu}_N \leq x \leq \hat{\mu}_S \\ \max(x), & \text{otherwise} \end{cases} \tag{3.8}$$

The MNF method requires that $\hat{\mu}_N \leq \hat{\mu}_S$. If this condition is not met then the MNF method will fail.

3.2.2 Threshold estimation

One approach to practically estimating λ by solving Equation (3.7), is to make the assumption that both the signal and noise component PDFs follow a Gaussian distribution, where the

© University of Pretoria

UNIVERSITEIT VAN PRETORIA
UNIVERSITY OF PRETORIA
YUNIBESITHI YA PRETORIA

noise distribution $f_N = \mathcal{N}(0, \sigma_n^2)$ is assumed to have zero mean and the signal distribution $f_S = \mathcal{N}(\mu_s, \sigma_s^2)$ some non-zero mean μ_s, then the threshold λ_i can be calculated from the following expression (derived in Appendix A),

$$\lambda = \frac{\mu_s \sigma_n^2 \pm \sigma_n \sigma_s \sqrt{2 \ln\left(\frac{\sigma_n}{\sigma_s}\right)(\sigma_n^2 - \sigma_s^2) + \mu_s^2}}{\sigma_n^2 - \sigma_s^2}. \tag{3.9}$$

The correct value for λ is then selected using Equation 3.8.

If $r(n)$ represents the received signal, then the Gaussian assumption for f_S requires that only the signal bearing portion of $r(n)$ be considered when calculating Equation (3.9). The signal distribution f_S is thus calculated as the PDF of $r(n)$ using only its positive elements. In other words, the signal portion $r_s(m)$ is roughly estimated to be,

$$r_s(m) = r(n), \quad r_i(n) \geq 0 \tag{3.10}$$

and the PDF of the signal portion is then estimated by using $r_s(m)$, such that $f_S = f(r_s(m))$. Therefore, the mean of the signal distribution can be calculated as,

$$\mu_s = \frac{1}{M} \sum_{m=1}^{M} r_s(m) \tag{3.11}$$

where $M \leq p$ is the number of positive elements in $r(n)$.

An estimate for the variance of the signal distribution σ_s is obtained by firstly calculating the variance σ_r^2 and power P_r of the received signal $r(n)$. The received power can be calculated as,

$$P_r = \frac{1}{p} \sum_{n=1}^{p} |r_s(n)|^2 \tag{3.12}$$

and the variance as,

$$\sigma_r = \frac{1}{M} \sum_{m=1}^{M} (r(n) - \mu_s)^2 \tag{3.13}$$

An estimate for the signal-to-noise ratio (SNR), denoted as γ, is then used, together with P_r, to obtain an estimate for the variance of the noise σ_n^2, such that,

$$\sigma_n^2 = \frac{P_r}{10^{(0.1\gamma)}} \tag{3.14}$$

The estimate for the variance of the signal component is then calculated as,

$$\sigma_s^2 = \sigma_r^2 - \sigma_n^2 \tag{3.15}$$

© University of Pretoria

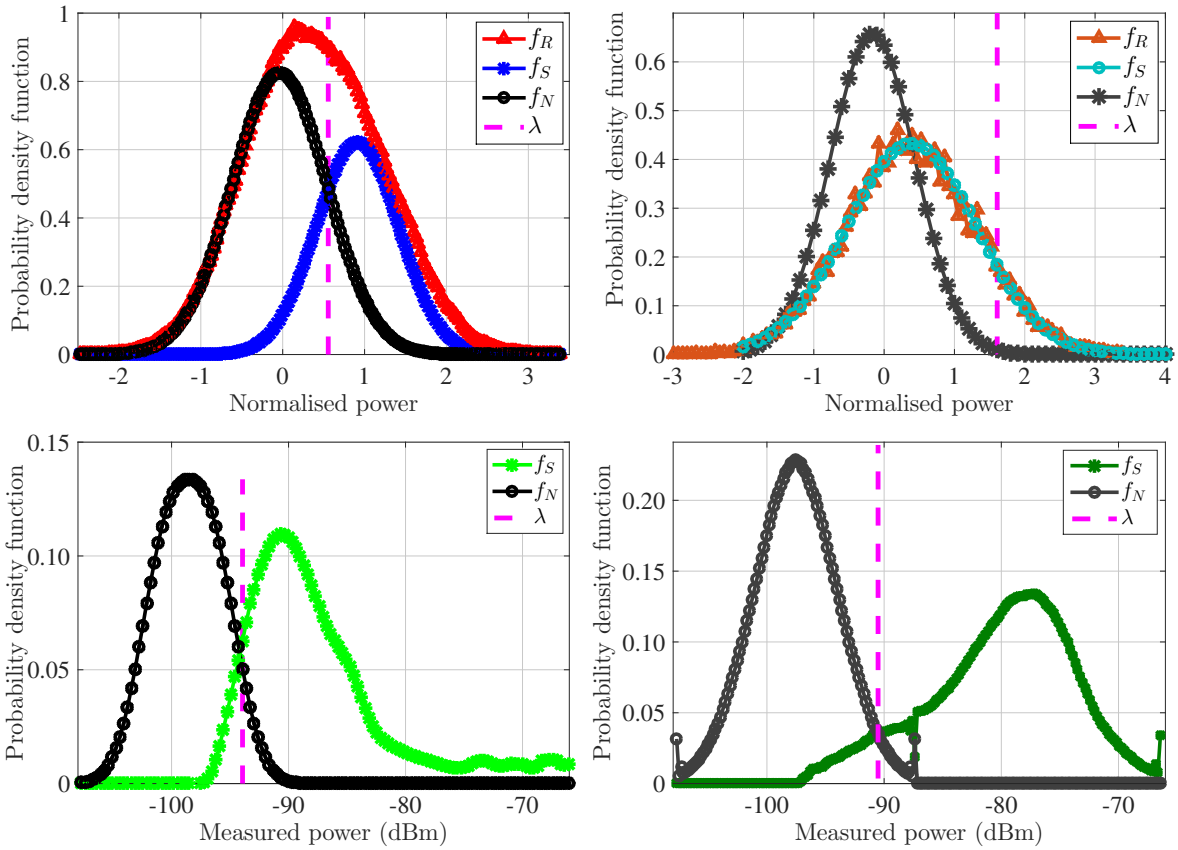

Figure 3.1: PDFs for the MNF (top left) and ROHT (top right) method, applied to a 40% occupied channel for data with a simulated SNR of 3 dB, and of the MNF method applied to real measurements from the TV broadcast (bottom left) and 900 MHz mobile cellular bands (bottom right).

3.2.3 Validation

Simulations were run to compare the accuracy of the MNF and ROHT methods. A vector of noise thresholds was calculated for each method and used to calculate the spectrum occupancy of a channel occupied by a known signal.

The MNF method is illustrated on the top left hand side of Figure 3.1 for a channel, with a SNR of 3 dB, that was simulated to be 40% occupied. Estimates for both the signal (blue line) and noise (black line) distributions were identified. In terms of normalized power, the threshold was calculated to be $\lambda = 0.556$, which resulted in an approximate error of 9.82%. Similarly, a threshold of $\lambda = 1.608$ was then obtained when the ROHT method was applied to the same data set, which lead to an error of approximately 88.64%, illustrated on

© University of Pretoria

UNIVERSITEIT VAN PRETORIA
UNIVERSITY OF PRETORIA
YUNIBESITHI YA PRETORIA

the top right hand side of Figure 3.1. The performance of the MNF and ROHT methods have been compared for other spectrum occupancy scenarios in Table 3.1, where the MNF method was clearly found to be significantly more accurate than the ROHT method for each scenario.

A practical example of the MNF method is provided in the bottom part of Figure 3.1 where the signal and noise distributions for instantaneous samples of the data that was measured in the TV broadcast (bottom left) and 900 MHz mobile cellar bands (bottom right) are illustrated. The PDFs to the left (black line) represent estimates for the noise component of $r(n)$, while the PDFs to the right (green line) represent estimates for the signal component of $r(n)$. The dashed purple lines represent calculated thresholds of $\lambda = -93.93$ dBm and $\lambda = -90.52$ dBm for the TV broadcast and mobile cellular bands respectively.

3.2.4 Occupancy calculation

For each measured band, the MNF method described in Section 3.2.1 was employed to calculate the detection threshold λ. The power of each individual measurement sample was then compared with λ and the number of samples that exceeded it counted and divided by the total number of samples ψ gathered for a particular band k. The percentage occupancy $O(k)$ of that band was then calculated according the following expression,

$$O(k) = 100\frac{\sum_{n=1}^{\psi} \rho(n,k)}{\psi}, \tag{3.16}$$

where,

$$\rho(n,k) = \begin{cases} 1, & r(n,k) > \lambda \\ 0, & r(n,k) \leq \lambda. \end{cases} \tag{3.17}$$

Table 3.1: The percentage error in occupancy when making use of the MNF and ROHT methods at SNR = 3 dB.

Occupancy (%)	20	40	60	80
MNF	11.74	9.82	2.27	1.80
ROHT	65.23	88.64	96.18	99.21

© University of Pretoria

UNIVERSITEIT VAN PRETORIA
UNIVERSITY OF PRETORIA
YUNIBESITHI YA PRETORIA

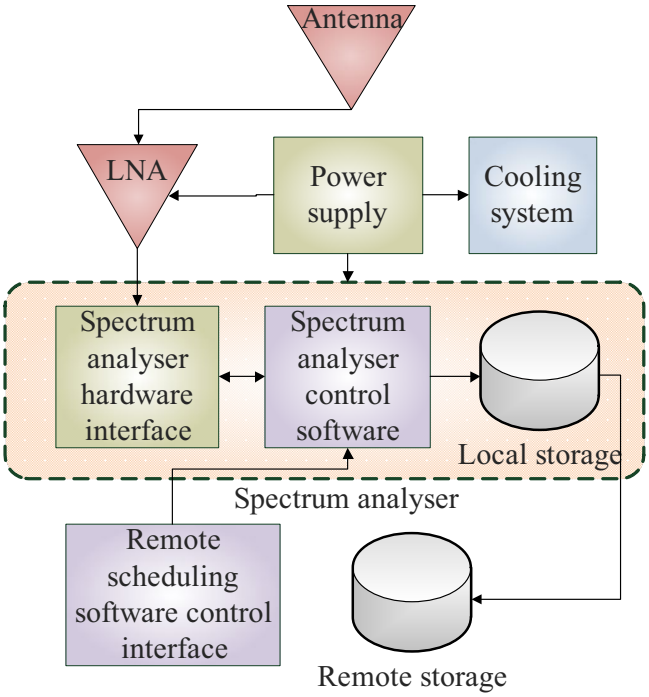

Figure 3.2: Overview of the spectrum measurement system.

3.3 SPECTRUM MEASUREMENT SYSTEM

A summary of the design, and configuration, of the measurement system is provided in this section [12].

3.3.1 Measurement setup

A block diagram of the measurement system is provided in Figure 3.2. The system was setup as follows: the output signal of a wideband antenna was fed into a low noise amplifier (LNA), which was in turn fed into the radio frequency front end of an Agilent EXA N9010A spectrum analyser. The spectrum analyser was controlled by a software application that received scheduling instructions from another software application that remotely controlled where and when measurements should be taken. Once measurements had been taken they were initially stored on a hard drive that formed part of the spectrum analyser. Since this local storage device had limited storage capacity, measured data was periodically moved to an external storage location. The spectrum analyser and LNA were housed in a metal weather resistant and air-conditioned cabinet at the physical measurement location.

© University of Pretoria

3.3.2 System calibration and sensitivity

An Agilent E5071C ENA series network analyser was employed to calibrated the radio frequency front end of the measurement system, while the wideband antenna was calibrated at the compact antenna test range of the University of Pretoria. The link budget for the measurement system, including the calibrated gains for the antenna G_a, the coaxial cables (LMR 600, G_{cl}, and Sucoflex 100, G_{cs}) and the LNA G_{lna}, is illustrated in Figure 3.3 [12, 114]. The calibrated gain of the system G_{tot}, illustrated by the solid black line in Figure 3.3, was calculated as follows,

$$G_{tot} = G_a + G_{cl} + G_{cs} + G_{lna}. \tag{3.18}$$

3.4 MEASUREMENT CAMPAIGNS

Various measurement campaigns were conducted to gather information about actual band usage. Descriptions of how these campaigns were conducted are provided in this section.

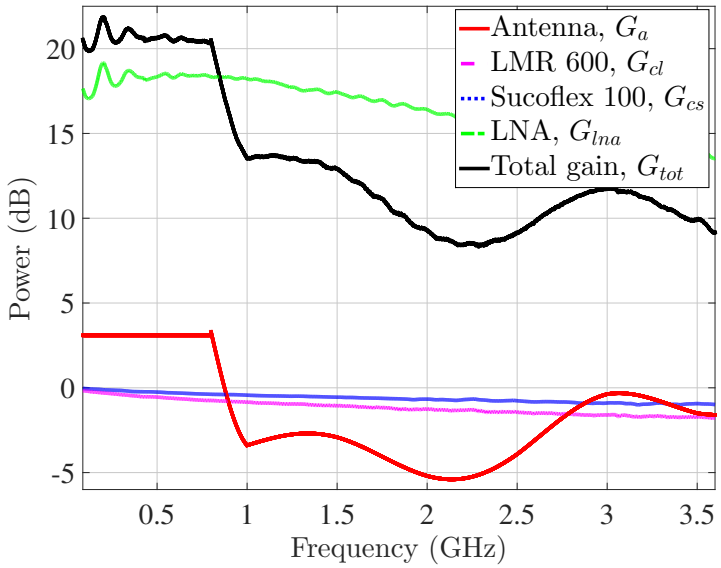

Figure 3.3: Link budget of hardware setup, modified from [12].

© University of Pretoria

UNIVERSITEIT VAN PRETORIA
UNIVERSITY OF PRETORIA
YUNIBESITHI YA PRETORIA

3.4.1 Measurement description

The measurement system, described in Section 3.3 [12], was used to measure the power spectrum of the broadcast TV bands and the bands used for mobile communication. Data was collected from the very-high frequency (VHF) (174 – 254 MHz) and ultra-high frequency (UHF) (470 – 854 MHz) bands, as well as from the downlink portion of the bands used for mobile communications, namely the mobile 900 MHz (M900) (880 – 960 MHz), mobile 1800 MHz (M1800) (1710 – 1880 MHz) and mobile 2100 MHz (M2100) (1900 – 2170 MHz) bands. For each band, a frequency resolution was chosen that would be fine enough to ensure that channel occupancy would be accurately detected. The bands measured are listed in Table 3.2, together with both the frequency and time resolutions employed for each band as well as the location at which the measurements were taken (as discussed in Section 3.4.3).

3.4.2 Measurement schedules

The time, regularity and duration of measurements were controlled by a remotely operated scheduling application. Measurements were taken over a period that consisted of either 500

Description	Band (MHz)	Frequency resolution (kHz)	Time resolution (ms)
University of Pretoria			
VHF	174 - 254	500	32
UHF	470 - 854	500	96
M900	920 - 960	100	50
M1800	1805 - 1880	100	100
M2100	2110 - 2170	100	50
Pinmill Farm			
M900	920 - 960	100	50
M1800	1805 - 1880	100	100

Table 3.2: Band descriptions for the two main measurement locations indicating spectral range as well as both frequency and time resolution.

© University of Pretoria

(TV broadcast bands) or 1500 (mobile bands) consecutive samples spaced according the time resolutions listed in column four of Table 3.2 (where each sample is a sweep of the entire band being measured). The sampling times were proportional to the resolution and size of the bands measured and were limited by the hardware processing time of the measurement system. Measurements were repeated every minute over a period of an hour for the TV broadcast bands (since little change could be observed over a longer period of time). However, measurements for the mobile cellular bands were repeated every seven minutes over a period of four weeks. This made it possible to compare traffic trends, for the mobile bands, for different times of day and days of the week. For all of the bands, measurements were evenly spaced so as to ensure that the measurement system did not fall behind schedule and also to give the file-backup application time to move the result-files to remote storage.

3.4.3 Measurement sites

Measurement data was collected from two different geographical locations in South Africa: the Hatfield campus of the University of Pretoria (site UP) and Pinmill Farm Office Park in Sandton, Johannesburg (site PF).

3.4.3.1 University of Pretoria measurement sites

As indicated in Table 3.2, measurements were taken for all of the bands at the University of Pretoria. However, measurements for each band were taken at different measurement sites. Photographs of the measurement sites are shown in Figure 3.4 and a map of these locations provided in Figure 3.5. Measurements for the TV broadcast bands were collected from all of the sites at the University of Pretoria so as to illustrate the hidden node problem by observing diversity in the results obtained. However, all of the results obtained for the M900 and M1800 bands were collected at location A and for the M2100 band at location C.

The measurement site locations were chosen to be fairly close together, with the furthest distance between any location being approximately 380 m between locations C and E. The reason for this was to demonstrate the effect of shadowing and the hidden node problem associated with SS in CR networks. Location A (GPS co-ordinates: $S25^\circ\ 45'\ 11''\ E28^\circ\ 13'\ 42''$) was situated on the roof of the Engineering 1 building (12 stories above ground level). Location B was situated at ground level with possible shadowing due to the surrounding

© University of Pretoria

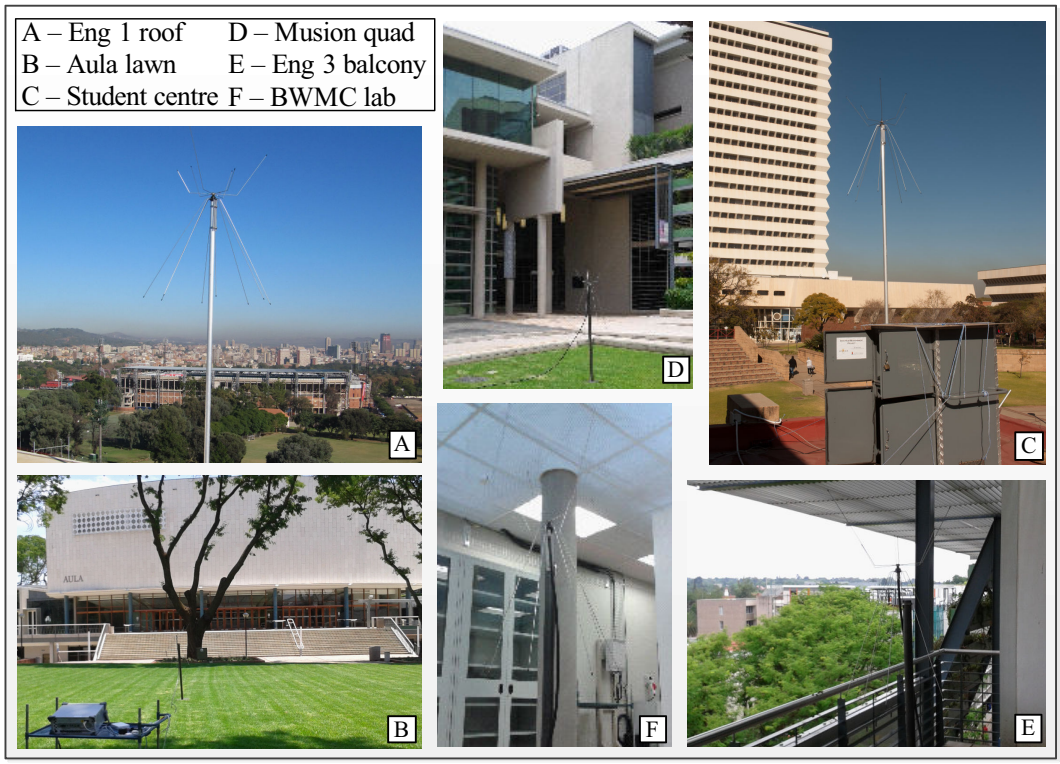

Figure 3.4: Photographs of the receiver locations at the Hatfield campus of the University of Pretoria.

structures. Location C was situated one floor above ground level on the roof of the student centre, also with possible shadowing. Location D was situated at ground level in a

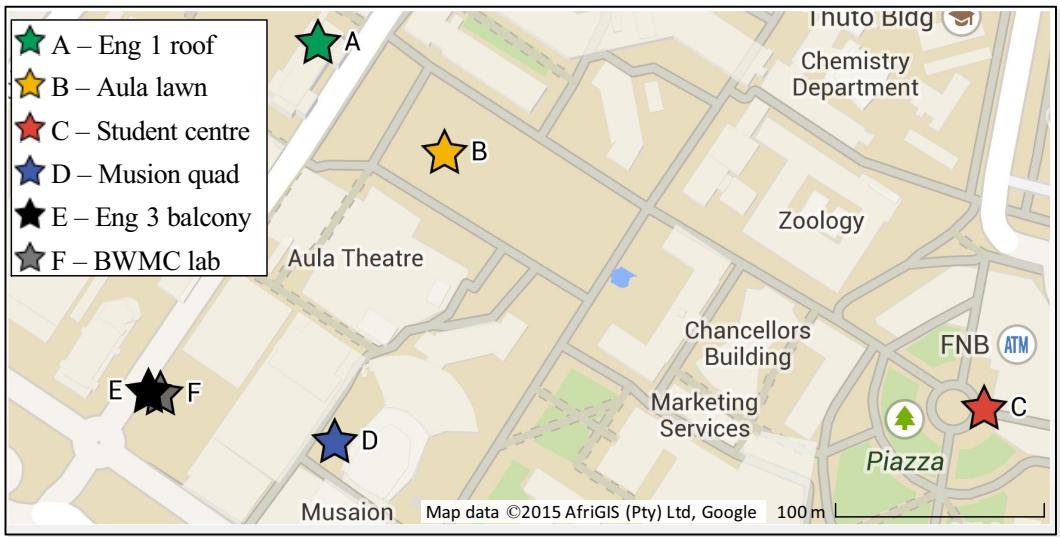

Figure 3.5: Receiver location map of the University of Pretoria's Hatfield campus [118].

© University of Pretoria

UNIVERSITEIT VAN PRETORIA
UNIVERSITY OF PRETORIA
YUNIBESITHI YA PRETORIA

heavily shadowed quadrangle between the Engineering 3 building, the Musaion and the Amphitheatre. Locations E and F were both situated on the 7th floor (this is the top floor) of the Engineering 3 building, with location E on the outer western balcony overlooking the central business district of the city and location F in a laboratory 20 m away. Location F was an indoor measurement site, while all of the others locations were situated outdoors.

3.4.3.2 Pinmill farm office park

To introduce some diversity into the results obtained for the M900 and M1800 bands, measurements were also carried out for these bands at site PF (GPS co-ordinates: $S26^\circ\ 6'\ 2''\ E28^\circ\ 4'\ 26''$). Photographs of the measurement site are provided in Figure 3.6 [119].

Figure 3.6: Photograph and location of the measurement system at Pinmill Farm office park in Sandton, Johannesburg [119, 120].

© University of Pretoria

3.5 SPECTRAL OPPORTUNITIES IN THE TELEVISION BROADCAST BANDS

In light of the impending switch over from analogue to digital television in South Africa [113], measurements were taken from the VHF and UHF bands to gain greater insight into their actual utilisation. Measurement results were compiled by averaging measurements taken over the course of the campaign (data was collected in June 2013 for location C and in December 2014 for rest of the locations at the University of Pretoria). Using these results practical challenges faced by CR networks, due to inaccurate SS, are illustrated in this section. A comparison is also made between the measured results and a locally available geo-location spectrum database (GLSDB) [30].

3.5.1 Transmitter locations

The power measured for the TV broadcast bands can be attributed to five separate TV broadcast sites located within the Tshwane metropolitan area (city of Pretoria). However some measurement sites were able to detect signals from two broadcast sites situated much further away. A map showing the locations of the Tshwane broadcast sites, in relation to site UP, is provided in Figure 3.7. Since different ERPs are used for each technology, a distinction has been made between the broadcast sites for analogue television (AT), digital terrestrial television (DTT) and digital mobile television (DMT). The broadcast sites are

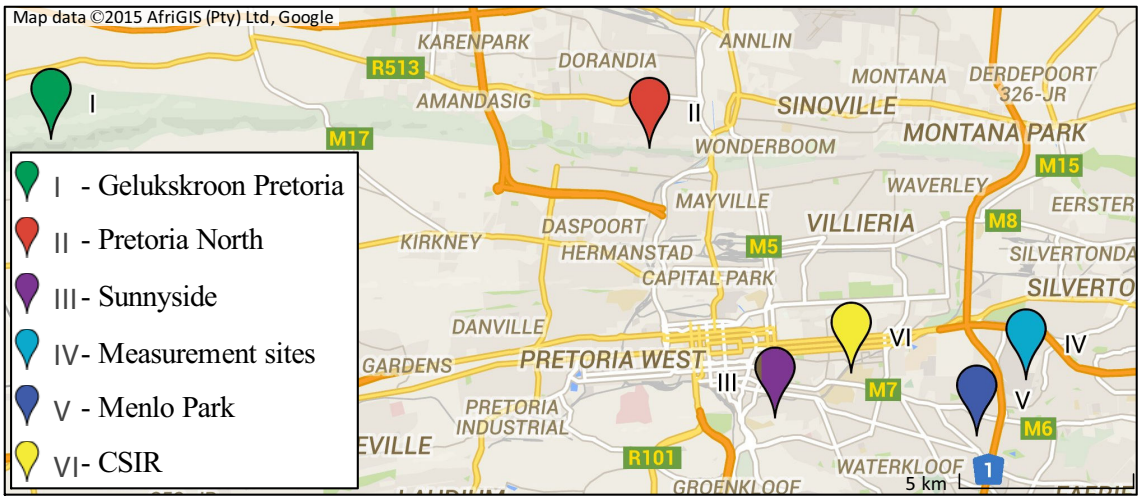

Figure 3.7: TV broadcast transmitter locations for the City of Tshwane [121].

© University of Pretoria

UNIVERSITEIT VAN PRETORIA
UNIVERSITY OF PRETORIA
YUNIBESITHI YA PRETORIA

Table 3.3: Broadcast locations and associated ERPs (kW).

Site	Lat.	Long.	AT	DTT	DMT
GPT	$S25.6892$	$E27.9839$	100.000	70.00	100.00
PN	$S25.6914$	$E28.1672$	0.125	0.02	2.50
SD	$S25.7661$	$E28.2058$	1.000	1.00	2.50
MP	$S25.7712$	$E28.2686$	0.040	0.04	0.25
CSIR	$S25.7554$	$E28.2829$	-	-	13.00

listed in Table 3.3 together with the associated effective radiated power (ERP) broadcast for each technology (all powers are in kW) [122]. The Tshwane broadcast sites are: Gelukskroon Pretoria (GPT), Pretoria North (PN), Sunnyside (SD), Menlo Park (MP) and the council for scientific and industrial research (CSIR). The other two sites, with ERPs in excess of 100 kW, are the Sentech tower (ST) in Johannesburg (approximately 54 km away from the UP) and the Welverdiend tower (WDT) situated near Carletonville (approximately 125 km away). With the exception of the CSIR, which is only used for DMT broadcasts, all sites are currently used for AT, DTT and DMT broadcasting.

3.5.2 Typical channel profiles for analogue and digital television

While AT and DTT signals for a single channel both cover 8 MHz of spectrum, they make use of this spectrum in different ways. The DTT signal is more spectrally efficient since a number of TV channels can be broadcast at the same time on that spectrum, while only one channel can be broadcast on the AT at any given time. To illustrate a typical AT signal, the power spectral density (PSD) of e.tv (channel 38) is shown in the left hand side of Figure 3.8. The luminance carrier, chrominance carrier, near instantaneous companded audio multiplex (NICAM) carrier and audio carrier are clearly visible. The vestigial side band to the left of the luminance carrier is also evident. The right hand side of Figure 3.8 shows the measured PSD of channel 35. This is a DTT transmission for DStv mobile. The format is digital video broadcasting–handheld (DVB-H) and is thus expected to have a flat power spectrum, the lack of which suggests that the signal may have experienced frequency selective fading.

© University of Pretoria

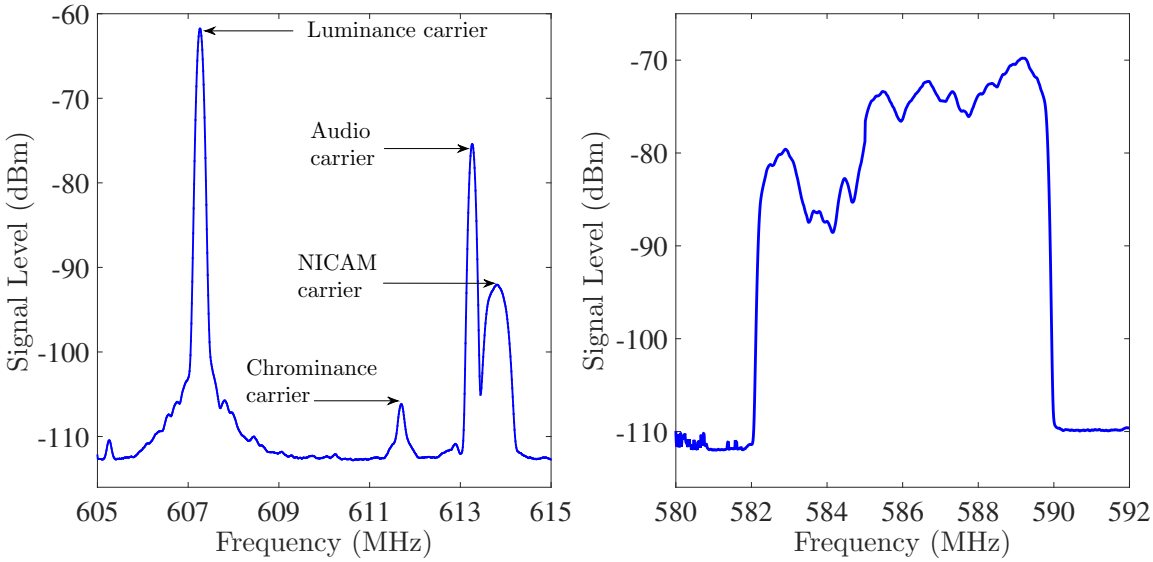

Figure 3.8: PSDs of a typical AT (left) and DTT (right) transmissions.

3.5.3 Very-high frequency band results

For each measurement location, plots of the measured PSD for the VHF band (channels 4-13) are provided in Figure 3.9. The University of Pretoria measurement location site, as shown in Figure 3.5, is indicated as a legend at the top right hand corner of each sub-plot, while the value of λ used to calculate CO is illustrated by a horizontal dashed line. From Figure 3.9 it can be seen that only three channels in the VHF bands (channels 4, 8, 11) are clearly distinguishable. However, weak signals from some other channels are evident at some of the locations. A very weak signal was detected at location A at 239.25 MHz. Since no assignment has been made for that channel, it is assumed to either be noise or an illegal transmission.

3.5.4 Ultra-high frequency band results

Similar to the VHF band, plots of the measured PSD for the UHF band (channels 21-68) are provided in Figure 3.10. Of particular interest were four anomalous signals that were not AT transmissions. Three of these signals occurred in channels 35, 54 and 58 and occupied the same amount of spectrum as a standard TV channel (8 MHz). These signals represent DMT and DTT transmissions. Channel 35 is being used for a DMT transmission that uses the DVB-H format and channels 54 and 58 have DTT trials running on them using the digital

© University of Pretoria

UNIVERSITEIT VAN PRETORIA
UNIVERSITY OF PRETORIA
YUNIBESITHI YA PRETORIA

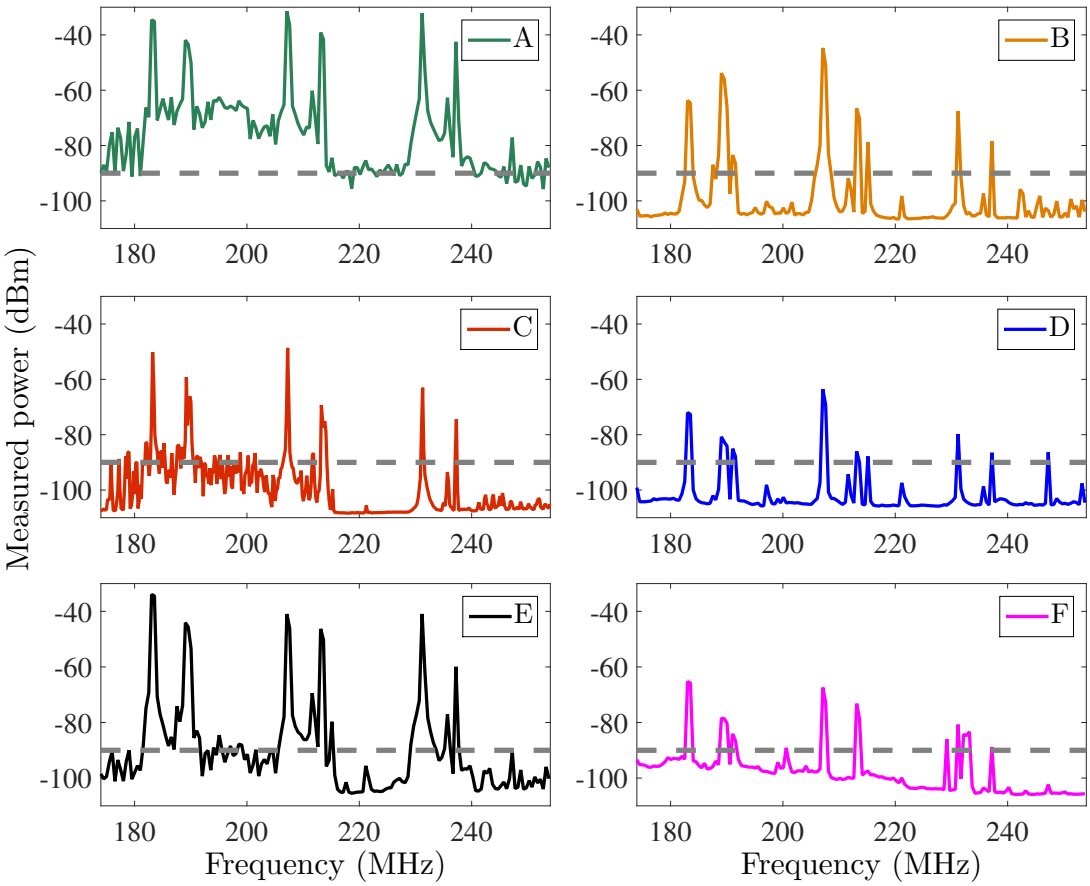

Figure 3.9: Measured power spectral density of the VHF bands.

video broadcasting second generation (DVB-T2) format. There is a signal present at 851.25 MHz (1 MHz bandwidth) that does not seem to correspond to either DVB-T2 or AT. This signal is very strong at locations C and A, while weaker versions were detected at all of the other measurement sites. It is assumed that this signal is either a studio transmitter link for the campus radio station or an illegal transmission. Another such signal was detected at location A at 835.25 MHz.

3.5.5 Spectral occupancy and availability

For the TV broadcast bands, two approaches to selecting the detection threshold λ were considered. In the first approach, the threshold was calculated from the minimum usable field strength used to calculate TV broadcast coverage, as suggested by ICASA [122]. The thresholds were thus used as -90 dBm (55 dBμV/m) and -80 dBm (65 dBμV/m) for the VHF and UHF bands respectively. These values are summarised in Table 3.4. The second

© University of Pretoria

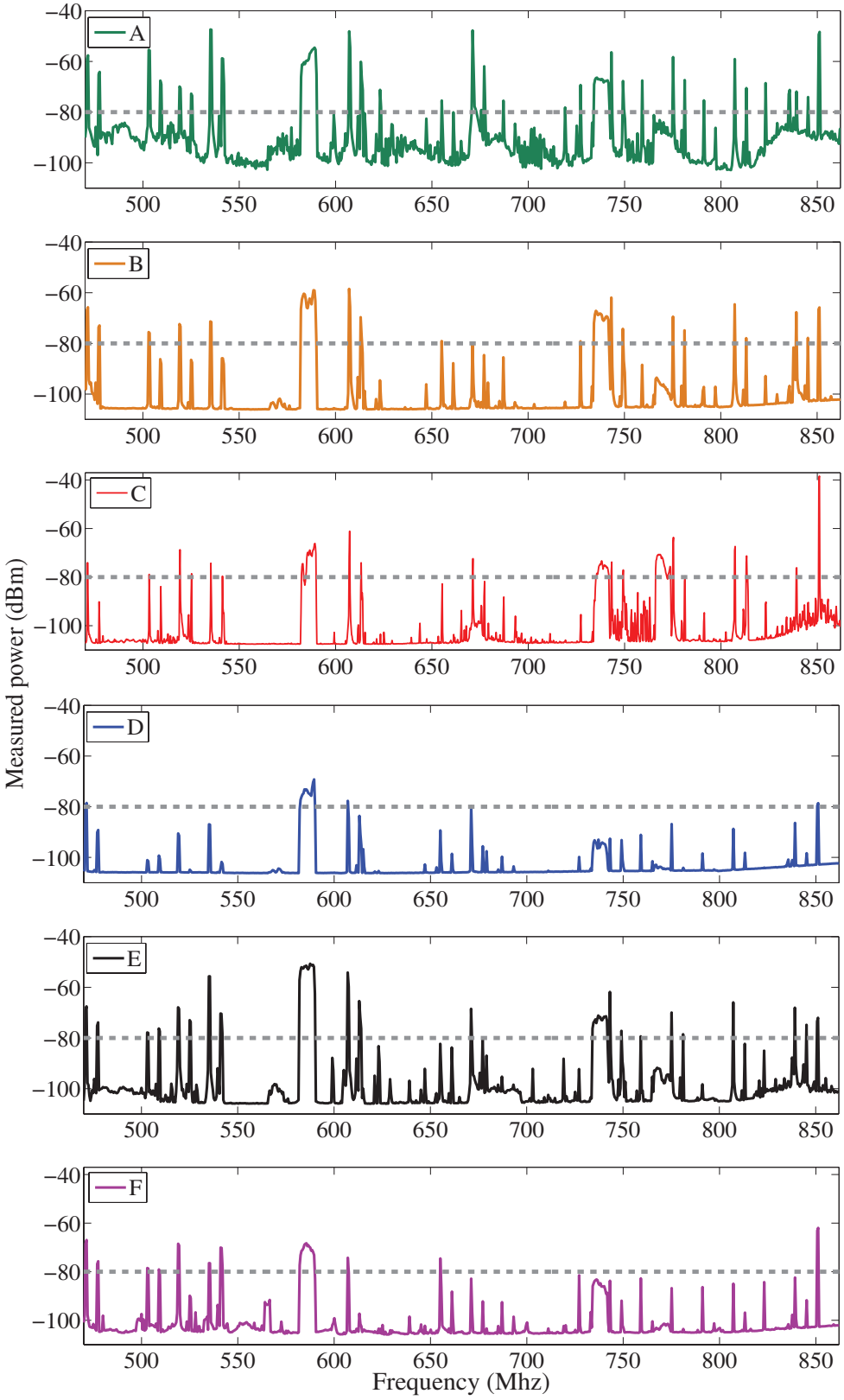

Figure 3.10: Measured power spectral density of the UHF bands at site UP.

© University of Pretoria

UNIVERSITEIT VAN PRETORIA
UNIVERSITY OF PRETORIA
YUNIBESITHI YA PRETORIA

Table 3.4: Minimum usable field strength for TV broadcast coverage [122].

Band	Frequency (MHz)	Channel	Strength (dBμV/m)	Power (dBm)
VHF (Band III)	174-254	4-11,13	55	-90
UHF (Band IV)	470-854	21-68	65	-80

approach was based on the MNF method, as described in Section 3.2.

The first approach was followed for calculating channel occupancy (CO) and the second approach for calculating spectral occupancy (SO). The difference between CO and SO is explained via the following definitions:

- ***Channel occupancy***: If the luminance carrier of a TV channel is measured to be above the threshold, then that TV channel is occupied (8 MHz of spectrum). The channel occupancy of the band is calculated as a percentage of the total number of TV channels allocated to the band.
- ***Spectral occupancy***: If any measured signal component is found to be above the chosen threshold, then that component is considered to be occupied spectrum. Any components that fall below this threshold constitute un-occupied spectrum.

Once occupancy has been calculated, the spectral availability (SA) of the bands can also be calculated. SA is defined as the amount of spectrum that is deemed to be unused and thus potentially available for unlicensed usage.

Calculated values for CO, SO and SA are listed in Table 3.5 for each measurement location. It is evident that SA, due to SS, varied according to location specific differences in SS accuracy. For example, at location D, CO was calculated to be 60% (SA of 32 MHz) and 10.42% (SA of 344 MHz), but at location A, this was 90% (SA of 8 MHz) and 45.83% (SA of 208 MHz) for the VHF and UHF bands respectively.

However, according to actual TV channel assignments for the region, CO should be 30% (SA of 56 MHz) and 48.98% (SA of 200 MHz) and according to the CSIR GLSDB, a minimum of 100% (SA of 0 MHz) and 75.51% (SA of 96 MHz) respectively.

© University of Pretoria

UNIVERSITEIT VAN PRETORIA
UNIVERSITY OF PRETORIA
YUNIBESITHI YA PRETORIA

Table 3.5: Measured spectral opportunities for the TV broadcast bands.

Band	CO (%)	CO SA (MHz)	SO (%)	SO SA (MHz)
Location A				
VHF	90.00	8.00	46.25	43.00
UHF	45.83	208.00	37.56	239.77
Location B				
VHF	40.00	48.00	23.13	61.50
UHF	29.17	272.00	15.98	322.64
Location C				
VHF	30.00	56.00	45.25	43.80
UHF	29.17	272.00	17.93	315.15
Location D				
VHF	60.00	32.00	16.88	66.50
UHF	10.42	344.00	9.88	346.06
Location E				
VHF	50.00	40.00	25.00	60.00
UHF	29.17	272.00	13.90	330.62
Location F				
VHF	40.00	48.00	25.63	59.50
UHF	16.67	320.00	13.29	332.97

For the same locations SO was calculated to be 16.88% (SA of 66.5 MHz) and 9.88% (SA of 346.06 MHz) at location D, and 46.25% (SA of 43 MHz) and 37.56% (SA of 239.77 MHz) at location A, for the VHF and UHF bands respectively. The difference between CO and SO can largely be attributed to inefficient use of spectrum by AT channels.

3.5.6 Spectrum sensing accuracy

Illustrated in Figure 3.11, a channel availability comparison has been made, for each measurement location at the University of Pretoria, between (a) the measured CO, (b) the actual TV channel assignment for the Tswhane metropolitan area (listed together with each broadcast

© University of Pretoria

UNIVERSITEIT VAN PRETORIA
UNIVERSITY OF PRETORIA
YUNIBESITHI YA PRETORIA

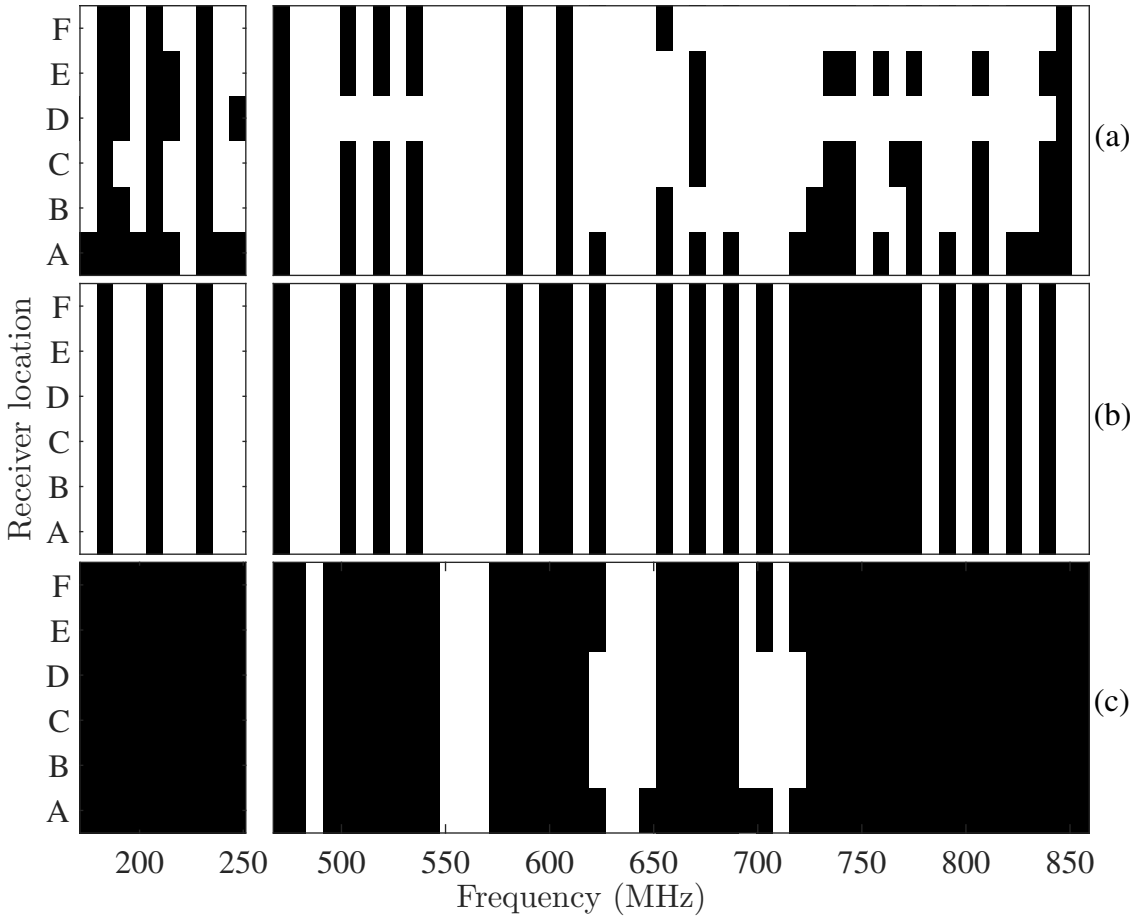

Figure 3.11: Comparison between TVWS opportunities for (a) measured CO, (b) actual TV channel assignment [122] and (c) the CSIR TVWS GLSDB [30].

site in Appendix B [122]) and (c) the CSIR TV white space GLSDB, based on the ITU-R P.1546-4 (B) propagation model [30].

The effect of the hidden node problem is clearly evident when comparing parts (a), (b) and (c) of Figure 3.11. SS accuracy fluctuated across the measurement locations and failed to detect the presence of a TV signal on a number of channels. Since the transmissions in the VHF band were very strong, SS was accurate at all locations (even weak signals from the ST and WDT transmitters were detected on some channels). However, this was not always the case for the UHF band. The SS error ϵ for both bands, as calculated against part (b) and part (c) of Figure 3.11, is summarised as a percentage in Table 3.6 (detected signals originating from the ST and WDT were not counted as errors).

For the UHF band, the highest degree of SS error was observed at location D ($\epsilon = 40.82\%$.),

© University of Pretoria

UNIVERSITEIT VAN PRETORIA
UNIVERSITY OF PRETORIA
YUNIBESITHI YA PRETORIA

Table 3.6: Percentage channel detection error ϵ for each measurement location at the University of Pretoria, due to SS, compared with TV band allocations and the CSIR GLSDB.

Band	A	B	C	D	E	F
TV stations						
VHF	0.00	0.00	0.00	0.00	0.00	0.00
UHF	8.16	22.45	22.45	40.82	22.45	34.69
CSIR GLSDB						
VHF	10.00	60.00	70.00	40.00	50.00	60.00
UHF	40.82	46.94	46.94	65.31	53.06	65.31

while the lowest SS error was observed at location A ($\epsilon = 8.16\%$). The CSIR GLSDB seems to be a more conservative approach and appeared to include transmissions from further afield, e.g. the ST. For the VHF band at location C, the difference in CO between SS and the GLSDB was as much as 70%. Under certain scenarios this should mean better protection for the primary user, however, technologies that rely on short range communication may benefit from a less conservative approach.

3.6 CHARACTERISATION OF SPECTRAL ACTIVITY IN THE MOBILE CELLULAR BANDS

Measurement results for the mobile cellular bands are presented and discussed in this section. Data was collected for the M900 and M1800 bands, at the University of Pretoria, during March and April 2012 and at Pinmill Farm during October and November 2012. Data was collected at the University of Pretoria for the M2100 band during May and June 2013.

3.6.1 Mobile 900 MHz bands

A plot of the average power measured across the M900 band, at site UP, is presented in part (a) of Figure 3.12. The corresponding heat map over a 24 hour period is provided in part (b) of the figure. It is immediately evident that there appears to be a significant amount of activity in these bands.

© University of Pretoria

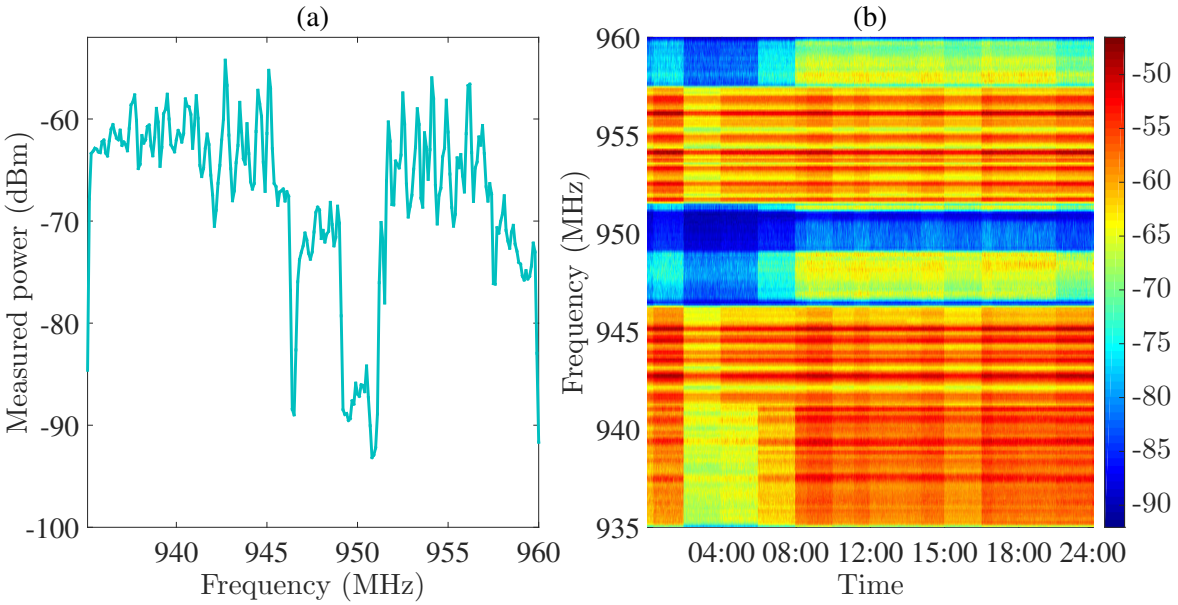

Figure 3.12: (a) Average measured power and (b) heat map over the course of an average day for the down-link of the M900 band at site UP.

3.6.1.1 Hourly occupancy

Two sub-plots comparing the measured average occupancy of the M900 band for site UP and site PF, over the course of a 24 hour period are provided in Figure 3.13. Both of the sub-plots exhibit similar trends with regard to how occupancy changes over the course of the day, e.g., low occupancy during average sleeping hours and high occupancy during business hours (this trend confirms the assumptions made in the previous sub-section). However, as suggested earlier, there is a notable difference between the two locations when comparing the utilisation of the measured bands. According to the measurements, site UP had an average occupancy of approximately 32% more than site PF. Also, the difference between the calculated occupancy at 04:00 (time of lowest occupancy) when compared with 16:00 (time of maximum occupancy), was found to be much larger at site PF (from 70.5% to 44.5% = 26%) than at site UP (from 94.8% to 84.4% = 10.4%).

3.6.1.2 Daily occupancy

The difference between the occupancy of the measurement sites is further described in Table 3.7, where the average occupancy over a seven day period for site UP, site PF and the difference between them, is tabulated. While there appears to be no significant difference

© University of Pretoria

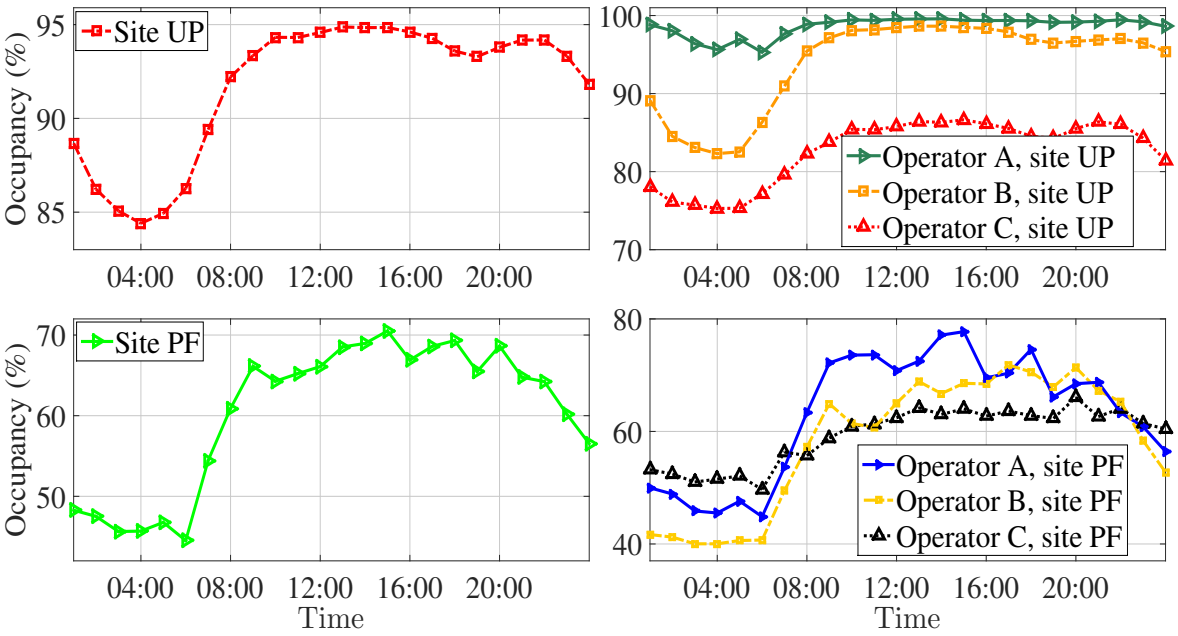

Figure 3.13: Average measured power of the down-link of the M900 band at site UP and site PF.

between occupancy over the days of the week (at most a 3% deviation from the average daily occupancy), the large difference in occupancy between the two sites is again evident (on average, approximately 92% for site UP and 60% for site PF).

Table 3.7: Daily occupancy comparison of an average week for the G900 band.

Day	Site UP (%)	Site PF (%)	Difference
Mon	91.67	60.72	30.95
Tue	91.96	57.41	34.45
Wed	91.80	58.92	32.88
Thu	93.23	62.09	31.04
Fri	92.25	63.32	28.93
Sat	91.78	63.16	28.62
Sun	90.77	56.82	33.95
Average	91.89	60.35	31.55

© University of Pretoria

UNIVERSITEIT VAN PRETORIA
UNIVERSITY OF PRETORIA
YUNIBESITHI YA PRETORIA

Table 3.8: Occupancy comparison between the different mobile operators for G900 band.

Operator	Site UP (%)	Site PF (%)	Difference (%)
A	98.61	63.22	35.39
B	93.92	58.50	35.42
C	82.64	59.29	23.35

3.6.1.3 Comparison amongst mobile operators

While differences exist between the measured occupancy of the two locations, there are also differences in occupancy between the bands allocated to the mobile operators listed in Table 3.2. This can clearly be seen in Figure 3.13, where the average occupancy for each operator is compared over a 24 hour period. At both measurement sites operator A was found to have the most traffic, followed closely by operator B and then by operator C. However, the relative occupancy of operator C to operator A at site UP (approximately 16.2% lower) was greater than at site PF (approximately 6.2% lower). The average occupancies of the different mobile operators for both measurement locations are listed in Table 3.8. A difference in occupancy of around 35% was found between site UP and site PF for both operator A and operator B, however, the difference for operator C was only around 23%. These trends may be indicative of the number of subscribers that each operator has around the measurement sites in question. It is also clear that there is a high user density at measurement site UP.

3.6.2 Mobile 1800 MHz bands

A plot of the average power measured across the M1800 band, at site UP, is presented in part (a) of Figure 3.14. The corresponding heat map over a 24 hour period is provided in part (b) of the figure. Clearly, there is less activity in the M1800 band than in the M900 band. However, looking at part (b), it appears that the first and last 10 MHz of the M1800 band are completely unoccupied, which accounts for the lower average occupancy calculated for the band in Section 3.6.2.1.

© University of Pretoria

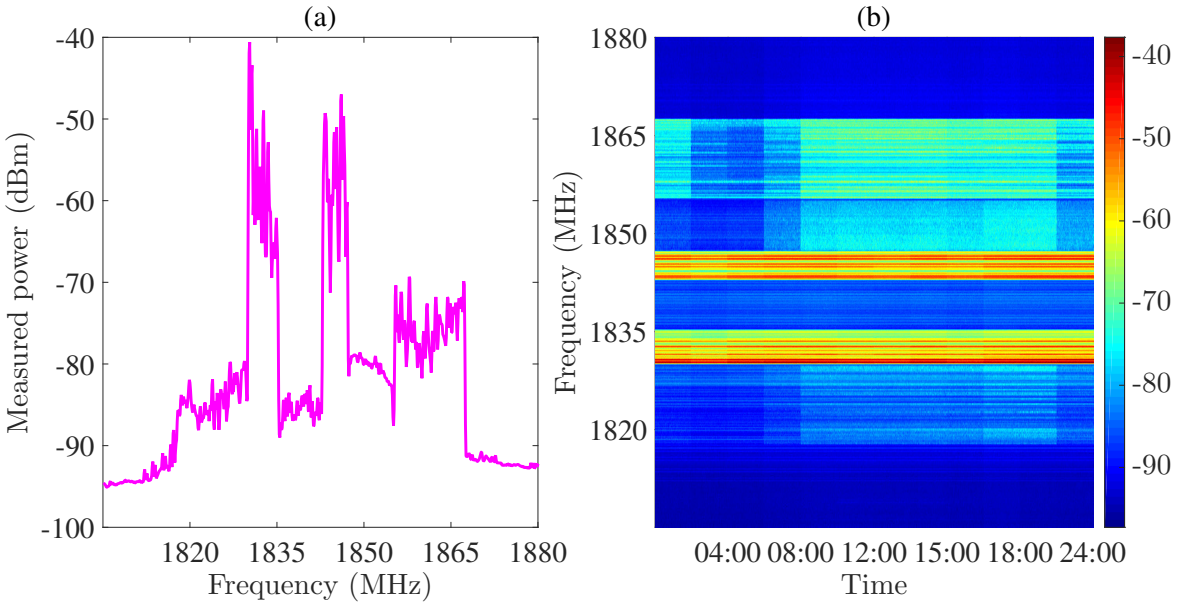

Figure 3.14: (a) Average measured power and (b) heat map over the course of an average day for the down-link of the M1800 band at site UP.

3.6.2.1 Hourly occupancy

The average occupancy of this band was calculated for a 24 hour period and has been plotted, for both site UP and site PF, in Figure 3.15. While the daily usage pattern of this band was similar to the M900 band, the overall level of occupancy was found to be significantly lower (roughly 55% lower than the M900 band). The difference between the two measurement sites (site UP and site PF) was found to be around 28% (fairly consistent with the findings from the M900 band). There was also a narrower period of time during which peak utilisation was evident. For site UP, peak utilisation was found to be between 09:00 and 22:00, while for site PF, this was found to be between 10:00 and 18:00.

3.6.2.2 Daily occupancy

The utilisation of the M1800 band over the days of the week is provided in Table 3.9. A slight variation in occupancy is evident, however, only around 4% difference was found between the occupancy on Sundays (lowest) as compared with the occupancy calculated for Thursdays (highest).

© University of Pretoria

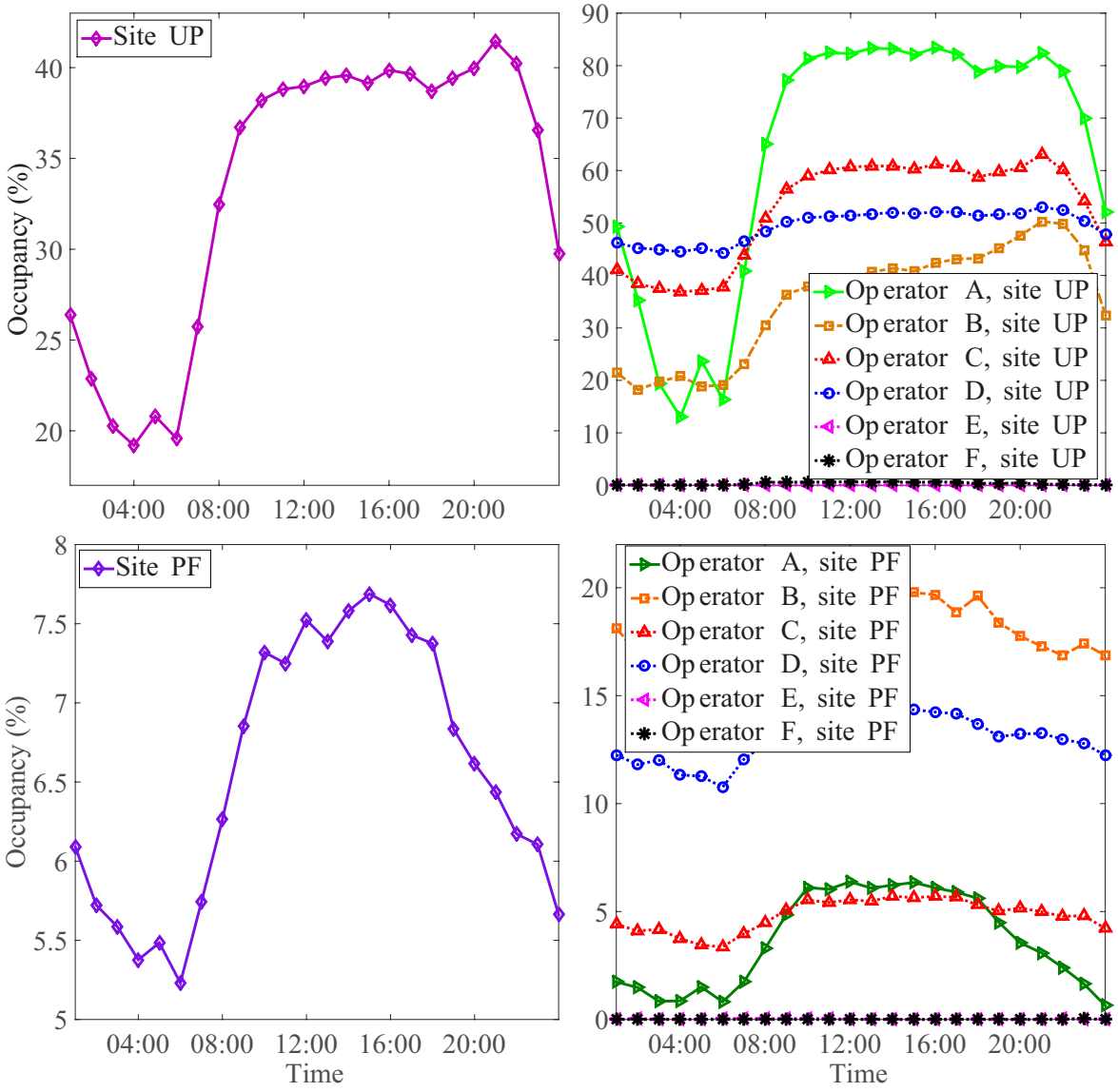

Figure 3.15: Average measured power of the down-link of the M1800 MHz band.

3.6.2.3 Comparison amongst mobile operators

Plots showing the difference in occupancy between the mobile operators assigned to the M1800 band are shown on the right hand side of Figure 3.15. Six operators are licensed to use this band, however, two of them were found not to be using their spectrum (denoted as operator E and operator F in Figure 3.15). These differences are listed in Table 3.10, however, unlike the M900 band the differences between the operators at the two locations are not consistent. At site UP, operator A was found to have the most traffic (67.59% where the band average was 34.43%), followed by operator C, operator D and then operator B. On the

© University of Pretoria

UNIVERSITEIT VAN PRETORIA
UNIVERSITY OF PRETORIA
YUNIBESITHI YA PRETORIA

Table 3.9: Occupancy comparison of the M1800 band for an average week.

Day	Site UP (%)	Site PF (%)	Difference
Mon	35.02	7.01	28.01
Tue	35.01	6.28	28.73
Wed	34.82	6.71	28.11
Thu	36.35	6.33	30.02
Fri	33.88	7.63	26.25
Sat	33.59	6.29	27.30
Sun	32.33	5.61	26.72
Average	34.43	6.55	27.88

other hand, operator B was found to have the most traffic (17.94% where the band average was 6.55%) at site PF, followed by followed by operator D, operator C and then operator A.

These trends may be indicative of the number of subscribers that each operator has around the measurement sites in question. It is also clear that there was a much higher user density at site UP than at site PF.

Table 3.10: Occupancy comparison between the different mobile operators for the M1800 band.

Operator	Site UP (%)	Site PF (%)	Difference (%)
A	67.59	3.656	63.93
B	35.27	17.94	17.33
C	52.76	4.824	49.94
D	49.47	12.92	36.55
E	0.044	0.002	0.042
F	0.347	0.001	0.346

© University of Pretoria

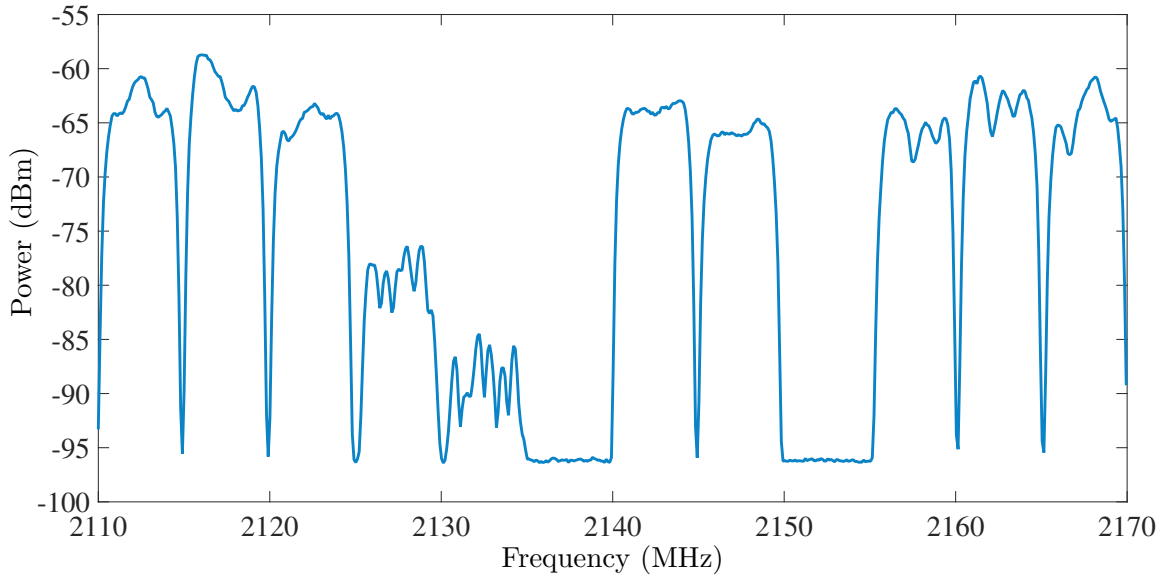

Figure 3.16: Average measured PSD of the M2100 band at site UP.

3.6.3 Mobile 2100 MHz bands

Measurements were also taken from the M2100 band which, at the time of measurement, was used for downlink data transmission using 3G wide code division multiple access (WCDMA). The PSD of this band, as measured at site UP, is shown in Figure 3.16 and heat maps for both a 24 hour (left) and a seven day (right) period are provided in Figure 3.17. From

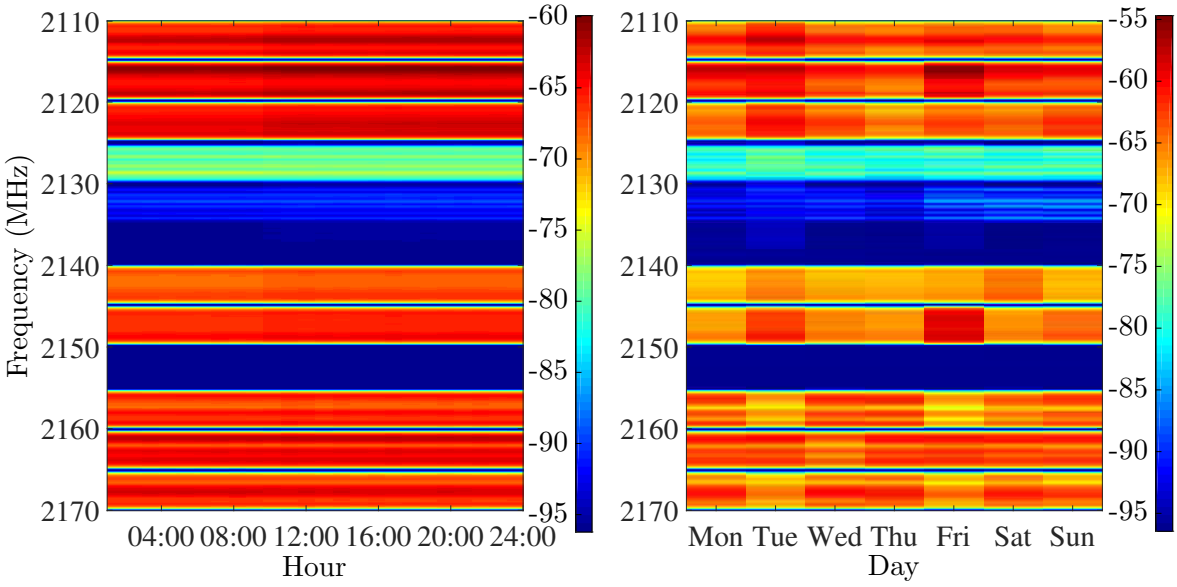

Figure 3.17: Heat maps of the M2100 band for an average day (left) and week (right).

© University of Pretoria

these plot it can be seen that the band is subdivided into 5 MHz channels with guard bands clearly visible in between each channel. The effects of frequency selective fading can be seen in Figure 3.16, as the tops of the channels are not flat as would be the case without frequency selective fading. Due to the nature of WCDMA, it is difficult to directly measure the number of mobile users on each channel. As such, the occupancy measurements performed for the M2100 band are simply a calculation of the spectral occupancy, i.e. the percentage of the band that is not considered noise.

3.6.3.1 Hourly occupancy

On the left hand side of Figure 3.18 the overall occupancy, calculated as per the MNF method, of the M2100 band can be seen for the average twenty-four hour period. It can be seen that the usage increases suddenly at approximately 09:00, with local minima at around 13:00, 16:00 and 19:00. This seems to correlate with lunch, the end of work day and supper times. The lowest occupancy was found to be after midnight at around 02:00. However, these fluctuations represent no more than a 2% difference in occupancy at any given time. This observation is corroborated by the heat map on left hand side of Figure 3.17, where it is hard to see any difference in average measured power over the course of an average day.

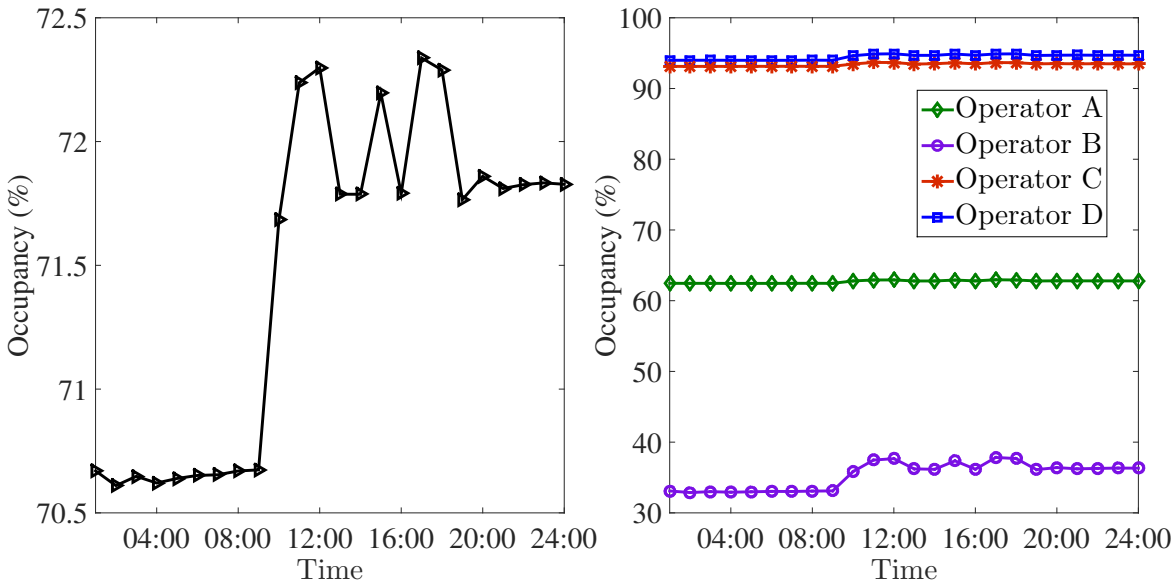

Figure 3.18: Plot of the overall (left) and per operator (right) occupancy of the M2100 band for an average 24 hour period.

© University of Pretoria

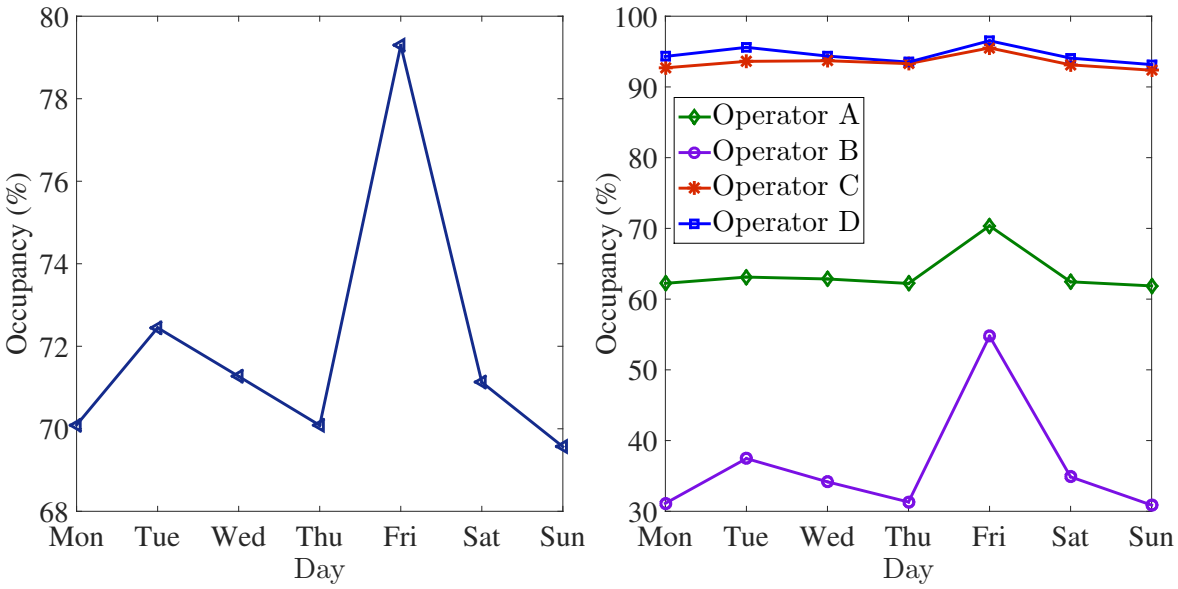

Figure 3.19: Occupancy of the M2100 band for an average week.

3.6.3.2 Daily occupancy

The right hand side of Figure 3.17 and the left hand side of Figure 3.19 respectively show the average measured power and occupancy of the M2100 band for the period of an average week. From the figure it is evident that Sunday was the day with lowest use and Friday the day with the highest usage. It is interesting to note that Monday, Thursday and Sunday were all found to have approximately the same level of occupancy, near the minimum occupancy levels for this band. The low activity on Sundays can be explained by the fact that the university campus is mostly devoid of students. However, the reasons for the low occupancy of Mondays and Thursdays are not as evident.

3.6.3.3 Comparison amongst mobile operators

There are four mobile operators assigned to the M2100 band. These are the same operator A, operator B, operator C and operator D that were reported to be operating in the M1800 band. Each operator has been assigned 15 MHz of bandwidth consisting of three 5 MHz channels. From the measurements shown in Figure 3.16, it appears that both operator A (2140 - 2155 MHz) and operator B (2125 - 2140 MHz) only use two thirds of their assigned spectrum in this band. Furthermore, since different signal levels were measured for the two channels being used by operator B, it appears that there may be two different base stations

© University of Pretoria

UNIVERSITEIT VAN PRETORIA
UNIVERSITY OF PRETORIA
YUNIBESITHI YA PRETORIA

serving site UP for operator B. Also, assuming that the transmission power would be similar for all base stations, it appears that either the base stations of operator B are located further away from site UP, than those serving the other operators, or there is something that is causing additional shadowing or fading.

The per operator occupancy levels for an average day are shown on the right hand side of Figure 3.18. The figure shows that operator D and operator C were found to have the highest spectral occupancy levels (approximately 94% and 93% respectively), with a low variability over an average day. Nonetheless, a small increase is seen at the 09:00 mark. Operator A was found to have the third highest occupancy level (approximately 63%), with a similar increase at 09:00. Operator B had the lowest occupancy levels (around 35%) and experienced a significant increase in activity at the 09:00 time mark.

The right hand side of Figure 3.19 shows the occupancy over the average week on a per operator basis. Consistent with the right hand side of Figure 3.18, the results show that operator C and operator D were using nearly all of their assigned bandwidth (95% and 93%, respectively) and exhibited little variability over the course of an average week. Operator A was the next most occupied (64%) with a significant increase evident on Fridays. Operator B was found to have an occupancy level of approximately only 36%, but this increased to approximately 55% on a Friday.

3.7 COMPARATIVE ANALYSIS

A comparison is made in Table 3.11 between the results obtained from measurements taken at location A of the University of Pretoria and the interpreted international results listed in Table 2.1. As discussed in Chapter 2, it is difficult to make a direct comparison due to

Table 3.11: Spectral utilisation in Pretoria compared with various international locations.

Band	Pretoria	New York	Chicago	Virginia	Barcelona	Dublin
TV	39.09	35.93	52.40	30.54	82.08	36.36
Mobile A	91.89	46.30	54.70	42.53	51.30	0.70
Mobile B	34.43	33.80	42.90	19.70	29.41	36.80

© University of Pretoria

UNIVERSITEIT VAN PRETORIA
UNIVERSITY OF PRETORIA
YUNIBESITHI YA PRETORIA

differing regulatory policies. However, this brief compassion does provide a rough indication as to how the results obtained in Pretoria compare with the rest of the world.

Three main observations can be made from this comparison. Firstly, that the TV broadcast bands in Pretoria and Dublin appear to have similar levels of occupancy (lower than cities like New York and Barcelona), secondly, that activity in mobile A was found to be significantly higher in Pretoria and thirdly that activity in mobile B was found to be similar to the other locations (especially New York and Dublin).

3.8 CONCLUSION

Technologies such as CR and GLSDB have been identified as candidates for taking advantage of TVWS for communication services. However, information about the spectral opportunities in these bands is required to determine the suitability of these technologies. Spectrum measurements were thus taken from the VHF and UHF bands, to quantify the current status of the TV broadcast bands in South Africa. Data was collected from various measurement sites at the Hatfield campus of the University of Pretoria and both the channel and spectral occupancies of these bands were calculated. Results indicated that a reasonable amount of spectrum is already available in these bands. Channel occupancies of only 40% and 29.17% were measured at location B of site UP which means that as much as 320 MHz of spectrum may currently be available.

Spectrum measurements were also taken from the bands utilised for mobile cellular communication at both site UP and site PF. Results indicated that these bands are already well utilised. At site UP, average spectral occupancies of 92% and 34% were found for the M900 and M1800 bands respectively, and an average spectral occupancy of 71% was found for the M2100 band. Thus, given the predictions for increased mobile services in the future, it is clear that the current capacity of these bands may not be enough to satisfy future spectrum needs. Technologies such as CR and GLSDB together with the freeing up of TVWS, for usage by mobile communications devices, may thus become critical to ensuring that future spectrum demands are met.

The work presented in this chapter has laid a foundation and provides motivation for the concepts that will be discussed in the chapters that follow.

© University of Pretoria

CHAPTER 4

PRIMARY USER TRAFFIC PREDICTION

4.1 INTRODUCTION

In a cognitive radio network (CRN) it is assumed that secondary users (SU) are able to coexist with primary users (PU) of the same spectrum. However, interference between these users is undesirable [9]. If a SU is to avoid a collision with the PU, then it will need to know when the PU is present. A cognitive radio (CR) will thus periodically perform spectrum sensing (SS) to detect the presence of a PU [50]. Yet, the SS process adds additional overhead for a SU. It is thus not ideal for a SU to be constantly sensing the band of interest. Nevertheless, reducing SS regularity poses a problem, since a PU may still collide with a SU if it enters a band in-between SS events. But, if a SU is able to predict the return of a PU ahead of time, then it has the opportunity to avoid collision by pro-actively vacating the band of interest before the actual arrival of the PU. Accurate prediction of PU behaviour thus has the potential to allow a SU to reduce SS regularity, while still avoiding collisions with the PU [80].

Various approaches to modelling and predicting PU traffic have been proposed in the literature, as presented in Section 2.5. However, one of the problems associated with traffic prediction in a CRN is the computational complexity of the algorithm. Ideally, PU traffic prediction needs to be performed both accurately and quickly for it to be successful. Consequently, a computationally simple yet fairly accurate approach to predicting PU occupancy, based on a sliding occupancy window (OW), is proposed in this chapter. The prediction error (PE) of this method is compared with that of the normalised least mean square (NLMS) and two-state Markov chain (MC) approaches to occupancy prediction.

© University of Pretoria

UNIVERSITEIT VAN PRETORIA
UNIVERSITY OF PRETORIA
YUNIBESITHI YA PRETORIA

The rest of this chapter is structured as follows. Section 4.2 is a brief discussion on the classification of PU traffic. The OW method for traffic prediction is presented in Section 4.3. Simulation results are provided in Section 4.4, which is followed by Section 4.5, where conclusions are drawn. Parts of this chapter were published in [123] and [124].

4.2 TRAFFIC CLASSIFICATION

The main purpose of traffic prediction in CRNs, is to provide SUs with information about PU behaviour before it actually happens. In order for a SU to be able to make these predictions, certain PU behavioural properties need to be ascertained. These behavioural properties may then be utilised in the prediction process, e.g., if PU behavioural patterns can be identified from historical data, then it is plausible that these patterns may be repeated in the future.

The first step in identifying these patterns is to classify the type of traffic that is to be predicted. It is assumed that at time t, for a particular frequency band ϑ, a SU i will gather a sequence of binary occupancy decisions (ON and OFF periods) $\boldsymbol{S}_{t,i,\vartheta}(n)$ that describe the occupation of the band by a PU for a period of p historical ON and OFF periods. This sequence is given as,

$$\boldsymbol{S}_{i,t,\vartheta}(n) = \{D_{t-1,i}, D_{t-2,i}, \ldots, D_{t-p,i}\}, \quad 1 \leq n \leq p \tag{4.1}$$

where $D_{t-p,i}$ is the binary occupancy decision from Equation (2.2). An ON period denotes the presence of a PU (e.g. at $t = t - p$, $D_{t-p} = 1$) and an OFF period the absence thereof (e.g. at $t = t - p$, $D_{t-p} = 0$). This sequence is then used to model the broader traffic pattern generated by the PU. For the sake of simplicity, PU traffic will be classified according to the following three scenarios,

- periodicity of ON and OFF times,
- randomness of ON and OFF times, and
- density of ON and OFF times.

© University of Pretoria

4.2.1 Periodicity

If after observing PU behaviour, it is repeatedly found that the ON and OFF times in $\boldsymbol{S}_{i,t,\vartheta}(n)$ are of a fixed length, then it may be assumed that PU traffic will continue to follow a fixed periodic pattern in the future. This distinction can be made by calculating the separation time between the consecutive local maxima of $\boldsymbol{S}_{i,t,\vartheta}(n)$, as suggested in [125]. If the separation time is found to be reasonably constant, then $\boldsymbol{S}_{i,t,\vartheta}(n)$ may be assumed to be periodic. In this case the usage pattern observed during the period of repetition is deterministic and may then be repetitively used to predict future PU activity on that band. Such a scenario is depicted in part (c) of Figure 4.1.

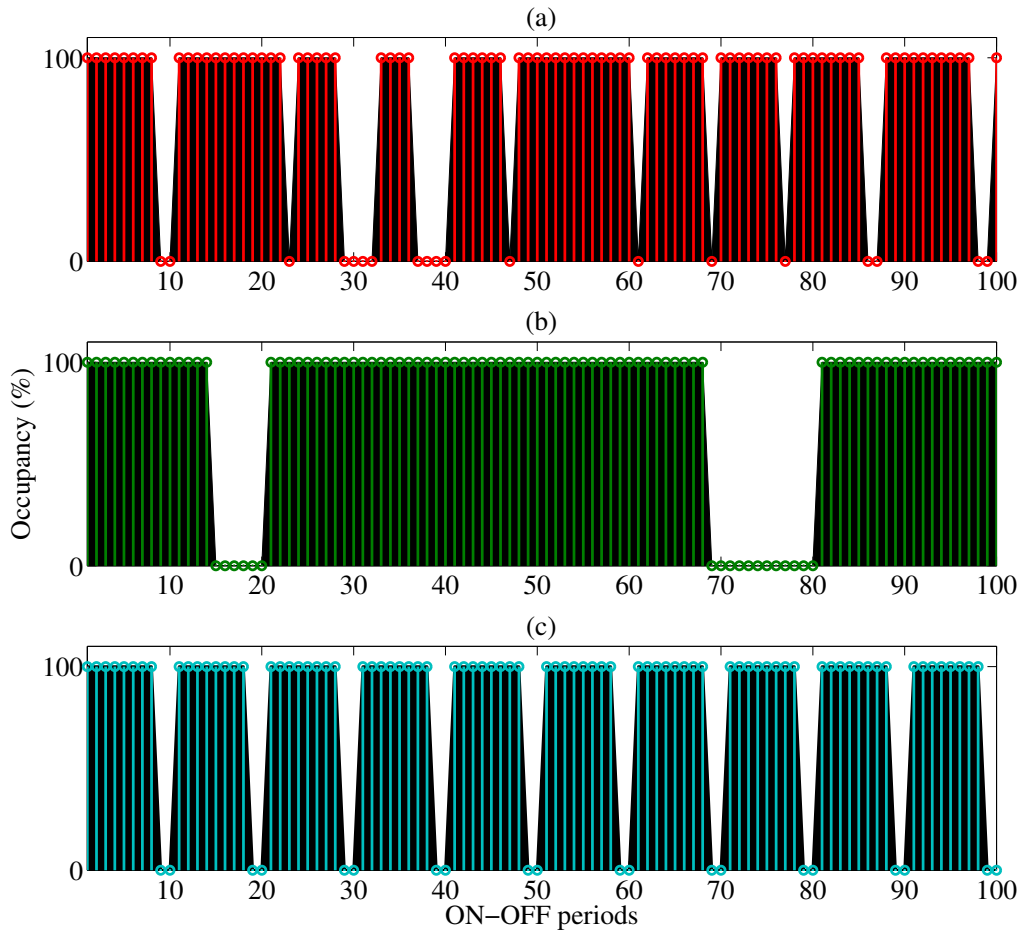

Figure 4.1: Binary data sets illustrating: (a) fast and (b) slow varying stochastic PU activity and (c) fast varying periodic PU activity (approximately 80% channel utilisation).

© University of Pretoria

UNIVERSITEIT VAN PRETORIA
UNIVERSITY OF PRETORIA
YUNIBESITHI YA PRETORIA

4.2.2 Randomness

If $\boldsymbol{S}_{i,t,\vartheta}(n)$ is found to be non-periodic, then it may be assumed that the arrival rate and duration of ON and OFF times may follow a stochastic distribution. An example of such a stochastic distribution is the alternative exponential ON-OFF model which has been adopted in this chapter for modelling these ON and OFF periods [126]. For this model, it is assumed that channel occupancy can be modelled as independently exponentially distributed processes, where the time intervals between the arrival and departure of a PU follow a negative exponential distribution. For channel ϑ the OFF period distribution is given as,

$$f\left(t_{\vartheta,0}\right) = \begin{cases} \Lambda_0 e^{-\Lambda_0 t_{\vartheta,0}}, & t_{\vartheta,0} \geq 0 \\ 0, & t_{\vartheta,0} < 0 \end{cases} \tag{4.2}$$

with mean $1/\Lambda_0$ and $t_{\vartheta,0}$ the duration of an OFF period. Similarly, the ON period distribution is given as,

$$f\left(t_{\vartheta,1}\right) = \begin{cases} \Lambda_1 e^{-\Lambda_1 t_{\vartheta,1}}, & t_{\vartheta,1} \geq 0 \\ 0, & t_{\vartheta,1} < 0 \end{cases} \tag{4.3}$$

with mean $1/\Lambda_1$ and $t_{\vartheta,1}$ the duration of an ON period. Such a scenario is depicted in parts (a) and (b) of Figure 4.1. Another example is the Poisson distribution. In this case the rate at which PUs either arrive or depart from the band of interest is considered. The rate at which they depart is described by the following distribution,

$$f\left(r_{\vartheta,0}|\Lambda_0\right) = \frac{{\Lambda_0}^{r_{\vartheta,0}}}{r_{\vartheta,0}!} e^{-\Lambda_0}, \tag{4.4}$$

with mean departure rate Λ_0 and $r_{\vartheta,0} \in \mathbb{N}$ the number PUs that will depart the band over a fixed time period. Similarly, the rate at which they arrive is given by the following distribution,

$$f\left(r_{\vartheta,1}|\Lambda_1\right) = \frac{{\Lambda_1}^{r_{\vartheta,1}}}{r_{\vartheta,1}!} e^{-\Lambda_1}, \tag{4.5}$$

with mean arrival rate Λ_1 and $r_{\vartheta,1} \in \mathbb{N}$ the number of arriving PUs.

The effect that these patterns will have on PE will be investigated in Section 4.4.

4.2.3 Traffic density

The average utilisation of an observed channel may also have a bearing on the way in which PU behaviour may be predicted. By calculating the average utilisation of $\boldsymbol{S}_{i,t,\vartheta}(n)$, information

© University of Pretoria

UNIVERSITEIT VAN PRETORIA
UNIVERSITY OF PRETORIA
YUNIBESITHI YA PRETORIA

can be obtained as to how frequently the ON period will change to OFF periods and vice versa. For example, if after observation, the average utilisation of a channel is found to be only 10%, then future time slots may be likely to follow a similar trend. A method for predicting PU behaviour, based on channel utilisation, will be discussed in Section 4.3.

For the sake of simplicity, PU traffic will be classified according to the following two parameters: pattern change rate and the average utilisation of the band. Traffic patterns can be described by using these parameters to adjust Λ_0 and Λ_1 according to the following expression,

$$\Lambda_0 = \tau \upsilon_0, \tag{4.6}$$
$$\Lambda_1 = \tau \upsilon_1,$$

where $\Lambda_0, \Lambda_1 \in (0, \infty)$. The rate at which PU occupancy patterns are changing is described by τ while υ_0 and υ_1 are a measure of ON and OFF period density respectively, where $\tau \in [1, \infty)$, $\upsilon_0 \in [0, 10]$ and $\upsilon_1 = 10 - \upsilon_0$.

As an example consider the data sets presented in Figure 4.1 where all three data sets are a binary representation of a high PU traffic density scenario consisting of $p = 100$ ON-OFF periods (approximately 80% channel utilisation) where $\upsilon_0 = 2$ and $\upsilon_1 = 8$. The first scenario (a), shown at the top of the figure, represents the case where stochastic PU activity is changing quite fast ($\tau = 1$). The second scenario (b), shown in the middle of the figure, represents the case where stochastic PU activity is changing more slowly ($\tau = 5$). The third scenario (c), shown at the bottom of the figure, represents a deterministic data set with fixed ON-OFF periods for fast changing PU activity. Each period was $T = 10$ time samples long, and consisted of eight ON samples followed by two OFF samples.

Traffic classification and prediction performance will be investigated in Section 4.4.

4.3 PREDICTION MODELLING

In this section an OW based method for modelling PU activity is proposed that uses traffic density to forecast future PU activity. The OW based method can in turn be used for making predictions about future PU traffic behaviour. In this chapter it is assumed that predictions are made by a single SU for the traffic of a single PU. Forecasting using multiple SUs will be

© University of Pretoria

UNIVERSITEIT VAN PRETORIA
UNIVERSITY OF PRETORIA
YUNIBESITHI YA PRETORIA

discussed in Chapter 5.

4.3.1 Primary user traffic prediction

If a function $f(\cdot)$ is used to perform a forecast, then let $\boldsymbol{F}_{t,\vartheta}(r)$ be the sequence of predicted ON-OFF values at time t for frequency channel ϑ based on the historical sequence $\boldsymbol{S}_{t,\vartheta}(n)$, such that,

$$\boldsymbol{F}_{t,\vartheta}(r) = f\left(\boldsymbol{S}_{t,\vartheta}(n)\right), \quad t+1 \leq r \leq t+k, \quad 1 \leq n \leq p \tag{4.7}$$

where k is the number of future ON-OFF samples predicted, $\{r, t, k\} \in \mathbb{N}$, $\boldsymbol{S}_{t,\vartheta} \in \{0, 1\}$ and $\boldsymbol{F}_{t,\vartheta}(r) \in \{0, 1\}$. The function $f(\cdot)$ could represent any of the prediction methods described in Chapter 2. $\boldsymbol{F}_{t,\vartheta}(r)$ may also be described as a sequence of binary forecast values, such that,

$$\boldsymbol{F}_{t,\vartheta}(r) = \{PD_{t+1}, PD_{t+2}, \ldots, PD_{t+k}\}, \quad t+1 \leq r \leq t+k \tag{4.8}$$

where PD_{t+k} is the binary forecast for time slot $t+k$.

4.3.2 Occupancy window approach

While many of the techniques discussed in Chapter 2 have been shown in the literature to be effective at predicting various forms of traffic, they all add a certain amount of complexity to the SS and prediction process. However, excessive complexity could slow the prediction process down leading to outdated predictions, especially under fast changing PU traffic conditions. Therefore, a simplified approach to prediction that relies on estimating the average utilisation of the band of interest over a window of observation of length p time slots, is proposed in this section.

Future predictions are made as a hard decision, based on the calculated occupancy level of the observation window. If the observation window for channel ϑ at time t is comprised of the sequence $\boldsymbol{S}_{t,\vartheta}(n)$, then the mean occupancy $\Phi_{t,\vartheta}$ of that observation window is calculated as follows,

$$\Phi_{t,\vartheta} = \frac{1}{p} \sum_{n=1}^{p} \boldsymbol{S}_{t,\vartheta}(n). \tag{4.9}$$

Once $\Phi_{t,\vartheta}$ is known, the predicted sequence $\boldsymbol{F}_{t,\vartheta}(r)$ is calculated by letting the binary forecasts

© University of Pretoria

UNIVERSITEIT VAN PRETORIA
UNIVERSITY OF PRETORIA
YUNIBESITHI YA PRETORIA

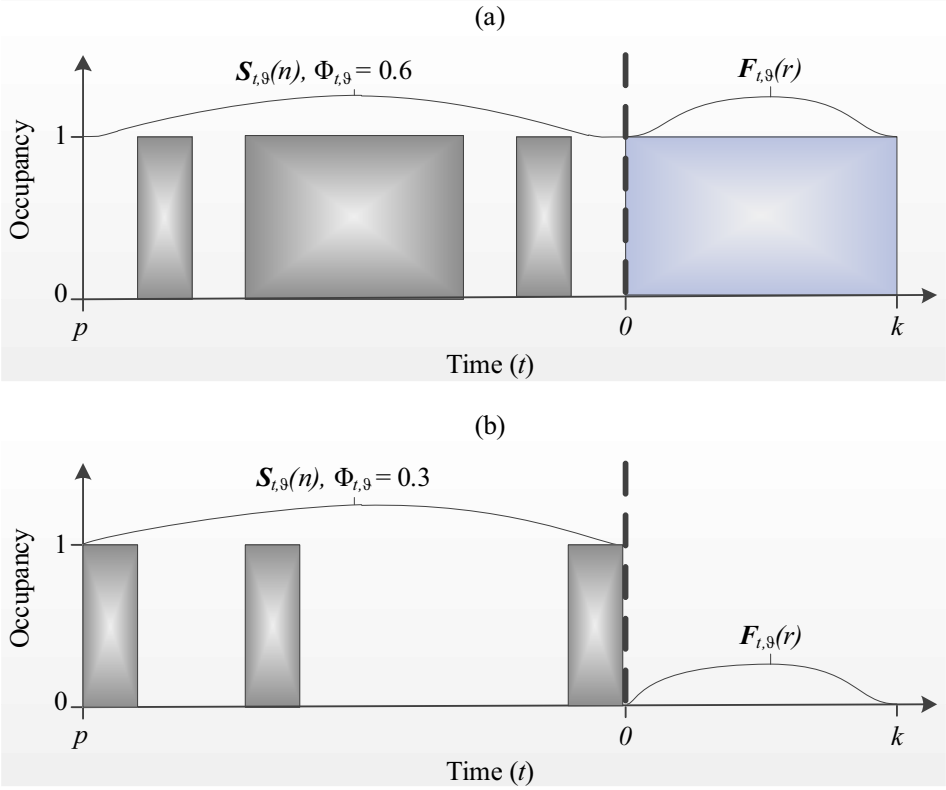

Figure 4.2: Occupancy window based prediction, where $\Phi_{t,\vartheta} = 0.6$ for (a), $\Phi_{t,\vartheta} = 0.3$ for (b) and $p = 10$ samples.

for each future time slot be populated according to the following expression,

$$PD_{t+r} = \begin{cases} 1, & \Phi_{t,\vartheta} \geq 0.5, \quad 1 \leq r \leq k \\ 0, & \Phi_{t,\vartheta} < 0.5, \quad 1 \leq r \leq k. \end{cases} \tag{4.10}$$

4.3.3 Occupancy window example

A generic example of how this OW approach works, is provided in Figure 4.2. Consider scenario (a) where $\Phi_{t,\vartheta} \geq 0.5$, and scenario (b) where $\Phi_{t,\vartheta} < 0.5$, with observation window length chosen as $p = 10$ and the number of predicted samples as $k = 5$ for both scenarios. In scenario (a),

$$\boldsymbol{S}_{t,\vartheta}(n) = \{0, 1, 0, 1, 1, 1, 1, 0, 1, 0\}, \tag{4.11}$$

which means that $\Phi_{t,\vartheta} = 0.6$. Therefore since $\Phi_{t,\vartheta} \geq 0.5$, the predicted sequence would be calculated as,

$$\boldsymbol{F}_{t,\vartheta}(r) = \{1, 1, 1, 1, 1\}. \tag{4.12}$$

© University of Pretoria

UNIVERSITEIT VAN PRETORIA
UNIVERSITY OF PRETORIA
YUNIBESITHI YA PRETORIA

However, in scenario (b),

$$\boldsymbol{S}_{t,\vartheta}(n) = \{1, 0, 0, 1, 0, 0, 0, 0, 0, 1\}, \tag{4.13}$$

which means that $\Phi_{t,\vartheta} = 0.3$. Therefore since $\Phi_{t,\vartheta} < 0.5$, the predicted sequence would be calculated as,

$$\boldsymbol{F}_{t,\vartheta}(r) = \{0, 0, 0, 0, 0\}. \tag{4.14}$$

Intuitively, it would seem that this method of prediction would be likely to be more suited to conditions where ON and OFF periods are made up of contiguous blocks in time, e.g slow varying PU activity. This assumption should thus be taken into consideration when selecting values for parameters p and k.

4.4 SIMULATION RESULTS

Simulations were run, in MATLAB, to compare the PE of the OW method with two other prediction methods, namely the: NLMS [104, 105] and MC [85, 92] methods (summarised in Chapter 2). Three simulations were run: Firstly to compare the PE for random PU traffic with periodic PU traffic, secondly to investigate the effect of traffic density on PE and thirdly to compare the complexity of each prediction method.

4.4.1 Simulation environment

To compare the performance of the prediction methods, simulations were run using the data sets illustrated in Figure 4.1. These data sets were generated with the aim of creating a high PU traffic density scenario (approximately 80% channel utilisation). The PE was defined as the percentage difference between the actual $\boldsymbol{X}_t(r)$ and predicted $\boldsymbol{F}_{t,\vartheta}(r)$ data sequences at time t, such that,

$$PE = 100\left(\frac{\sum_{r=1}^{k} \boldsymbol{F}_{t,\vartheta}(r) - \boldsymbol{X}_{t,\vartheta}(r)}{k}\right). \tag{4.15}$$

The PE was calculated for each method under various traffic classification scenarios. For all three simulations, the performance of each prediction method was compared with the scenario where the predicted sequence was made up of discrete uniformly distributed pseudo-random binary integers. For the rest of this thesis, this will be referred to as random prediction (RND).

© University of Pretoria

UNIVERSITEIT VAN PRETORIA
UNIVERSITY OF PRETORIA
YUNIBESITHI YA PRETORIA

Table 4.1: Simulation parameters for the traffic density and complexity simulations.

Parameter	υ_0	υ_1	τ	k	p
Value	$[0, 10]$	$10 - \upsilon_0$	$\{1; 5\}$	$\{1; 10\}$	21

4.4.1.1 Deterministic and stochastic traffic patterns

For the first simulation the PE was compared using data sets (a) and (c) from Figure 4.1, so as to compare the PE for periodic traffic with that of stochastic traffic (Poisson distributed). To aid the comparison, the effect that the number of observations p had on the PE, was investigated. The effect on PE, as the step-ahead prediction length k was increased, was also observed. These parameters were investigated for the following range of values: $1 \leq p \leq 25$ for observation time, and $1 \leq k \leq 10$ for prediction length.

4.4.1.2 Traffic density and complexity

The second and third simulations compared the PE for different levels of traffic occupancy and pattern change rates, as discussed in Section 4.2.3. Only the stochastic traffic patterns were considered, i.e. part (a) and (b) of Figure 4.1. The observation length was set at $p = 21$ and forecast lengths of either $k = 1$ or $k = 10$ were employed. Simulations were run for ten different channel occupancy values (from 0%, $\upsilon_0 = 0$, to 100% occupied, $\upsilon_0 = 10$) and results where compared for two different pattern change rates ($\tau = 1$ and $\tau = 5$). These parameters are summarised in Table 4.1.

4.4.2 Prediction performance: Deterministic and stochastic traffic

Calculated prediction accuracies, as observation period p is increased, are illustrated in Figure 4.3. For these results, the prediction length was fixed at $k = 5$ future time samples. For both data sets, the prediction models clearly provided an improvement over RND. Also, the proposed OW method was found to consistently be more accurate or provide at least the same accuracy as the MC and NMLS methods respectively.

When using periodic data, part (a), the prediction accuracies obtained for the MC and NLMS

© University of Pretoria

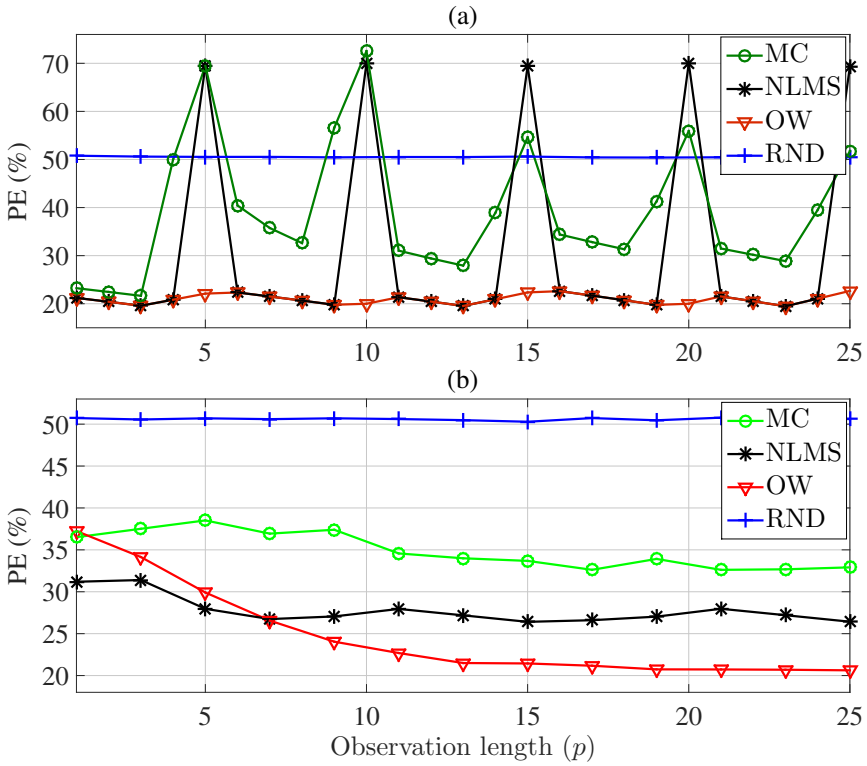

Figure 4.3: PE as observation length p is increased and $k = 5$, for (a) periodic and (b) stochastic data (Poisson distribution).

methods appear to exhibit a periodic fluctuation. The period of this fluctuation is linked to the period T of the data set. Since the data set is deterministic and periodically repetitive, it is concluded that $p = T$ should be chosen to perform prediction. Also, p does not seem to have any other significant effect on PE.

From the results obtained using stochastic data, part (b), it is evident that increasing p leads to a reduction in the PE of all three methods, particularly for the OW method. Over the range $p = \{1, \ldots, 25\}$, there was approximately a 4% improvement for the MC method, a 5% improvement for the NLMS method and a 17% improvement for the OW method. Observing Figure 4.3, it seems that the PE of the NLMS and OW methods begins to settle as $p > 11$, whereas the MC method appears to need a longer time to do so.

In Figure 4.4, the prediction methods are compared for PE as step-ahead prediction length k is increased. In this case, the observation period was fixed at $p = 20$. For periodic data, part (b), a periodic fluctuation in PE is again evident. As with the observation period, it is recommended that k be chosen according to the period T of the data set. It is also noticeable

© University of Pretoria

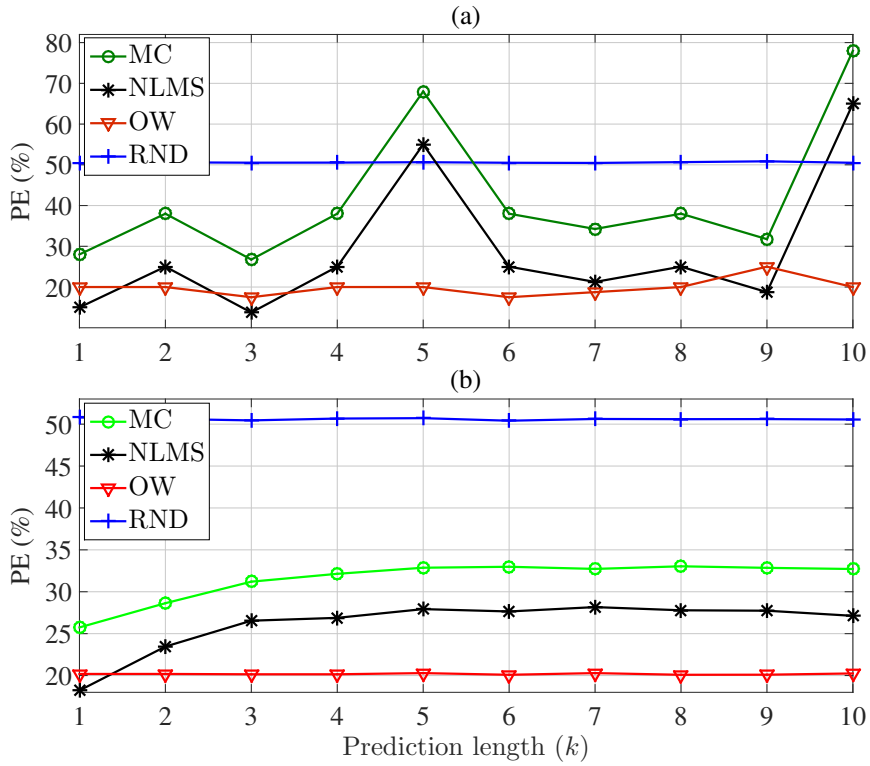

Figure 4.4: PE as prediction length k is increased and $p = 21$, for (a) periodic and (b) stochastic data (Poisson distribution).

that there is little difference in the PE of the MC and NLMS methods. Thus, apart from periodic fluctuations, k does not appear to have any other major effect on PE for periodic data.

However, for stochastic traffic, part (b), results show that PE gradually increases when the NLMS and MC methods are employed for $1 \leq k \leq 6$. Further increase in k appears to have no effect on the PE. The OW method seems to be less susceptible to this increase in PE than the other two methods, since there is less than a 1% increase in PE of (over the range $k = \{1, \ldots, 10\}$), compared with approximate increases in PE of 7% and 9% for the MC and NLMS methods receptively. All three prediction methods significantly outperformed RND for the entire range of future prediction lengths k.

Thus, as k was increased, it was again evident that the proposed OW method was consistently more accurate than both the MC and NMLS methods for a traffic occupancy rate of 80%. Yet, it will be shown in the next section that this is not necessarily the case for all traffic density scenarios.

© University of Pretoria

UNIVERSITEIT VAN PRETORIA
UNIVERSITY OF PRETORIA
YUNIBESITHI YA PRETORIA

4.4.3 Prediction performance: Traffic density

Prediction performance for stochastic traffic patterns, investigated over the full range of channel occupancy values, is presented in this sub-section.

4.4.3.1 Fast changing traffic

Plots showing the PE for fast changing PU traffic (when $\tau = 1$) are provided in Figure 4.5 (for alternative exponentially distributed traffic) and Figure 4.6 (for Poisson distributed traffic). It is evident that all of the prediction methods either matched or outperformed RND (the control method) over the full range of channel occupancies. Consistent with Figure 4.4, predictions made further into the future (i.e. $k = 10$) were found to be less accurate than for the immediate future (i.e $k = 1$). However, the most notable observation was that the PE of all of the methods was found to be the lowest when a band was either completely empty (0%) or when it was completely occupied (100%) and highest when the channel had an occupancy of 50%. This can be explained by the effect of randomness on the prediction methods, since the PU traffic pattern is more random when the occupancy is 50% and completely non-random when the occupancy is either 0% or 100%.

In the previous section simulations were only run for a traffic density of $\upsilon_0 = 2$. In that scenario, all of the prediction methods experienced improved PE values as p was increased. However, after further analysis of Figure 4.5 and Figure 4.6, it is clear that as the PU traffic occupancy approaches 50%, i.e. becomes more random, the inverse is actually true. When the traffic pattern is random the accuracy of the prediction methods degrades as an identifiable traffic pattern becomes less prevalent.

The major differences found, when comparing the results obtained under alternative exponentially distributed traffic to those obtained for Poisson distributed traffic, were: Firstly, that the PE for all three methods was slightly worse for Poisson distributed traffic when the PU traffic density approached 50%. But, secondly, for the OW method, the PE was found to be lower when $\upsilon_0 \leq 3$ or $\upsilon_0 \geq 7$. This meant that the OW method was consistently better than the other methods when $k = 10$. The third difference was that the difference in PE, between predictions made for the near future compared with those made further into the future, was larger for the NLMS and MC methods but much smaller for the OW method.

© University of Pretoria

UNIVERSITEIT VAN PRETORIA
UNIVERSITY OF PRETORIA
YUNIBESITHI YA PRETORIA

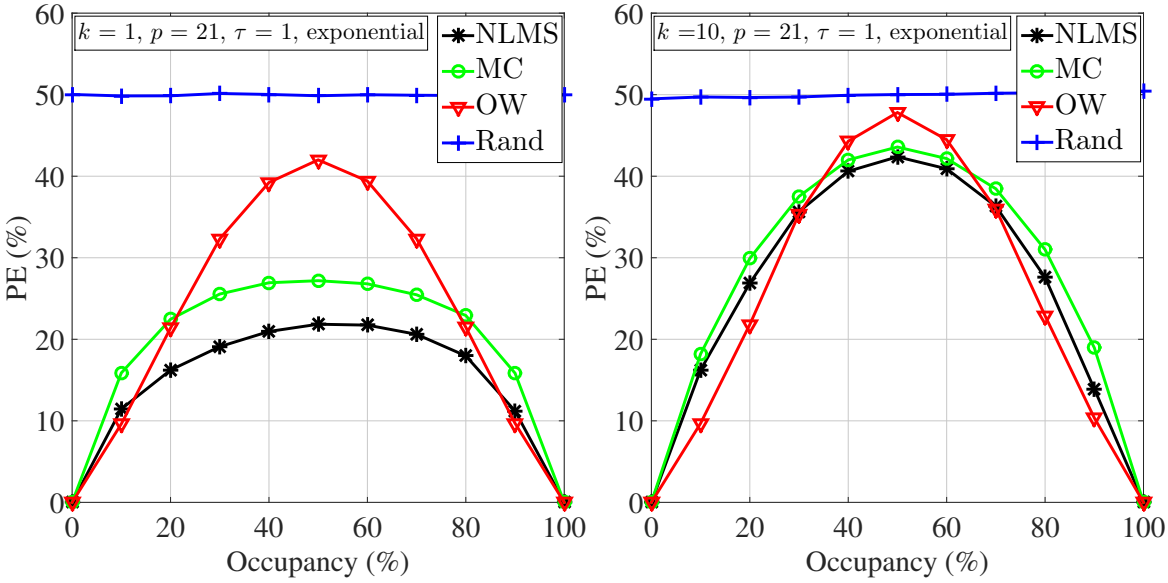

Figure 4.5: Prediction error over the full range of channel occupancies for a fast varying stochastic PU traffic pattern (alternate exponential distribution with $k = \{1, 10\}$, $p = 21, \tau = 1$).

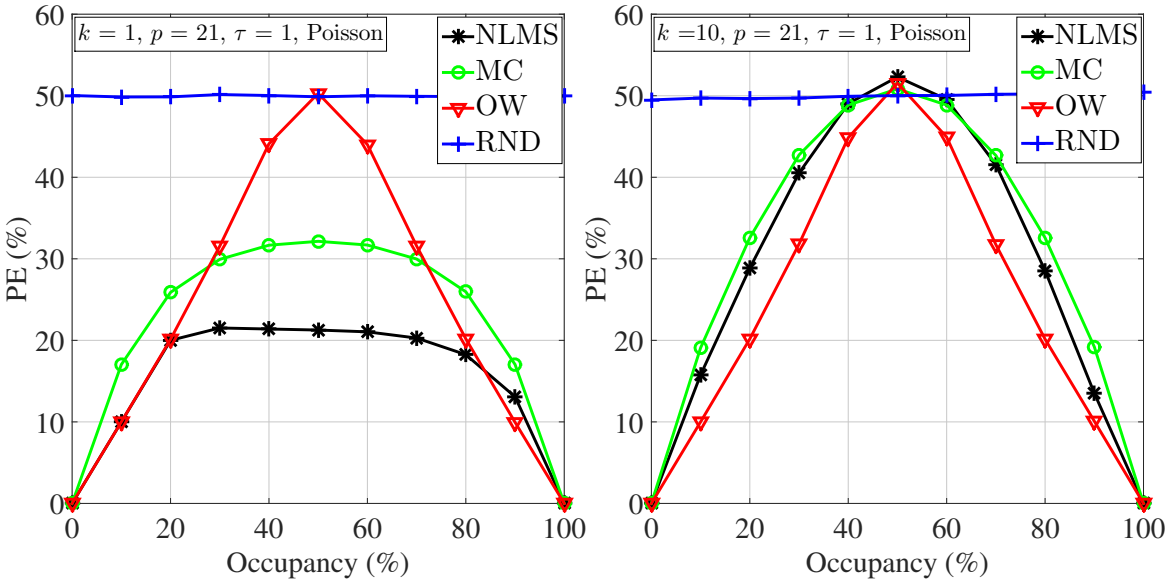

Figure 4.6: Prediction error over the full range of channel occupancies for a fast varying stochastic PU traffic pattern (Poisson distribution with $k = \{1, 10\}$, $p = 21, \tau = 1$).

It is thus evident that the achievable prediction performance of each method varies according to the PU traffic conditions and in an optimal scenario should thus be employed accordingly.

© University of Pretoria

4.4.3.2 Slow changing traffic

Plots showing the PE for slow changing stochastic traffic (when $\tau = 5$) are provided in Figure 4.7 (for alternative exponentially distributed traffic) and Figure 4.8 (for Poisson distributed traffic). PE trends similar to the fast changing traffic scenario were observed. The major differences though were: Firstly, for the MC and NLMS methods, the PE appeared to generally be significantly lower under slow changing traffic conditions than under fast changing traffic conditions. Secondly, the variation in PE values as channel occupancy changed were found to be less pronounced, with PE almost flat when $1 \leq \upsilon_0 \leq 9$. This may be attributed to the fact that a slower changing PU traffic pattern is less random and thus more predictable (intuitively it makes sense that for a binary pattern, the larger the number of contiguous bits that are the same, the easier it becomes to predict future bits). Thirdly, PE for the OW method also improved for alternate exponentially distributed traffic, but generally became worse under Poisson distributed traffic.

The OW method was thus clearly found to be generally less suitable for slow changing traffic conditions than for fast changing traffic conditions.

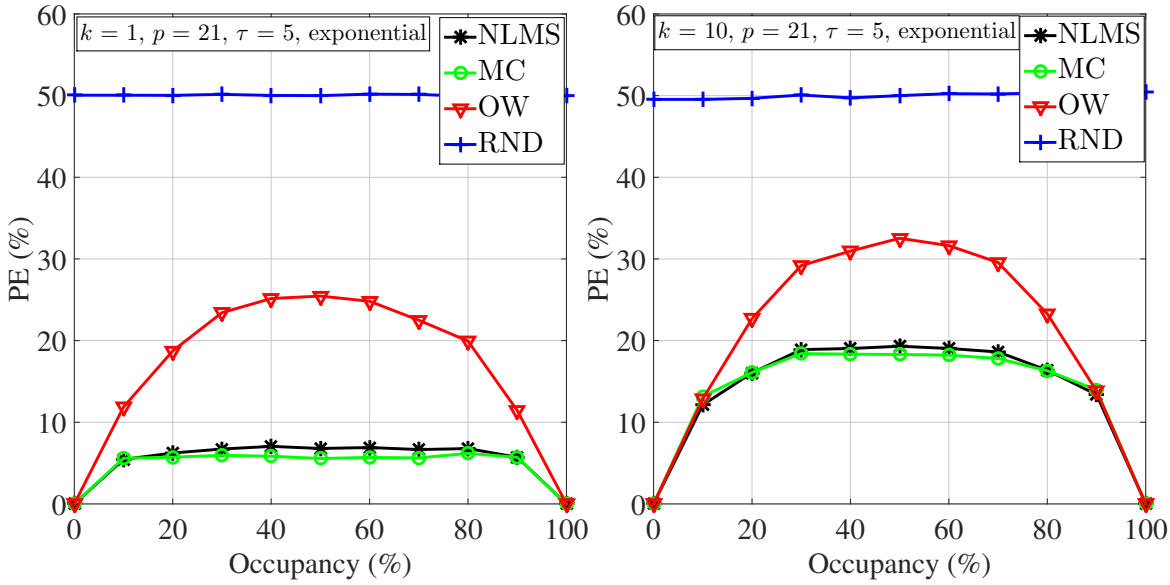

Figure 4.7: Prediction error over the full range of channel occupancies for slow varying PU traffic (alternate exponential distribution with k={1,10}, $p = 11, \tau = 5$)

© University of Pretoria

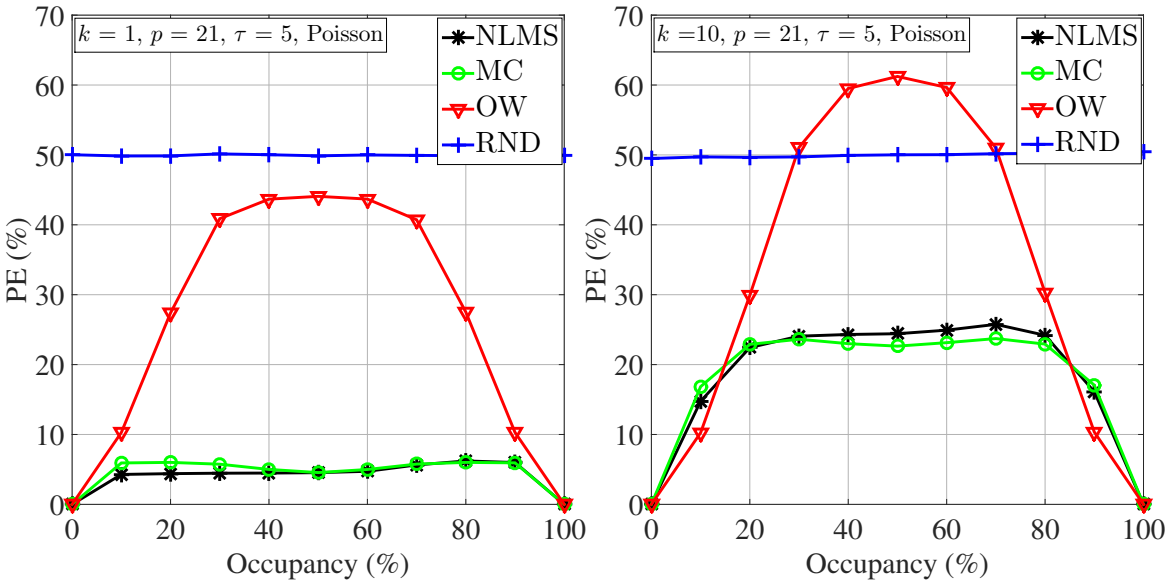

Figure 4.8: Prediction error over the full range of channel occupancies for slow varying PU traffic (Poisson distribution with k={1,10}, $p = 21, \tau = 5$)

4.4.3.3 Traffic distribution

Individual differences between the performance of the prediction methods for different occupancy levels, traffic change rates and prediction lengths were observed. These differences suggest that the choice of prediction method should be related to the traffic pattern of the actual channel for which a prediction is to be made. Selected PE results are listed in Table 4.2, to further highlight these differences in the context of the underlying PU traffic distribution. PE values for different different levels of future prediction length k and traffic density τ are compared for each method, when channel occupancy was either set at $\upsilon_1 = 5$ or at $\upsilon_1 = 8$ for a fixed observation length of $p = 21$, for both alternate exponentially and Poisson distributed PU traffic patterns.

With the exception of the OW method, at higher levels of traffic occupancy ($\upsilon_1 \geq 8$), all of the prediction methods returned either similar or slightly better results for alternate exponentially distributed traffic than for Poisson distributed traffic. For both traffic pattern distributions, most of the traffic scenarios investigated found that the NLMS method generally had the best performance, while the OW method was generally found to be the worst performing method. The OW method was particularly poor when the occupancy level was 50% ($\upsilon_1 = 5$) and the underlying traffic pattern followed a Poisson distribution. Under certain conditions the OW

© University of Pretoria

UNIVERSITEIT VAN PRETORIA
UNIVERSITY OF PRETORIA
YUNIBESITHI YA PRETORIA

Table 4.2: Comparison between selected PE results for $v_1 = 5$ and $v_1 = 8$ when $p = 21$, for both alternate exponentially and Poisson distributed traffic patterns.

Method	Poisson				Alternate Exponential			
	$\tau = 1$		$\tau = 5$		$\tau = 1$		$\tau = 5$	
	$k = 1$	$k = 10$	$k = 1$	$k = 10$	$k = 1$	$k = 10$	$k = 1$	$k = 10$
$v_1 = 5$								
NLMS	21.26	52.30	4.54	24.42	21.85	42.38	6.79	19.31
MC	32.14	50.83	4.56	22.64	27.19	43.58	5.56	18.30
OW	50.29	51.55	44.07	61.23	42.02	47.81	25.45	32.54
RND	49.87	50.02	49.93	49.99	49.88	50.02	50.00	50.00
$v_1 = 8$								
NLMS	18.25	28.55	6.07	24.19	17.97	27.59	6.78	16.37
MC	25.96	32.58	5.18	22.93	22.92	31.00	5.19	16.31
OW	20.19	20.15	15.09	30.27	21.48	22.89	19.94	23.28
RND	49.89	50.23	50.19	50.30	49.89	50.22	49.92	50.34

method actually had the lowest PE of all of the methods. For both traffic distributions this occurred when predictions were made further into the future ($k = 10$) and the traffic pattern was fast changing ($\tau = 1$), but in this case performed best under the Poisson distributed traffic scenario. The PE of all of the methods, became more similar at either high or low levels of traffic occupancy.

The PEs of the MC and NLMS methods were found to be similar for slow changing traffic ($\tau = 5$), with the MC method marginally better. However, for a faster varying traffic pattern ($\tau = 1$), the NLMS method was found to be better (particularly when $k = 1$ where PE was found to be between 5% and 11% better).

While PE is of primary importance to the proactive decision making process, the complexity of each method could influence its actual viability in a CRN. This will be discussed in Section 4.4.4.

© University of Pretoria

UNIVERSITEIT VAN PRETORIA
UNIVERSITY OF PRETORIA
YUNIBESITHI YA PRETORIA

4.4.4 Prediction performance: Complexity

To gain some insight into the complexity associated with predicting future PU behaviour, average execution times were simulated and normalised for each prediction method using unit length feature scaling. Only the stochastic PU traffic patterns were considered.

4.4.4.1 Observation and prediction length

The normalised simulation times for each prediction method are compared with RND, for various values of p and k, in Figure 4.9. Prediction method complexities, when $k = 1$ and $k = 10$, were illustrated on the left and right hand side of the figure respectively. Alternate exponentially distributed traffic was employed with $\tau = 1$ and a logarithmic scale was employed to highlight the differences between the most and least complex methods.

From these plots it can be seen that the MC method experienced the highest level of complexity particularly as p was increased. The NLMS method was found to be less complex than the MC method but did not experience significant increases in complexity with increasing values of p. The OW method was found to be much less complex than by the MC and NLMS methods and was either comparable or even less complex than employing RND. In general,

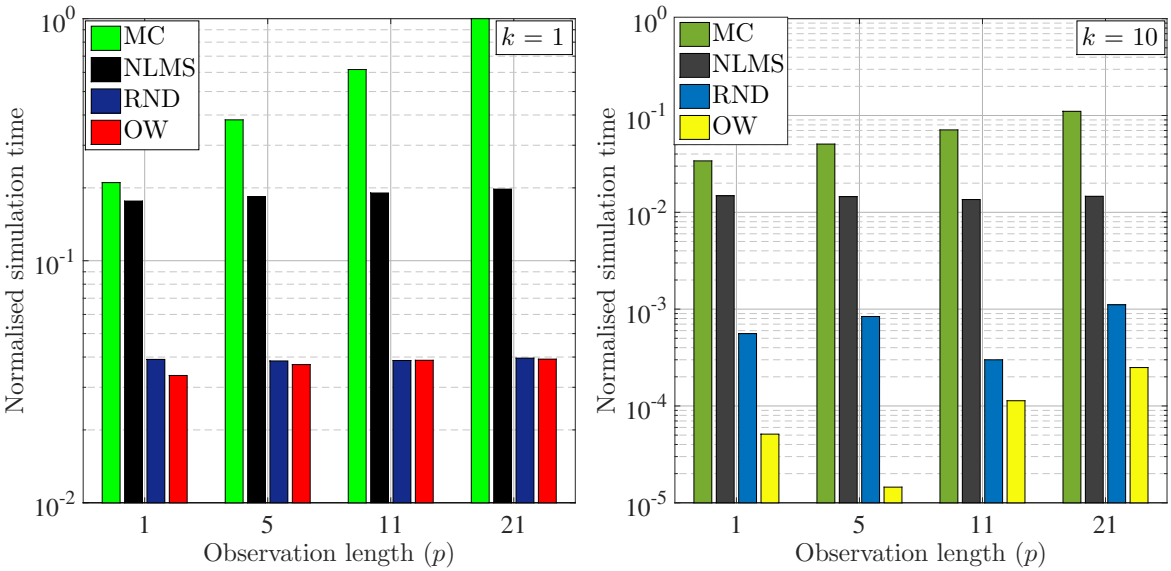

Figure 4.9: Normalised simulation times for each prediction method for various values of p and k (alternate exponentially distributed traffic when $\tau = 1$).

© University of Pretoria

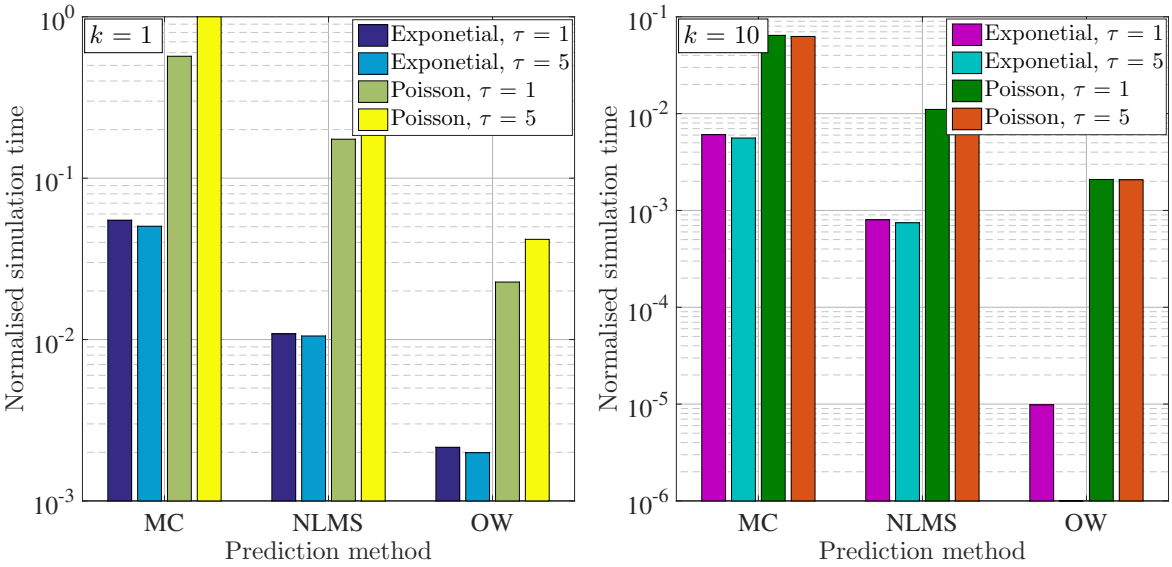

Figure 4.10: Comparison of normalised simulation times between different stochastic traffic distributions and pattern change rates for each prediction method (with $p = 21$).

all of the methods took proportionately longer to simulate when $k = 1$ than when $k = 10$. This was expected since predictions only needed to made every ten periods when $k = 10$ compared with every single period when $k = 1$.

4.4.4.2 Traffic distribution

Normalised simulation times, for different underlying traffic distributions and pattern change rates, are illustrated in Figure 4.10. The observation length was chosen to be $p = 21$. All three prediction methods experienced higher complexity for Poisson distributed traffic than for alternate exponentially distributed traffic. However, the traffic change rate τ did not seem to have any significant effect on complexity.

4.4.4.3 Channel occupancy

Normalised simulation times for all three prediction methods, for different levels of traffic occupancy, are illustrated in Figure 4.11. Poisson distributed traffic was employed with $\tau = 1$ and $p = 21$. Clearly, the level of channel occupancy had no effect on the complexity experienced by the MC and NLMS methods, while for the OW method only minor variations were observed.

© University of Pretoria

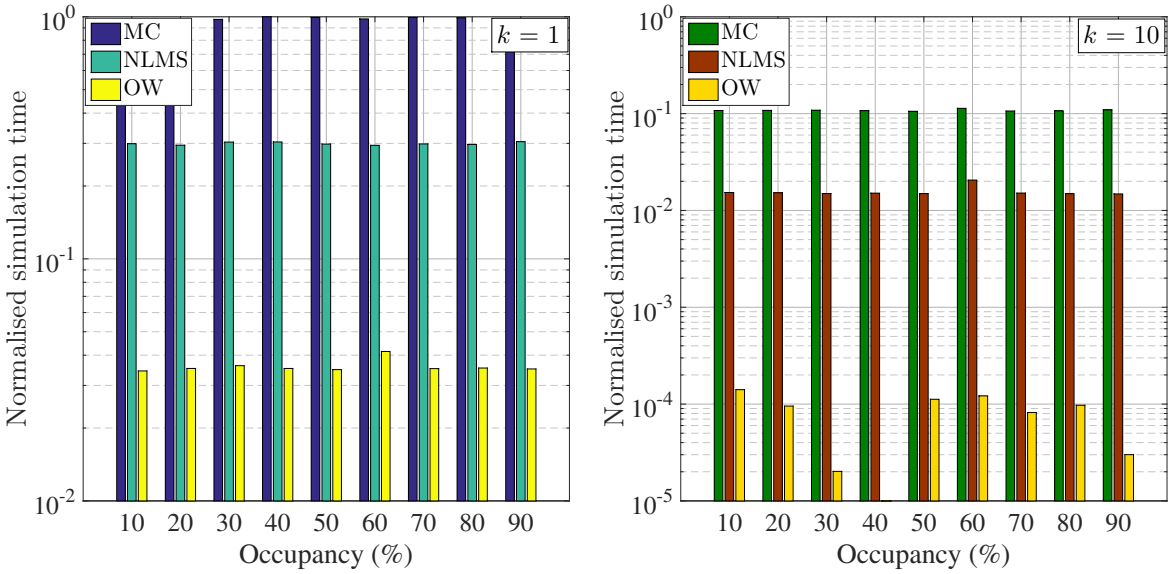

Figure 4.11: Normalised simulation times for different levels of channel occupancy for each prediction method (with $p = 21$ and $\tau = 1$).

4.5 CONCLUSION

In this chapter a simple method for predicting PU occupancy was proposed and compared with two other prediction methods in the literature. Both the accuracy and complexity of these methods was investigated for different PU traffic patterns. PU traffic pattern criteria included: Randomness, traffic distribution, channel occupancy and pattern change rate. Different observation and prediction lengths were also considered. The prediction methods were found to provide different levels of performance depending on the underlying traffic pattern. Although the MC and NLMS methods were generally found to be more accurate than the OW method, the OW method was found to either match or outperform the other methods under certain traffic conditions, e.g. under fast changing traffic conditions, when the traffic pattern becomes less random and when predictions are made further into the future (higher values of k). Also the OW method was consistently found to be significantly less complex than the other methods. Thus it can be concluded that under the right PU traffic conditions, the OW method would be well suited to a CR environment where complexity can be a performance limiting factor. This work forms the basis of the discussion that follows in Chapter 5 where the issue of exploiting SU diversity, to improve PE, will be investigated.

© University of Pretoria

CHAPTER 5

COOPERATIVE PREDICTION IN COGNITIVE RADIO NETWORKS

5.1 INTRODUCTION

In this chapter the premise that if collaboration between secondary users (SU) may improve the spectrum sensing (SS) process, then collaboration between SUs should also allow for better accuracy in the prediction process, is explored [111, 112]. Firstly a hard decision based model for performing cooperative prediction, where the results of individual SU predictions are fused together to make a combined prediction, is presented. Secondly, a sub-optimal cooperative forecasting algorithm has been formulated to minimise the likelihood of cooperative prediction error (CPE) and a heuristic for solving it proposed. Thirdly, the use of pre-fusion and post-fusion based prediction scenarios are introduced and their performance is compared with that of the single SU prediction scenario (this scenario was discussed in Chapter 4). Finally, the issue of algorithmic complexity in the prediction process is also dealt with. It is shown that diversity, both in terms of physical location and local forecasting accuracy, can be exploited to improve primary user (PU) prediction accuracy in a cognitive radio network (CRN). An optimal balance is sought between the accuracy that forecasting and cooperation provides and the costs and delays that this may introduce into the CRN.

The rest of this chapter is organised as follows: The system model that was considered, for the combination of cooperation and prediction, is described in Section 5.2. Techniques for collaboratively modelling and forecasting PU behaviour are discussed in Section 5.3. Optimal cooperative prediction is discussed in Section 5.4. Both the benefits and costs of cooperative

© University of Pretoria

UNIVERSITEIT VAN PRETORIA
UNIVERSITY OF PRETORIA
YUNIBESITHI YA PRETORIA

prediction are then quantified via the simulation results presented and discussed in Section 5.5. The chapter is then concluded in Section 5.6. Parts of this chapter were published in [127] and [124].

5.2 SYSTEM MODEL FOR COOPERATIVE PREDICTION

5.2.1 Prediction scenario

A scenario where multiple SUs cooperate to predict future spectrum availability is depicted in Figure 5.1. It is assumed that all cooperating SUs are aware of the radio environment within which they are operating and that they are willing to collaboratively analyse the same channels. The aim of this collaboration is to generate a forecast for the future availability of the band. The cooperative prediction scheme described in this chapter assumes the use of both a forecast engine (where predictions are made about future PU behaviour) as well as a fusion centre (FC) (where information from cooperating SUs is combined). Individual SUs perform SS, after which individual decisions are used to perform predictions based on information fusion. A decision is then made about the future availability of the band.

Two different cooperative fusion scenarios are illustrated in Figure 5.1. Namely a pre-fusion scenario (illustrated by the solid green arrows) where each SU performs prediction before fusion is performed and a post fusion scenario (indicated by the dashed blue arrows) where prediction is only performed after the SS results of each SU have already been combined. These fusion scenarios will be discussed in greater detail in Section 5.3.

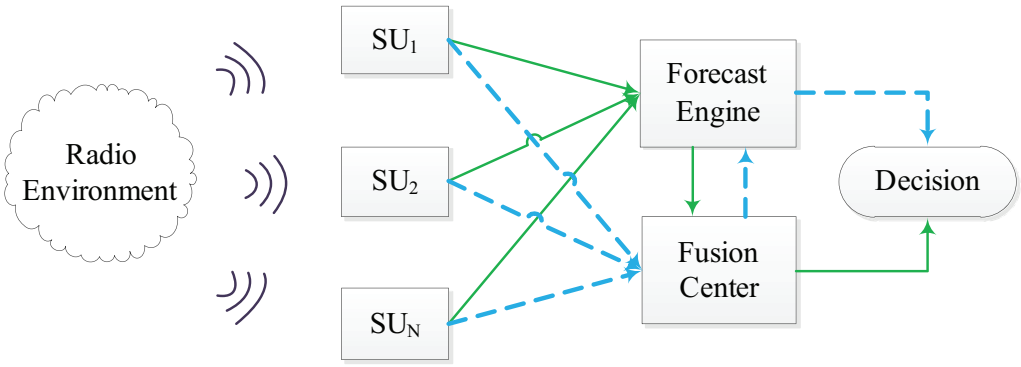

Figure 5.1: Cooperative prediction scenario.

© University of Pretoria

UNIVERSITEIT VAN PRETORIA
UNIVERSITY OF PRETORIA
YUNIBESITHI YA PRETORIA

5.2.2 Radio environment

Taking into account both large and small scale path loss, the received signal $r_i(n)$ at any SU i was assumed to be given by the following expression,

$$r_i(n) = x(n)a_i(n)L_i + \gamma(n), \tag{5.1}$$

where $x(n)$ is the transmitted PU signal, $a_i(n)$ is the fading on the channel between SU i and the PU base station (BS), $\gamma(n)$ is additive white Gaussian noise and L_i is the free space path loss experienced by SU i and was calculated according to the following expression,

$$L_i = \left(\frac{c}{4\pi d_i f_i}\right)^2, \tag{5.2}$$

where d_i is the distance in meters between the transmitting PU and the receiving SU i, f_i is the signal frequency in hertz and $c \approx 3 \times 10^8$ is the speed of light. A frequency flat fading environment has been assumed, where the channel follows a Rician distribution,

$$f_i(x) = \frac{x}{\sigma^2} \exp\left\{-\frac{x^2+\rho^2}{2\sigma^2}\right\} I_0\left\{\frac{x\rho}{\sigma^2}\right\}, \tag{5.3}$$

with Rician K-factor,

$$K = 10\log\left(\frac{\rho^2}{2\sigma^2}\right), \tag{5.4}$$

where ρ is the line of site amplitude, I_0 is the zero order modified Bessel function and σ^2 is the noise variance of the signal.

The geographical distribution of SUs, considered in this chapter, is illustrated in Figure 5.2. The green line represents the cell boundary of a PU BS (shown as a red square), while ten cooperating SUs are illustrated as blue circles. The radius of the PU cell is $R = 1.414$ km. Each SU, SU1 through SU10, has been assigned a different Rician K-factor ($K = [0; 18; 9; 1; 14.5; 4; 20; 6; 8; 12]$). The K-factor describes the severity of fading on the channel, which means that each SU will be able to detect PU activity with different degrees of success.

This grouping of SUs was chosen to represent a scenario where there was diversity amongst SUs with regard to their quality of received PU signal. A scenario like this was chosen based on the premise that diversity would be a key factor in the success of cooperative prediction. Preliminary investigations indicated that the cooperative prediction process would be less successful if the level of diversity amongst SUs were to be diminished.

© University of Pretoria

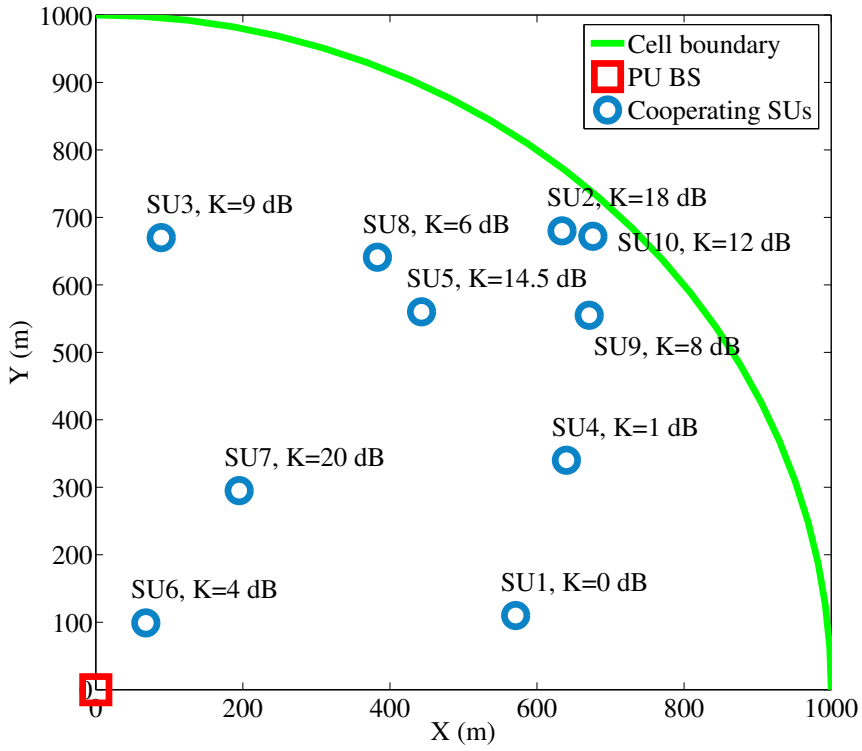

Figure 5.2: Geographical distribution of cooperating SUs

It is assumed that no errors are made when the SUs report either their individual SS or forecast results to the FC. Other large scale fading effects such as diffraction and scattering have been ignored. The assumption has also been made that channel conditions change at a slower rate than the time for which a prediction has been made, i.e. the PU traffic pattern must not change during the predicted time slots. A necessary condition, to support this assumption, is that SUs remain stationary during this time (the geographical distribution of SUs must remain constant so that no Doppler shift can interfere with the sensing and prediction process).

5.3 COOPERATIVE PREDICTION

The historical behaviour of PUs can be used to model and then predict future behaviour, as discussed in Chapter 4, which can in turn be used by CRs to make proactive decisions. Multiple SUs may be used to collaboratively perform forecasting. This forecast is obtained by fusing the SS data obtained by multiple SUs to obtain a single improved forecast. In this section the manner in which prediction and fusion are combined will be investigated.

© University of Pretoria

5.3.1 Single and multi-user prediction

In this chapter it will be assumed that, at time t, prediction may be performed by either a single SU i or by multiple concurrently active SUs. In the single SU case, prediction is performed by a single SU using $\boldsymbol{F}_{i,t,\vartheta}(r)$ from Equation (4.7) in Chapter 4. For the multiple SU case a set, comprised of N cooperating SUs, is used to calculate a combined forecast. Therefore, let the combined forecast, be denoted by $\boldsymbol{G}_{t,\vartheta}(r)$ such that,

$$\boldsymbol{G}_{t,\vartheta}(r) = C^N \left\{ \boldsymbol{F}_{i,t,\vartheta}(r) \right\}, \quad t+1 \leq r \leq t+k \tag{5.5}$$

where $C^N \{\cdot\}$ indicates a combination of N individual SU predictions, k is the number of future samples predicted, ϑ is the channel number for which the prediction is being made, $\{i, t, \vartheta, r, k\} \in \mathbb{N}$ and $\boldsymbol{F}_{i,t,\vartheta}(r) \in \{0, 1\}$.

5.3.1.1 Fusion rule

When more than one SU begins to collaborate ($N > 1$), then the process of forecasting becomes a function of multiple SUs. There are a number of ways in which the information collected by individual SUs may be combined.

One of the most popular approaches to cooperative SS in the literature is the M-out-of-N rule [128]. This is a voting-based fusion rule which can be extended to cooperative forecasting. In this approach, a forecast value of $\boldsymbol{G}_{t,\vartheta}(r) = 1$ is made if at least M out of the N cooperating SUs predict the presence of a PU. The forecast is thus given as,

$$\boldsymbol{G}_{t,\vartheta}(r) = \begin{cases} 1, & \sum_{i=1}^{N} \boldsymbol{F}_{i,t,\vartheta}(r) \geq M \\ 0, & \text{otherwise} \end{cases} \tag{5.6}$$

where $r = t+1, t+2, \ldots, t+k$. The M-out-of-N rule becomes the OR rule when $M = 1$, and the AND rule when $M = N$. When using this approach, a suitable value for M will need to be chosen. In this chapter, $M = \left\lceil \frac{N}{2} \right\rceil$ was used.

5.3.2 Fusion scenarios

Two fusion scenarios have been considered. In the first scenario, all collaborating SUs first perform prediction on a individual basis and then fuse their decisions (pre-fusion prediction).

© University of Pretoria

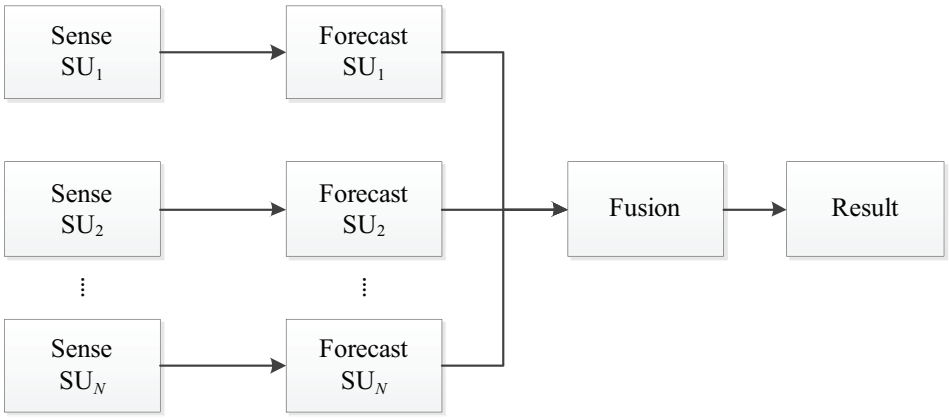

Figure 5.3: Pre-fusion cooperative prediction

In the second scenario, collaborating SUs first fuse historical PU data at the FC before performing a single prediction (post-fusion prediction).

5.3.2.1 Pre-fusion prediction

The pre-fusion prediction scenario is illustrated by the block diagram shown in Figure 5.3. Firstly, using Equation (4.1) in Chapter 4, each collaborating SU obtains a sequence of SS results $\boldsymbol{S}_{i,t,\vartheta}(n)$, which is followed by an individual prediction by each SU about future channel availability $\boldsymbol{F}_{i,t,\vartheta}(r)$. After the prediction process, all of the individual SU predictions are fused together to obtained a combined prediction result $\boldsymbol{G}_{t,\vartheta}(r)$. The expressions given in Equation (5.6) represents the pre-fusion prediction scenario.

5.3.2.2 Post-fusion prediction

The post-fusion prediction scenario is illustrated by the block diagram shown in Figure 5.4. All collaborating SUs perform SS to obtain a sequence of historical PU information $\boldsymbol{S}_{i,t,\vartheta}(r)$. This data is then immediately fused to obtain a collaborative SS decision $\boldsymbol{H}_{t,\vartheta}(r)$, which may be described by the following expression,

$$\boldsymbol{H}_{t,\vartheta}(n) = \begin{cases} 1, & \frac{1}{N}\sum_{i=1}^{N} \boldsymbol{S}_{i,t,\vartheta}(n) \geq M \\ 0, & \text{otherwise} \end{cases} \qquad 1 \leq n \leq p \tag{5.7}$$

where $\{n, p\} \in \mathbb{N}$, $\boldsymbol{H}_{t,\vartheta}(n) \in \{0, 1\}$ and p is the observation length described in Chapter 4. Only then is a single prediction made for future channel availability, using the result of the

© University of Pretoria

UNIVERSITEIT VAN PRETORIA
UNIVERSITY OF PRETORIA
YUNIBESITHI YA PRETORIA

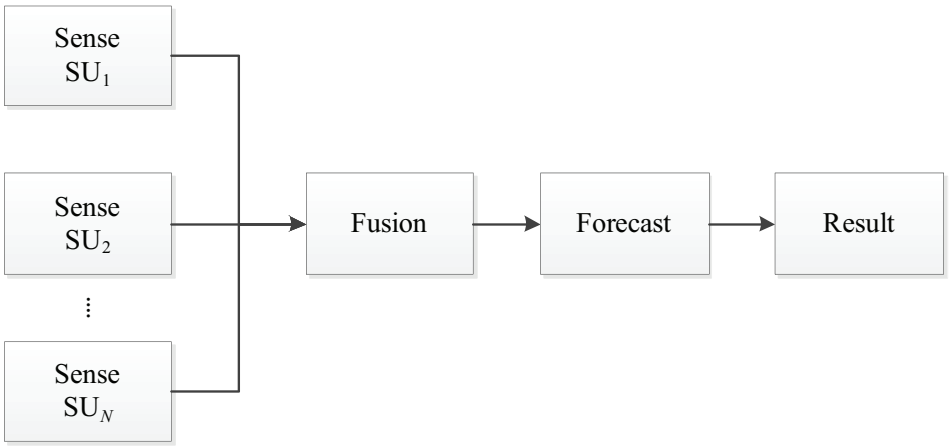

Figure 5.4: Post-fusion cooperative prediction.

combined SS decision, such that,

$$\boldsymbol{G}_{t,\vartheta}(r) = f\left(\boldsymbol{H}_{t,\vartheta}(n)\right), \quad t+1 \leq r \leq t+k, \quad 1 \leq n \leq p \tag{5.8}$$

where $\{r, k\} \in \mathbb{N}$ and $\boldsymbol{G}_{t,\vartheta}(r) \in \{0, 1\}$.

5.3.3 Prediction approach

The occupancy window prediction approach, described in Chapter 4, was employed to calculate the local prediction error $\bar{\epsilon}_{fr}$. This error does not take into account the possibility that the information it uses to make the prediction may be incorrect due to poor SS, but is simply a prediction of future PU traffic based on information obtained through SS by a single SU. Equation 4.15, from Chapter 4, may be used to calculate $\bar{\epsilon}_{fr}$. Each SU i will detect different versions of $\boldsymbol{S}_{i,t,\vartheta}(n)$ due to imperfect SS and may also experience variations in its ability to preform a local forecast. To allow for variations in local prediction error $\bar{\epsilon}_{fr}$, the local forecast error for a single SU i has been defined as,

$$\epsilon_{fr,i,t} = v_{i,t}\bar{\epsilon}_{fr}, \tag{5.9}$$

where $v_{i,t}$ is randomly chosen from a continuous uniform distribution with probability density function $f_v(x)$ and a lower boundary of ς, such that,

$$v_{i,t} = \varsigma + (1-\varsigma)f_v(x). \tag{5.10}$$

For the simulation results shown in Section 5.5.4, the lower boundary ς acts as a spreading factor that allows for accuracy variations among cooperating SUs.

© University of Pretoria

UNIVERSITEIT VAN PRETORIA
UNIVERSITY OF PRETORIA
YUNIBESITHI YA PRETORIA

5.4 OPTIMAL FORECASTING

The idea behind a cooperative prediction scheme is to minimise CPE by exploiting diversity amongst SUs. However, in order to so, it is necessary to perform predictions, and combine the data collected by cooperating SUs, in as optimal a fashion as possible. Therefore, an algorithm is presented in this section based on the system model and cooperative prediction approach described both in this chapter and in Chapter 4.

5.4.1 Problem formulation

Using Equation (5.8) the CPE at time t, denoted by $\epsilon_{cp,t}$, may be given as,

$$\epsilon_{cp,t} = \frac{\sum_{j=1}^{k} \boldsymbol{G}_{t,\vartheta}(j) - \boldsymbol{X}_{t,\vartheta}(j)}{k}, \tag{5.11}$$

where k is the number of future samples predicted and $\boldsymbol{X}_{t,\vartheta}(r)$ is the actual data sequence transmitted by the PU at time t on channel number ϑ. Since it is desirable to minimise $\epsilon_{cp,t}$, the cooperative prediction problem may be formulated as,

$$\begin{aligned}
\min_{\epsilon_{cp,t}} \quad & \epsilon_{cp,t} = \frac{\sum_{i=1}^{k} \boldsymbol{G}_{t}(i) - \boldsymbol{X}_{t}(i)}{k}, \\
\text{s.t.} \quad & 1 \leq n \leq p \\
& 1 \leq k \leq z \\
& 1 \leq i \leq N_{mx} \\
& 0 \leq \epsilon_{cp,t} \leq \bar{\epsilon}_{cp} \\
& n < t \leq \xi \\
& \rho, \nu \geq 1 \\
& 1 \leq \tau \leq \xi \\
& 0 \leq \varsigma \leq 1 \\
& p, k, n, z, i, t, \tau, \rho, \nu \in \mathbb{N} \\
& \boldsymbol{G}_{t,\vartheta}, \boldsymbol{X}_{t,\vartheta} \in \{0, 1\}.
\end{aligned} \tag{5.12}$$

In Equation (5.12), n is the number of observations gathered by the local prediction algorithm and may not exceed the limit of p observations, z is the maximum number of future samples that may be predicted, i is the number of cooperating SUs, N_{mx} is the maximum number of

© University of Pretoria

UNIVERSITEIT VAN PRETORIA
UNIVERSITY OF PRETORIA
YUNIBESITHI YA PRETORIA

cooperating SUs that may be combined, $\bar{\epsilon}_{cp}$ is the maximum error threshold for cooperative prediction, ξ is the maximum number of iterations allowed by the algorithm (assuming a single iteration at each time increment), ρ is the observation length resolution, ν is the amount by which i may be changed, τ is the iteration interval that determines the sign of ρ (discussed in the following subsection) and ς controls the variation in prediction accuracy experienced by individual SUs (using Equation 5.9).

5.4.2 Cooperative forecasting algorithm

A cooperative forecasting algorithm (CFA) can be employed to find a solution for Equation (5.12). A sub-optimal heuristic for this problem is proposed and described in Algorithm 2. In this case, it is assumed that cooperating SUs report their individual forecasts to a centralised FC to calculate $G_{t,\vartheta}(n)$.

The CFA begins by calculating $F_{i,t,\vartheta}(r)$ for a single SU ($i = 1$) at time $t = 0$, with $\{n, i, z\} = 1$ initially. It then enters a recursive process that begins by calculating $G_{t,\vartheta}(n)$ for SU i and the corresponding value for $\epsilon_{cp,t}$ ($G_{t,\vartheta}(r) = F_{i,t,\vartheta}(r)$ at $t = 0$). If $\epsilon_{cp,t}$ is found to be greater than the cooperative error threshold $\bar{\epsilon}_{cp}$ on the first iteration of the loop ($t = 0$), then the CFA will increase i and n by an amount ρ and ν respectively $\rho, \nu \in \mathbb{N}$ (these variables represent the amount by which i and n will be adjusted at each iteration of the CFA).

This process is repeated for τ iterations. If after τ iterations $\epsilon_{cp,t} > \epsilon_{cp,t-\tau}$, then n is decreased by ρ and i is kept constant to allow for the possibility that increasing n may actually degrade prediction performance. This is repeated until either $\epsilon_{cp,t} \leq \epsilon_{cp,t-\tau}$ or $n \leq \rho$. Thereafter either both i and n are increased (when $i < N_{mx}$) or only n is increased (if $i = N_{mx}$), at every iteration of the algorithm.

The CFA repeats itself until one of the stopping criteria are met: Either a lower cooperative prediction error than the threshold is found $\epsilon_{cp,t} \leq \bar{\epsilon}_{cp}$, the maximum number of historical observations has been exceeded $n > p$, the maximum number of cooperating SU has been exceeded $i > N_{mx}$ or the maximum number of iterations allowed by the algorithm has been reached $t > \xi$.

© University of Pretoria

Algorithm 2 Cooperative forecasting algorithm.

$t = 0$
$\{n, i, z\} = 1$
Compute $\boldsymbol{F}_{i,t,\vartheta}(r)$ from Equation (4.7)
while $(\epsilon_{cp,t} > \bar{\epsilon}_{cp})$ AND $(n \leq p)$ AND $(i \leq N_{mx})$ AND $(t \leq \xi)$ **do**
    Compute $\boldsymbol{G}_{t,\vartheta}(r)$ from Equation (5.5)
    Compute $\epsilon_{cp,t}$ from Equation (5.12)
    if $(\epsilon_{cp,t} \leq \bar{\epsilon}_{cp})$ **then**
        $n = n$
        $i = i$
        return $\epsilon_{cp,t}$ and $\boldsymbol{G}_{t,\vartheta}(r)$
    else if $\epsilon_{cp,t} > \bar{\epsilon}_{cp}$ **then**
        if $(t > \delta)$ **then**
            if $(\epsilon_{cp,t} > \epsilon_{cp,t-\delta})$ AND $(n > \rho)$ **then**
                $n = n - \rho$
                $i = i$
            else
                if $(i < N_{mx})$ **then**
                $n = n + \rho$
                $i = i + \nu$
                else
                $n = n + \rho$
                $i = i$
                end if
            end if
        else
            $n = n + \rho$
            $i = i + \nu$
        end if
    end if
    $t++$
end while

© University of Pretoria

UNIVERSITEIT VAN PRETORIA
UNIVERSITY OF PRETORIA
YUNIBESITHI YA PRETORIA

5.5 SIMULATION RESULTS

In this section, simulation results are presented to verify the performance of the suggested cooperative prediction techniques and illustrate the benefits of diversity in the prediction process. Using MATLAB, four different simulations were performed: Firstly to investigate the accuracy of the maximum normal fit (MNF) method as applied to the system model described in this chapter, secondly to investigate cooperative prediction accuracy, thirdly to show how optimisation can improve CPE and fourthly to quantify the costs and delays that this may introduce into the CRN.

5.5.1 Simulation environment

5.5.1.1 Spectrum sensing parameters

The first simulation was run to investigate the performance of the MNF method, described in Section 3.2.1. This simulation was run to generate the test data, based on the system model described in this chapter, from which the rest of the simulations could be performed. SS results were obtained for the ten different SU scenarios depicted in Figure 5.2, for a signal-to-noise ratio (SNR) range of $\gamma = [0, 30]$ dB in 2 dB increments. The observation length was fixed at $p = 10$ for this simulation.

5.5.1.2 Cooperative prediction parameters

The second simulation investigated the performance of cooperative prediction when compared with prediction by a single SU as the number of cooperating SUs i was increased up to $N = 10$. The difference between the prediction performance of the pre-fusion and post-fusion prediction scenarios was compared over an SNR range of $\gamma = [-4, 28]$ (8 dB increments). The probability of correct local forecast $P_{fr,i,t} = 1 - \bar{\epsilon}_{fr} = \overline{P}_{fr}$ was assumed to be equal amongst SUs, i.e. $\varsigma = 1$, and four fixed levels of local prediction accuracy $\overline{P}_{fr,t} = [0.6; 0.7; 0.8; 0.9]$ were considered. These parameters are summarised in Table 5.2 and Table 5.3.

© University of Pretoria

UNIVERSITEIT VAN PRETORIA
UNIVERSITY OF PRETORIA
YUNIBESITHI YA PRETORIA

Table 5.1: General simulation parameters for all four computer simulations.

Parameter	p	ξ	N_{mx}	τ	ρ	z	ν	$\overline{\epsilon}_{cp}$
Value	25	17	10	3	2	1	1	0

5.5.1.3 Parameters for optimal forecasting

The third simulation investigated the performance of the CFA. The values used for $\overline{\epsilon}_{fr}$ were based on those presented in [123] and only odd numbered values of n were considered ($n \in 2\mathbb{N}-1$). Diversity in local forecast accuracy was facilitated by selecting various values for ς such that $\varsigma = [0.0; 0.2; 0.4; 0.6; 0.8; 1.0]$. Limits of $p = 25$, $k = 1$, $N_{mx} = 10$, $\overline{\epsilon}_{cp} = 0$, $\rho = 2$, $\nu = 1$ and $\xi = 17$ were set. Through a process of trial an error, $\tau = 3$ was chosen to allow for both positive and negative adjustments of n in the CFA.

5.5.1.4 General parameters

All of the simulations were run for a length of $T = 60000$ time samples. For the first and third simulations, the CRN environment consisted of $\vartheta = 100$ channels spaced 200 kHz apart, beginning at $f_0 = 700$ MHz. The transmit power of the PU BS was set to $P_{tx} = 30$ W. The

Table 5.2: General simulation parameters for all four computer simulations.

Parameter	Value
T	60000 time samples
$\overline{P}_{fr}$	[0.6; 0.7; 0.8; 0.9]
ς	[0.0; 0.2; 0.4; 0.6; 0.8; 1.0]
L_i (dB)	70.9, 80.3, 81.6, 85.9, 86.4,
	86.5, 86.8, 88.1, 88.7, 88.9
K	[0; 18; 9; 1; 14.5; 4; 20; 6; 8; 12]
$\overline{\epsilon}_{fr}$	[0.303; 0.281; 0.236; 0.216; 0.187; 0.178;
	0.177; 0.174; 0.171; 0.168; 0.164; 0.169; 0.173]

© University of Pretoria

Table 5.3: Simulation parameters for the third simulation: CPA performance.

Parameter	N	P_{tx} (W)	BW (kHz)	f_0 (MHz)	R (m)	γ (dB)	ϑ	M
Value	10	30	200	700	1414	[-4, 28]	100	$\left\lceil \frac{N}{2} \right\rceil = 5$

$N = 10$ SUs were randomly distributed within a quarter circle with radius $R = 1414$m. The calculated free space path loss L_i and the assigned Rician K-factor K_i for each SU are listed in Table 5.2. For the fusion rule $M = \left\lceil \frac{N}{2} \right\rceil = 5$ was employed.

5.5.2 Spectrum sensing performance

Simulations were run to test the performance of the MNF method, described in Section 3.2.1. The individual noise thresholds λ_i and the resulting probabilities of error $P_{e,i}$ were calculated, as described in Section 2.3.3.2, for each of the SUs shown in Figure 5.2. The calculated values for λ_i (shown in dBm) have been plotted on the left hand side of Figure 5.5, while the SS error probabilities $P_{e,i}$ have been plotted on the right hand side. A plot comparing the probability of detection $P_{d,i}$ to the probability of false alarm $P_{f,i}$ for each SU, for various SNR values, is provided in Figure 5.6.

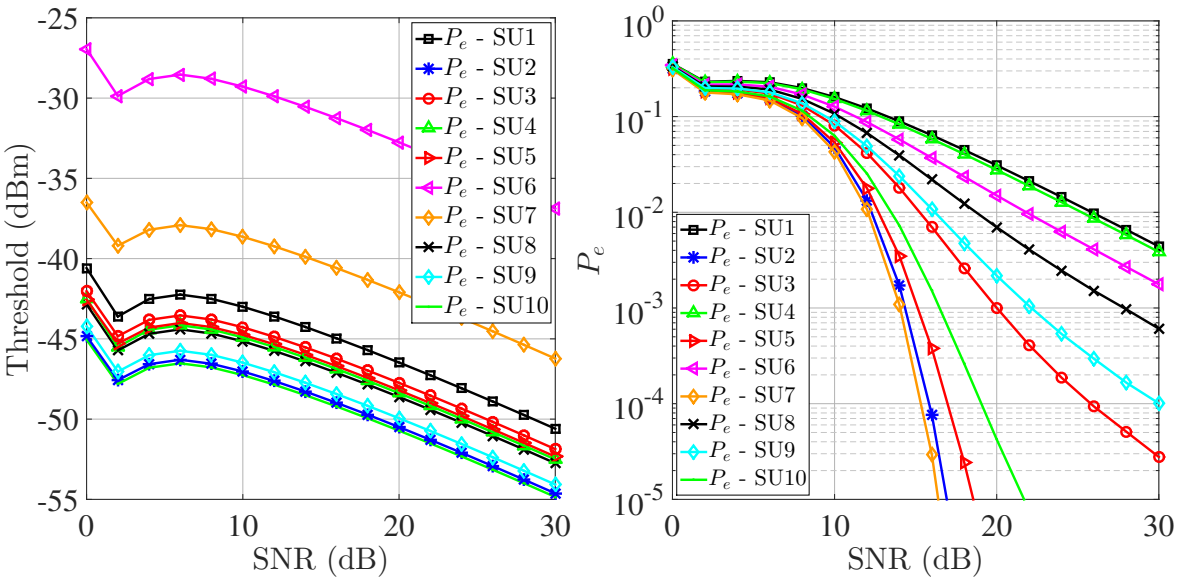

Figure 5.5: Calculated detection thresholds (left) and SS error probabilities (right), as SNR is increased, for the SUs described in Section 5.2.2.

© University of Pretoria

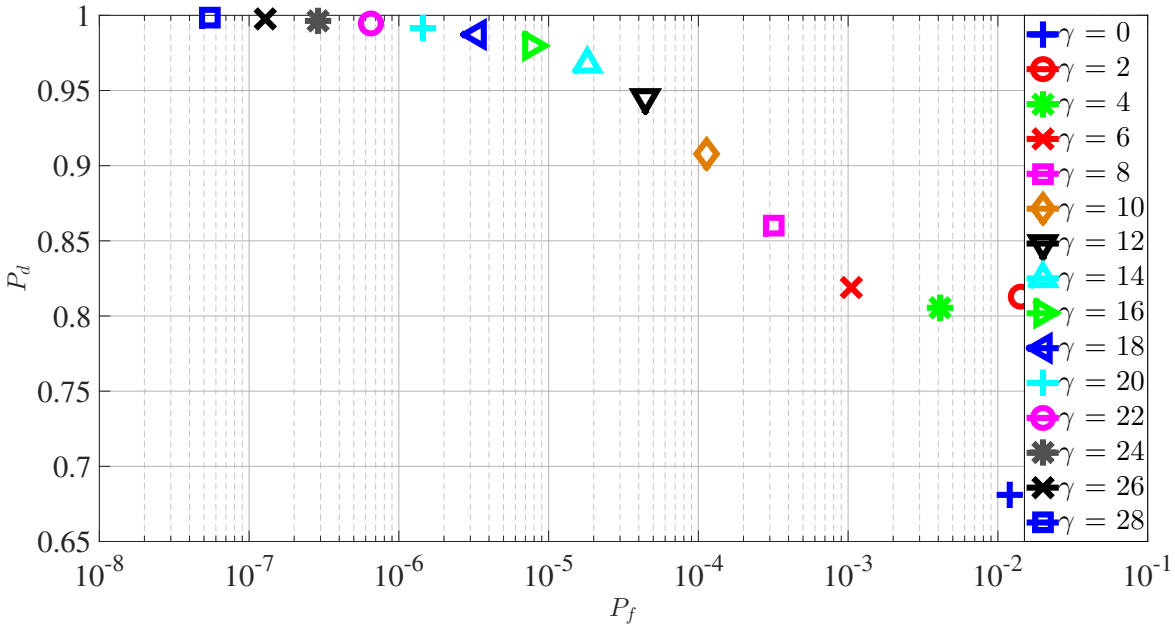

Figure 5.6: Single SU SS performance as SNR is increased: P_d vs. P_f.

The calculated threshold values λ_i exhibited an approximately inverse proportional relationship to SNR. However, this was not found to be true for SNR values below $\gamma = 6$ dB (since there is a greater overlap between the distributions of the information bearing and noise components of the signal, it becomes harder to calculate estimates for μ_s, σ_s^2 and σ_n^2 when $\gamma \leq 6$ dB). As expected $P_{e,i}$ improves as both the SNR and Rician K-factor are increased, since it becomes easier to estimate λ_i.

The $P_{e,i}$ values represent the ability that each SU has to detect the presence of the PU, based on the quality of the signal that it can detect, and were used as the basis of the cooperative prediction simulations that will be described in the remainder of this chapter.

5.5.3 Cooperative prediction performance

To quantify the benefit that cooperation brings to the prediction process, simulations were run that compared the CPE that could be obtained by employing both pre-fusion prediction (PRF) and post-fusion prediction (POF) as compared with the no-fusion scenario (NOF). For the PRF and POF scenarios all ten SUs where employed in the prediction process, while for the NOF scenario prediction was performed using only SU1 (shown in Figure 5.2). SU1 was used for the NOF scenario as it was the SU that was least able to detect the presence

© University of Pretoria

of the PU due to the poor channel conditions at its geographical location. The simulations were run for the range of SNR values listed in Table 5.3.

Each scenario was tested for a range of forecast probabilities $P_{fr} = [0.6; 0.7; 0.8; 0.9; 1.0]$. P_{fr} is the probability that a correct forecast was made by SU i and is the inverse of the prediction error (PE), discussed in Chapter 4, such that $P_{fr} = 1-\text{PE}$. Thus $P_{fr} = 0.6$ represents a poor prediction with a PE of 40%, while $P_{fr} = 1.0$ represents a perfect prediction with a PE of 0%.

5.5.3.1 The influence of local prediction error

The PRF results are illustrated in Figure 5.7, the POF results in Figure 5.8 and the NOF results in Figure 5.9. For these plots, the number of cooperating SUs was fixed at $i = 10$. For all three scenarios, the CPE improves exponentially as both the SNR and P_{fr} are increased. However, this reduction in CPE is larger when fusion is employed for prediction, most notably when the PRF scenario is adopted. When fusion is employed the CPE can be reduced to a value that is below the P_{fr} of the individuals SUs, as SNR is increased.

For the PRF scenario, the CPE when $P_{fr} < 1.0$ continues to improve with an increase in SNR until it reaches its best value around $\gamma = 24$ dB. For the POF scenario, however, the best

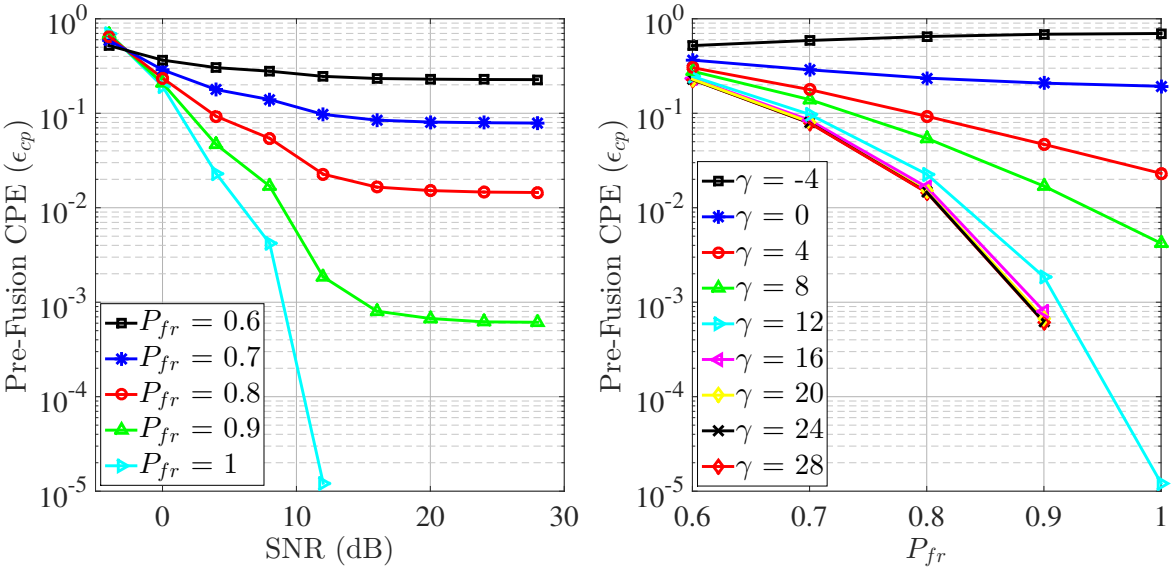

Figure 5.7: Cooperative prediction error for the pre-fusion scenario.

© University of Pretoria

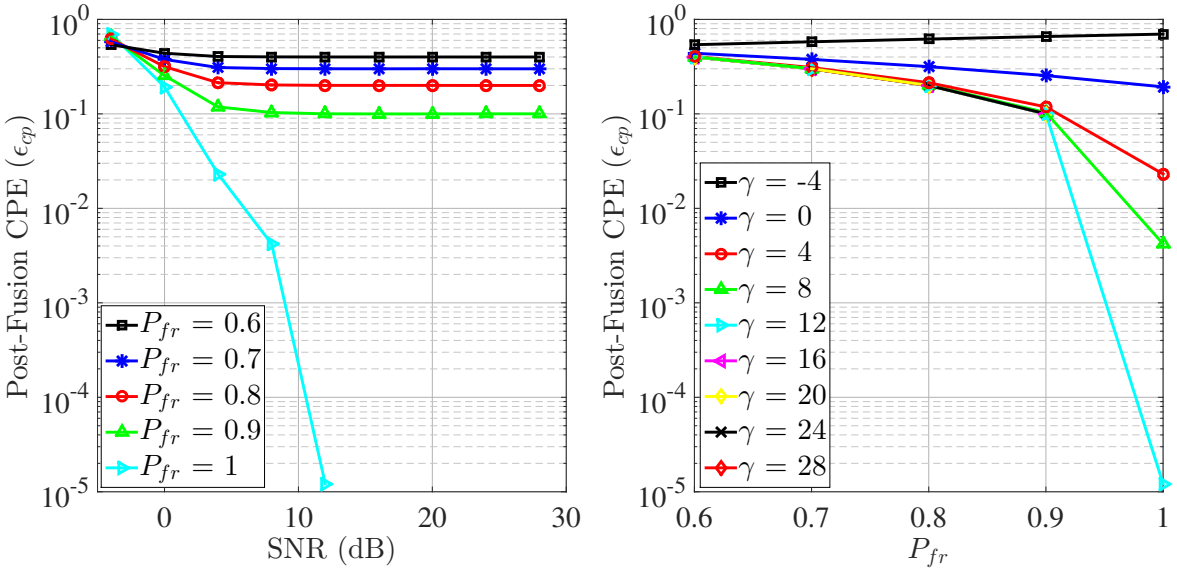

Figure 5.8: Cooperative prediction error for the post-fusion scenario.

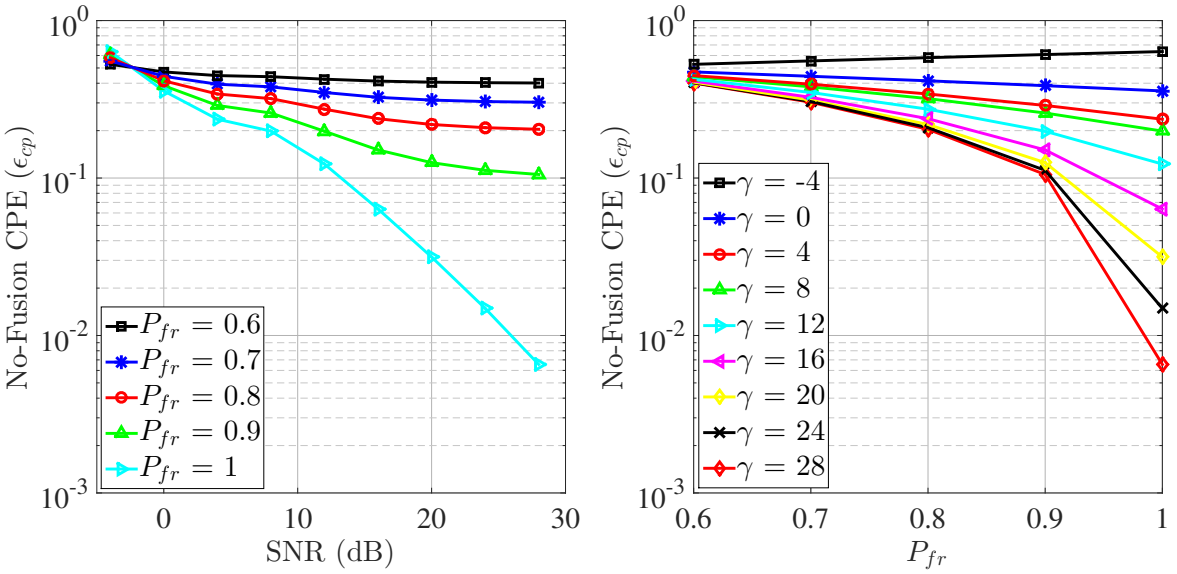

Figure 5.9: Cooperative prediction error when fusion is not employed.

CPE is reached much earlier at around $\gamma = 8$ dB. This means that there is a benefit derived from fusion for a much wider range of noise conditions under the PRF scenario. Improved PE, due to cooperation, is evident at SNRs as low as $\gamma = 0$ dB.

Selected results have been listed in Table 5.4 to highlight how much PE can be reduced by employing cooperative prediction. A CPE comparison is made for SNR values of $\gamma = 4$ and $\gamma = 16$, and for $P_{fr} = 0.7$ and $P_{fr} = 0.9$. When $\gamma = 4$ dB, the POF scenario led to a CPE

© University of Pretoria

UNIVERSITEIT VAN PRETORIA
UNIVERSITY OF PRETORIA
YUNIBESITHI YA PRETORIA

Table 5.4: Selected PE results that highlight the benefit of cooperation.

Scenario	$P_{fr} = 0.7$		$P_{fr} = 0.9$	
	$\gamma = 4$	$\gamma = 16$	$\gamma = 4$	$\gamma = 16$
Single				
SU1	39.43	32.55	28.90	15.08
Fusion				
POF	30.94	29.98	11.84	9.99
PRF	17.81	8.46	4.69	0.08
Reduction				
POF	8.49	2.57	17.06	5.09
PRF	21.62	24.09	24.21	15.00

reduction of 8.49% and 17.06%, for $P_{fr} = 0.7$ and $P_{fr} = 0.9$ respectively. However, the CPE was reduced by 21.62% and 24.21% respectively, for the PRF scenario. When $\gamma = 16$, the difference between PRF and POF was even larger.

Thus it can be concluded that the PRF scenario provided much larger reductions in CPE than the POF scenario, while it was clear that both fusion scenarios are of benefit to the prediction process.

5.5.3.2 Population size

Three dimensional plots, where CPE is plotted against both SNR and the number of co-operating SUs employed to perform prediction, are presented in Figure 5.10 and Figure 5.11. Each plot represents a different value for $\overline{P}_{fr}$ (in this case the same for all SUs, i.e. $\varsigma = 1$). The simulated CPE for a low to medium level of local forecast accuracy are illustrated in Figure 5.10 and for a medium to high level of local forecast accuracy in Figure 5.11. The CPE axes of each plot have been inverted to improve readability and only the PRF fusion scenario was considered.

In all four scenarios, the CPE improved exponentially as γ was increased, as previously

© University of Pretoria

UNIVERSITEIT VAN PRETORIA
UNIVERSITY OF PRETORIA
YUNIBESITHI YA PRETORIA

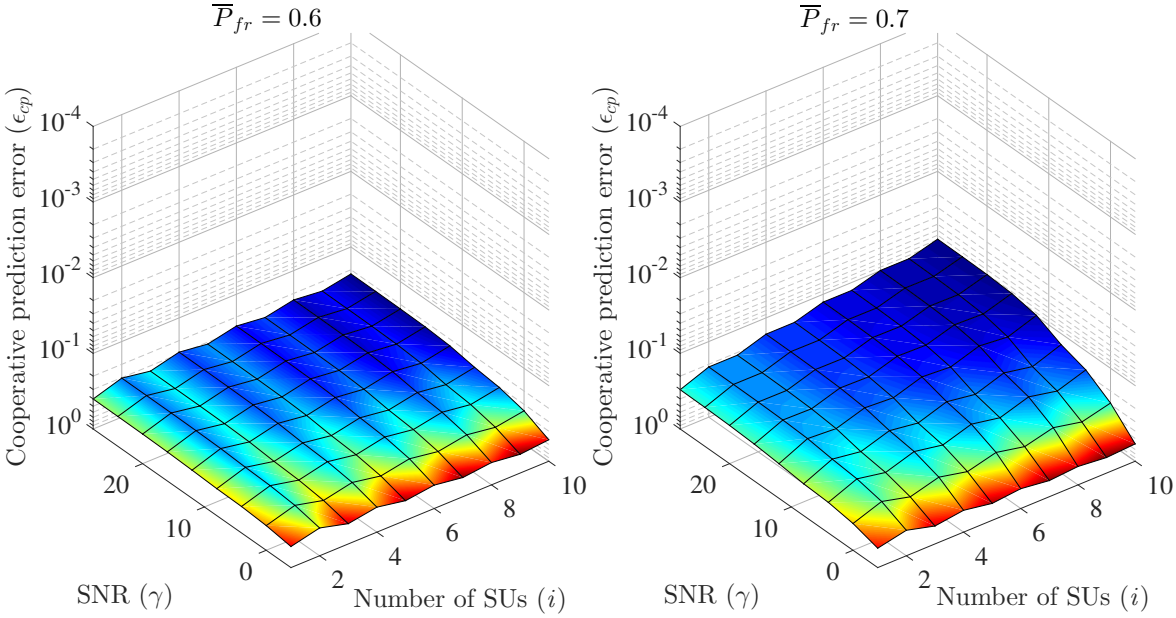

Figure 5.10: Cooperative prediction error for PRF when $\overline{P}_{fr} = [0.6; 0.7]$.

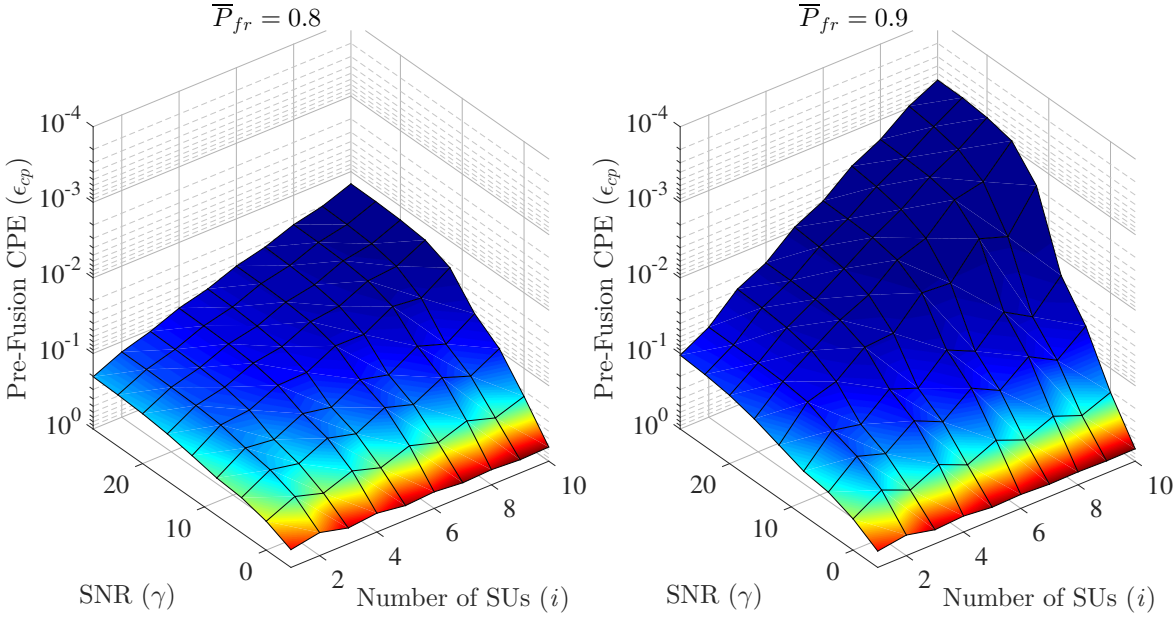

Figure 5.11: Cooperative prediction error for PRF when $\overline{P}_{fr} = [0.8; 0.9]$.

illustrated. This improvement was compounded by a linear improvement in ϵ_{cp} as the number of cooperating SUs i was increased. However, the real benefit of cooperation was only realised for higher values of P_{fr} for which the gains due to both increasing γ and i improved with local prediction accuracy. This can be quantified by comparing the minimum values obtained for ϵ_{cp} ($i = 10$ and $\gamma = 28$). When $P_{fr} = 0.6$, this was $\epsilon_{cp} = 0.227$ and when $P_{fr} = 0.9$, it had improved to $\epsilon_{cp} = 6.135 \times 10^{-4}$. Clearly the prediction gains due to SU diversity were much more pronounced for high values of $\overline{P}_{cp}$ than when local prediction was performed

© University of Pretoria

poorly.

The benefit of SU cooperation, for higher local prediction accuracy, can clearly be seen in the bottom plot of Figure 5.11 ($\overline{P}_{fr} = 0.9$). When $\gamma = 16$, a forecast error of $\epsilon_{cp} = 6.723 \times 10^{-4}$ was observed for $i = 10$ cooperating SUs compared with $\epsilon_{cp} = 0.151$ for SU1 attempting to make a forecast on its own. The corresponding benefit of SU cooperation was much lower when local forecast accuracy was poor ($\overline{P}_{fr} = 0.6$). Values of $\epsilon_{cp} = 0.2333$ and $\epsilon_{cp} = 0.4128$ were obtained respectively.

5.5.4 Optimal cooperative prediction

The CFA was used to calculate the results presented in Figure 5.12 and Figure 5.13.

5.5.4.1 Uniform local prediction error

In Figure 5.12, the CPE is illustrated for the case where $\varsigma = 1$, i.e. for no diversity in local forecast error $\epsilon_{fr,i,t}$. Values for ϵ_{cp} have been plotted, on the left hand side of the figure, for each iteration of the CFA for various values of γ. The corresponding values for variables i and n are illustrated on the right hand side of the figure. From these plots it can been

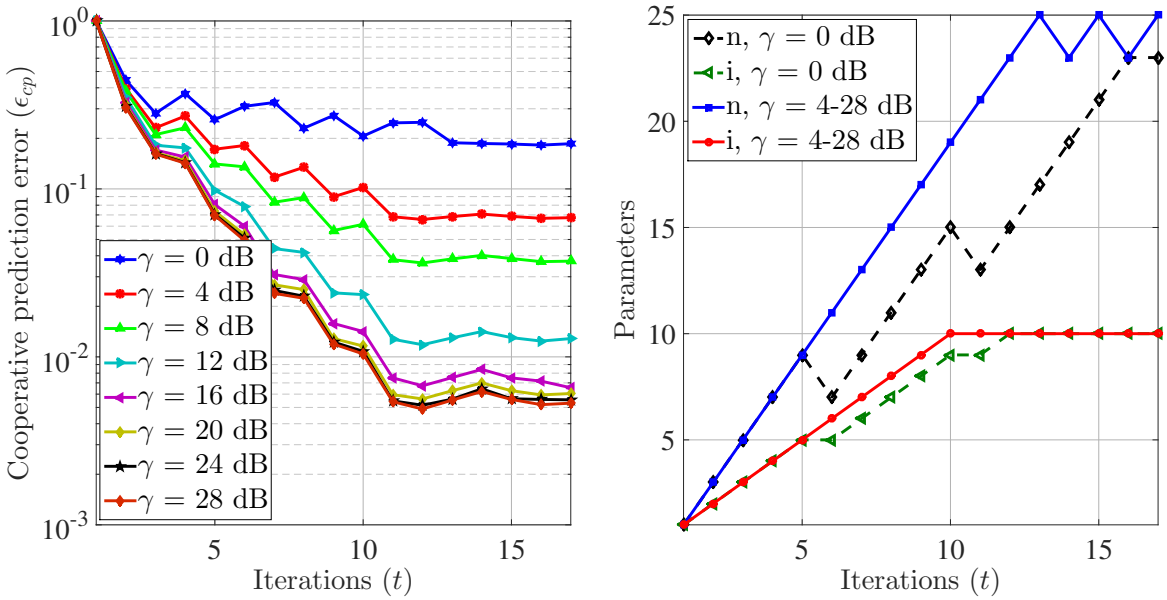

Figure 5.12: Cooperative prediction error at each iteration of the CFA for different values of γ (left) and the corresponding values for parameters i and n (right).

© University of Pretoria

UNIVERSITEIT VAN PRETORIA
UNIVERSITY OF PRETORIA
YUNIBESITHI YA PRETORIA

seen that ϵ_{cp} generally improved as the algorithm was iterated, reaching the optimal solution when $t = 12$ after which no further improvement was made. This could be seen for all values of γ, where i and n steadily increased up to their optimal values, except for when $\gamma = 0$ dB. When $\gamma = 0$ dB, i and n sometimes had to be decreased to cope with local SS inaccuracies. This meant that it took longer to find the optimal solution, which was only reached when $t = 16$.

5.5.4.2 Local prediction error diversity

In Figure 5.13 the effect of diverse local prediction accuracy, when $\varsigma = [0, 1]$, is illustrated. Using the CFA, the optimal value obtained for ϵ_{cp} is compared over a range of SNR values and for different values of ς. Clearly diversity in the ability of SUs to perform local forecasts lead to a improvement in the CPE. For example, for $\gamma = 16$ dB, the CPE obtained when $\varsigma = 1.0$ was $\epsilon_{cp} = 6.405 \times 10^{-3}$, but due to diversity it had been reduced to $\epsilon_{cp} = 3.800 \times 10^{-5}$ when $\varsigma = 0.0$.

For lower SNR values there was an approximately exponential decrease in ϵ_{cp} with SNR, which

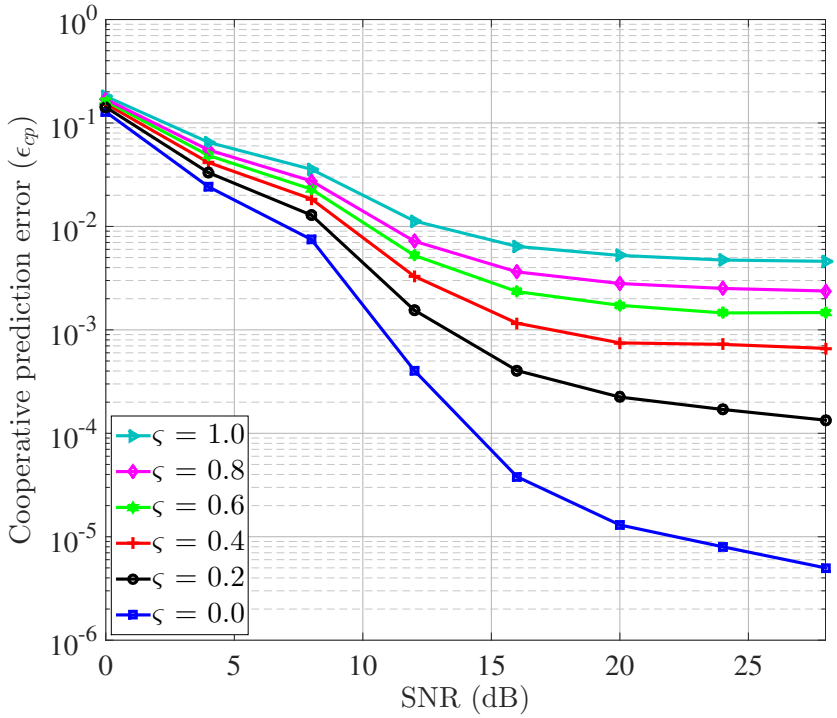

Figure 5.13: Cooperative prediction error with local forecast diversity.

© University of Pretoria

then began to flatten out as SNR became larger. For $\varsigma = [0.4; 0.6; 0.8; 1.0]$, the minimum value for ϵ_{cp} appeared to have been reached when $\gamma = 24$ dB. However, ϵ_{cp} was still decreasing at $\gamma = 28$ dB for a large diversity in local forecast accuracy ($\varsigma = [0.0; 0.2]$).

5.5.5 The cost of cooperative forecast

Although obtaining the lowest possible CPE is important, the cost associated with doing so must also be considered. Many CR functions are time critical and would be negatively affected if the SS and prediction process were to be an over complicated and time consuming process. Estimates for the complexities associated with each fusion scenario, over a range of local forecast accuracies, are illustrated in Fig 5.14. These estimates were calculated by normalising average simulation times using unit length feature scaling. Selected complexity results are also listed in Table 5.5, to complement Figure 5.14.

As may be expected, there was a price to pay for the improvement in prediction accuracy due to fusion. For the PRF scenario, the most accurate approach, fusion was found to be 10.7 times more complex than for the NOF scenario (when $P_{fr} = 0.8$). However, the POF scenario was found to be only 1.3 times more complex than the NOF scenario.

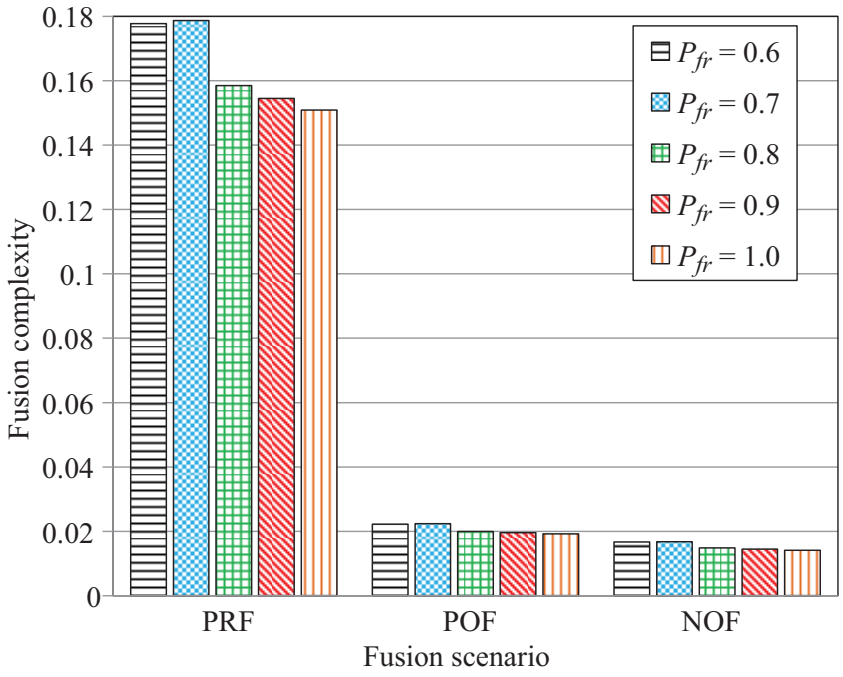

Figure 5.14: Estimated complexity of (a) prediction method and (b) fusion scenario.

© University of Pretoria

UNIVERSITEIT VAN PRETORIA
UNIVERSITY OF PRETORIA
YUNIBESITHI YA PRETORIA

Table 5.5: Selected complexity estimates for the prediction methods and fusion scenarios.

Scenario	$P_{fr} = 0.6$	$P_{fr} = 0.7$	$P_{fr} = 0.8$	$P_{fr} = 0.9$
PRF	0.178	0.179	0.158	0.154
POF	0.022	0.022	0.020	0.020
NOF	0.017	0.017	0.015	0.014

Therefore, when performing cooperative prediction it is important to select the correct combination of prediction method and fusion scenario, so as to ensure a reasonable balance between prediction accuracy and complexity.

5.6 CONCLUSION

In this chapter it was shown that cooperation allowed SUs to predict PU behaviour with greater accuracy than they would have on their own. The performance of various prediction methods and cooperative prediction fusion scenarios were investigated for different PU traffic conditions. A sub-optimal cooperative forecasting algorithm was also presented. From the simulation results obtained, cooperative prediction was shown to provide greater accuracy than when a single SU, experiencing poor channel conditions, was used to predict PU activity. The pre-fusion fusion scenario was clearly found to provide greater accuracy than the post fusion scenario, however, this was achieved at a significant increase in required computational complexity. A trade-off was thus found to exist between cooperative prediction accuracy and computational complexity. The CPA was also found to be effective at reducing CPE even further. In Chapter 6 the benefit of forecasting, with regard to energy efficiency in a network of cooperating SUs, will be investigated.

© University of Pretoria

CHAPTER 6

FORECASTING FOR ENERGY EFFICIENT SPECTRUM SENSING

6.1 INTRODUCTION

Since it was shown in [129] that sensing devices consume significantly more power when they are active, it may be concluded that the spectrum sensing (SS) process increases the energy consumption of sensing devices. More often than not, these devices will be energy constrained [130, 131]. Thus excessive SS, although critical for providing accurate information about the radio environment, may lead to premature depletion of the sensing devices battery and consequently shorten its lifetime [64]. Energy efficiency (EE) is thus a pertinent issue in a cognitive radio network (CRN) [132].

In [64] an optimal scheduling method for sensor node activation was proposed in an attempt at maximising the network lifetime (collective lifetime of all cooperating sensor nodes in the network) of a cooperative SS based CRN by minimising the active time of each sensor node. However, forecasting as a technique for reducing the amount of time spent on SS, was not considered. If accurate predictions can be made regarding the availability of spectral white spaces, then these predictions may allow for a reduction in SS regularity [12, 80]. Forecast values could be used to replace SS events, and a reduction in SS events could allow for lower overall power consumption in the sensor node network. For the rest of this chapter, primary user traffic prediction will be referred to as spectral opportunity forecasting (SOF).

In this chapter, a contribution is made through an investigation into the integration of the work presented in Chapter 4 on SOF and optimal scheduling for sensor node activation [64]

© University of Pretoria

UNIVERSITEIT VAN PRETORIA
UNIVERSITY OF PRETORIA
YUNIBESITHI YA PRETORIA

with the aim of further increasing sensor network lifetime. The idea that total network lifetime can be maximised by minimising the number of sensor nodes that need to be activated at any given time, is explored. The idea that the network lifetime of cooperating sensing devices could be even further increased, by replacing SS operations by forecast values, is demonstrated in this chapter. Mathematical expressions, that describe the relationship between SOF accuracy, the probability of detection and the probability of false alarm, have thus been derived and used to characterise the effect that the introduction of SOF has on sensor network lifetime. Promising simulation results were obtained that show a significant improvement in the collective lifetime of the sensor node network when SOF was introduced.

This chapter is organised as follows: Optimal scheduling for sensor node activation is summarised in Section 6.2. SOF and how it can be integrated into a cooperative SS framework is discussed in Section 6.3. Simulation results are presented in Section 6.4. Finally, conclusions are drawn in Section 6.5. This chapter is based on the work published in [133].

6.2 OPTIMAL SENSOR NODE ACTIVATION

Consider a CRN scenario, as illustrated in Figure 6.1, consisting of M secondary sensing nodes $S = [s_1, s_2, \ldots, s_M]$, where each node reports its individual decision to a centralised fusion centre (FC). If each node can be activated in such a way that only the minimum number of nodes needs to perform SS at the same time, then the energy consumption and thus the lifetime, of this network of cooperating secondary users (SU) can be prolonged.

6.2.1 Problem formulation

This chapter is based on an optimal scheduling problem for sensor node activation, presented in [64], that was aimed at maximising network lifetime. To maximise network lifetime, the nodes in the network needed to be activated so as to minimise energy consumption. The sensors were thus grouped into a series of non-disjoint subsets $S_1, S_2, \ldots, S_K$ with time coefficients $t_1, t_2, \ldots, t_K \in (0, 1]$ such that the network lifetime was given as,

$$T_N = t_1 + t_2 + \ldots + t_K. \tag{6.1}$$

The subsets that allowed the minimum number of sensors to be activated, while still adhering to cooperative detection and false alarm thresholds, where then selected. The problem

© University of Pretoria

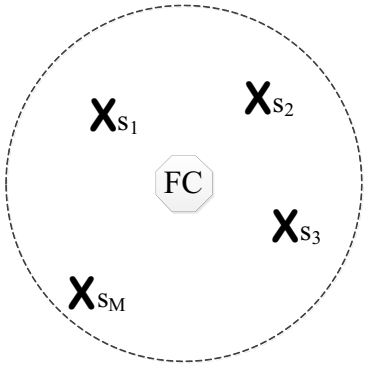

Figure 6.1: Example of a multi-SU sensing network with centralised FC.

was formulated as a non-linear optimisation problem that had the following set of decision variables, $x_i = \{x_1, x_2, \ldots, x_M\}$, where x_i was the activation status of sensor node s_i. The residual lifetime of s_i was denoted t_i and all sensor nodes were assumed to have the same residual lifetime. Based on the proof in [128], the OR rule for cooperative spectrum sensing (where $k = 1$) was assumed to be optimal. The problem was thus formulated as follows,

$$\begin{aligned}
\min_{t_{ij}, x_{ij}} \quad & \sum_{j=1}^{K} \sum_{i=1}^{M} x_{ij} t_{ij}, \qquad (6.2)\\
\text{s.t.} \quad & 1 - \prod_{i=1}^{M} (1 - x_{ij} P_{d,i}) \geq \overline{Q}_d, \quad j = 1, 2, \ldots, K \\
& 1 - \prod_{i=1}^{M} (1 - x_{ij} P_{f,i}) \leq \overline{Q}_f, \quad j = 1, 2, \ldots, K \\
& \sum_{j=1}^{K} x_{ij} t_{ij} \leq 1, \quad i = 1, 2, \ldots, M \\
& t_{ij} \in (0, 1], \\
& x_{ij} \in \{0, 1\},
\end{aligned}$$

where $x_{ij} = 1$ only if $s_i \in S_j$. For an individual sensor the probability of detection was denoted by $P_{d,i}$ and that of false alarm by $P_{f,i}$. For M cooperating sensors, $\overline{Q}_d$ was the cooperative detection probability threshold and $\overline{Q}_f$ the cooperative false alarm probability threshold. The network lifetime T_N was calculated as,

$$T_N = \omega G, \qquad (6.3)$$

where $G \leq K$ was the number of available and feasible subsets activated and $\omega \in (0, 1]$ the granularity or activation time interval of a subset S_j. Every time a sensor was selected as part

© University of Pretoria

UNIVERSITEIT VAN PRETORIA
UNIVERSITY OF PRETORIA
YUNIBESITHI YA PRETORIA

of a feasible subset, its residual lifetime was decreased by ω units of time, i.e. $t_{ij} = t_{ij} - \omega$. Once an individual sensor's lifetime had been depleted, it could no longer be activated.

In this chapter, the problem has been reformulated as a linear integer programming problem (as described in [64]) and two greedy algorithms have been considered to solve it. Namely implicit enumeration (IE) and the λ-greedy (λG) algorithm [64]. Simulation results, where these algorithm are complemented by SOF, will be presented in Section 6.4.

6.2.2 Implicit enumeration

For the IE approach, based on Equation (6.2), a least weighted sub-problem (LWSP) was set up as follows,

$$\begin{aligned} \min_{x_i} \quad & \sum_{i=1}^{M} w_i x_i, \\ \text{s.t.} \quad & 1 - \prod_{i=1}^{M} (1 - x_i P_{d,i}) \geq \overline{Q}_d, \\ & 1 - \prod_{i=1}^{M} (1 - x_i P_{f,i}) \leq \overline{Q}_f, \\ & x_i \in \{0, 1\}, \end{aligned} \tag{6.4}$$

where w_i is the weight of the ith sensor and $x_i = 1$ only if $s_i \in S_j$. The non-linear constraints of this LWSP were then transformed into linear constraints using the following transformation,

$$\begin{cases} a_i = \frac{\ln(1-P_{d,i})}{\ln(1-\overline{Q}_d)} > 0, \\ b_i = \frac{\ln(1-P_{f,i})}{\ln(1-\overline{Q}_f)} > 0. \quad i = 1, 2, \ldots, M \end{cases}$$

The non-linear problem could thus be reformulated as the following linear integer multi-dimensional knapsack problem,

$$\begin{aligned} \min_{x_i} \quad & \sum_{i=1}^{M} w_i x_i, \\ \text{s.t.} \quad & \sum_{i=1}^{M} a_i x_i \geq 1, \\ & \sum_{i=1}^{M} b_i x_i \leq 1, \end{aligned} \tag{6.5}$$

where $w_i, a_i, b_i > 0$ and $x_i \in \{0, 1\}$.

© University of Pretoria

UNIVERSITEIT VAN PRETORIA
UNIVERSITY OF PRETORIA
YUNIBESITHI YA PRETORIA

6.2.3 λ-Greedy algorithm

For the λG approach, a Lagrangian multiplier was introduced. The second constraint in Equation (6.5) was thus moved to the objective function. In this case the LWSP was formulated as follows,

$$\begin{aligned} \min_{x_i} \quad & \sum_{i=1}^{M} (w_i + \lambda b_i) x_i, \\ \text{s.t.} \quad & \sum_{i=1}^{M} a_i x_i \geq 1, \\ & w_i, a_i, b_i > 0, \end{aligned} \tag{6.6}$$

where $w_i, a_i, b_i > 0$, $\lambda \geq 0$ and $x_i \in \{0, 1\}$. To fill the knapsack, sensor node efficiency was calculated as,

$$e_i = \frac{a_i}{(w_i + \lambda b_i)}. \tag{6.7}$$

The following expression was then used to calculate the critical values of the Lagrangian multiplier λ,

$$\lambda(i, j) = \frac{a_j w_i - a_i w_j}{a_i b_j - a_j b_i)}, \tag{6.8}$$

where $\frac{a_i}{(w_i + \lambda b_i)}$ and $\frac{a_j}{(w_j + \lambda b_j)}$ represent two arbitrary efficiency values. All positive values for λ as well as the extreme cases of $\lambda = 0$ and $\lambda = \infty$ were considered so as to find the best sub-optimal solution.

6.3 FORECASTING SPECTRAL OPPORTUNITIES

Since power is consumed every time a sensing node is activated, EE would be further improved if SS regularity could be reduced. This could be achieved by introducing SOF. If it is assumed that SOF can be performed with a reasonable level of accuracy, then SS decisions could be replaced by the predicted status of a particular sensing node, as was considered in [80]. This means that the number of SS operations required of each node could be reduced, and thus the lifetime of each sensor would be improved. If the sensing period is denoted as t_s and the number of sensing periods that a forecast is made for is denoted by k_{fr}, then the amount of time that could be saved by SOF in between sensing operations, is $k_{fr} t_s$ (assuming that

© University of Pretoria

UNIVERSITEIT VAN PRETORIA
UNIVERSITY OF PRETORIA
YUNIBESITHI YA PRETORIA

the time and energy spent on SOF is negligible). In other words, for every SS operation k_{fr} SS operations could be replaced by forecast values. An example of the benefit that this may have, on energy consumption, is illustrated in Figure 6.2.

Considering the description provided for $P_{d,i}$ and $P_{f,i}$ in Section 2.3.3, let the probability of detection, given that a forecast was made $P_{d|fr,i}$, be given as,

$$\begin{aligned} P_{d|fr,i} =& Pr\left\{D_i = 1|H_1, F\right\} \\ =& P_{d,i}P_{fr,i}, \end{aligned} \tag{6.9}$$

where F is the condition that a forecast was made. The probability of obtaining a correct forecast at sensor node i is denoted by $P_{fr,i}$. This relationship is based on the assumption that $P_{fr,i}$ is independent of $P_{d,i}$. To accommodate for the possibility of SS and forecasting errors, let the probability of obtaining an error, given that a forecast was made $P_{e|fr,i}$, be given as,

$$\begin{aligned} P_{e|fr,i} =& Pr\left\{D_i = 1|H_0, F\right\} + Pr\left\{D_i = 0|H_1, F\right\}, \\ =& P_{e,i}P_{fr,i}. \end{aligned} \tag{6.10}$$

The assumption is then made that $P_{e|fr,i}$ can be described as,

$$P_{e|fr,i} = P_{f|fr,i} + P_{md|fr,i}, \tag{6.11}$$

where $P_{f|fr,i}$ is the probability of false alarm, given that a forecast was made and $P_{md|fr,i}$ is the probability of miss-detection given that a forecast was made. But, $P_{md|fr,i} = 1 - P_{d|fr,i}$, therefore, substituting Equation (6.11) into Equation (6.10) leads to the following expression,

$$P_{e|fr,i} = P_{fr,i}(P_{f,i} + 1 - P_{d,i}). \tag{6.12}$$

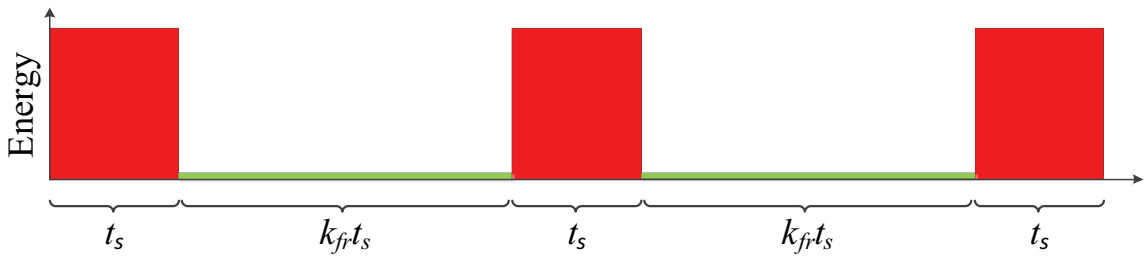

Figure 6.2: Illustration of the impact that SOF could have on energy consumption.

© University of Pretoria

UNIVERSITEIT VAN PRETORIA
UNIVERSITY OF PRETORIA
YUNIBESITHI YA PRETORIA

Equation (6.9) and Equation (6.11) can then be expanded such that,

$$P_{e|fr,i} = P_{f|fr,i} - P_{d,i}P_{fr,i} + 1. \tag{6.13}$$

Then Equation (6.12) and Equation (6.13) can be solved to obtain an expression for $P_{f|fr,i}$, such that,

$$P_{f|fr,i} = P_{fr,i}(1 + P_{f,i}) - 1. \tag{6.14}$$

When SOF is combined with optimal scheduling, $P_{d,i}$ is replaced by $P_{d|fr,i}$ and $P_{f,i}$ is replaced by $P_{f|fr,i}$ in Equation (6.2).

6.4 ENERGY EFFICIENCY SIMULATION

Simulations were run to compare the effect that SOF had on T_N. Together with SOF, the IE and λG optimisation methods were compared with random subset selection. The complexity of these approaches was also considered. All results presented represent the average of 1000 simulation iterations.

6.4.1 Parameters

All simulations presented in this section were run for a range of sensor deployments $2 \leq M \leq 20$ and a base granularity of $\omega = 0.1$ was assumed for all feasible subsets S_j. In accordance with the IEEE 802.22 standard's recommendations for spectrum sensing [134], cooperation thresholds of $\overline{Q}_d = 0.9$ and $\overline{Q}_f = 0.1$ were employed. Also, based on the work presented in [128], the OR rule was chosen for performing cooperative SS. The following specific simulation parameters were used to generate the simulation results.

6.4.1.1 Sensor node distribution

To simplify calculations, only the distributions of P_d and P_f were considered and not the actual physical locations of the sensor nodes. Two different scenarios were considered (illustrated in Figure 6.3). In the first scenario a standard uniform distribution $U(x)$ was employed,

$$U_M(x) = \begin{cases} \frac{1}{b-a}, & a \leq x \leq b \\ 0. & x < a \text{ or } x > b \end{cases} \tag{6.15}$$

where $a = 0$ and $b = 1$. In the second scenario variations of the Rayleigh distribution were

© University of Pretoria

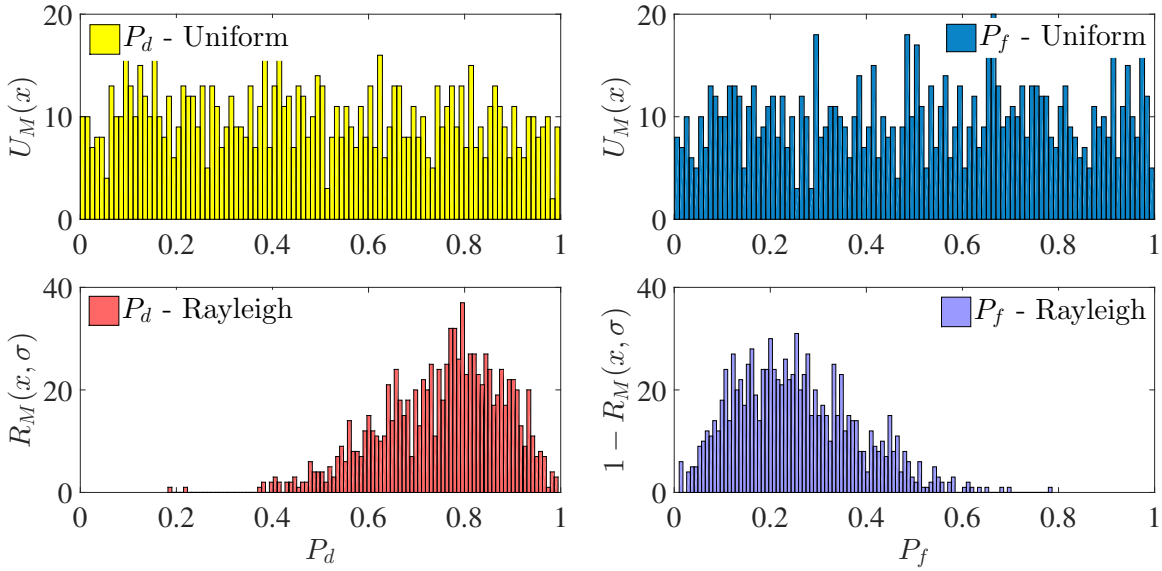

Figure 6.3: Sensor distribution of P_d and P_f for the uniform (top) and Rayleigh scenarios (bottom).

considered. For P_f, the following amplitude scaled Rayleigh distribution was employed,

$$R_M(x,\sigma) = \frac{0.2x}{\sigma^2} e^{(-x^2/2\sigma^2)}, \tag{6.16}$$

with the scale parameter of the distribution chosen to be $\sigma = 1$. However, for P_d, Equation (6.16) was changed to be $1 - R_M(x,\sigma)$.

6.4.1.2 Forecasting parameters

In this chapter $P_{fr,i}$ was calculated using the normalised least mean square (NLMS) method, described in Chapter 4. Only prediction lengths of $k_{fr} = [0;1;5;10]$ were considered (i.e. $k_{fr} = 0$ means that no forecast was made and $k_{fr} = 10$ means that a forecast was made ten sensing periods into the future). The values employed for k_{fr} are listed in Table 6.1.

Table 6.1: Table of P_{fr} versus k_{fr} calculated for a single SU using the NLMS prediction method.

k_{fr}	0	1	5	10
P_{fr}	1.0	0.76	0.64	0.63

© University of Pretoria

UNIVERSITEIT VAN PRETORIA
UNIVERSITY OF PRETORIA
YUNIBESITHI YA PRETORIA

When SOF was employed the granularity ω_{fr}, used to calculate T_N in Equation (6.3), was scaled by k_{fr} such that,

$$\omega_{fr} = \omega\left(k_{fr} + 1\right), \tag{6.17}$$

where ω is the granularity that would have been employed had no forecast been made.

6.4.1.3 Cooperation thresholds

The effect that different cooperative detection thresholds had on EE was also investigated. A range of cooperative detection $\overline{Q}_d = \{0.6; 0.7; 0.8; 0.9\}$ and false alarm $\overline{Q}_f = \{0.1; 0.2; 0.3; 0.4\}$ threshold values were considered. For these simulations only the uniform distribution was considered for P_d and P_f with $k_{fr} \in \{1, 10\}$.

6.4.2 Simulation results

6.4.2.1 Forecasting

The effect that SOF had on T_N is illustrated in Figure 6.4 and Figure 6.5. Results obtained under the uniform distribution are denoted by subscript U and those obtained under the Rayleigh distributions are denoted by subscript R. For both distribution scenarios a clear improvement in T_N was evident when compared with the approach proposed in [64], where $k_{fr} = 0$. This was in spite of the fact that SOF accuracy decreased when k_{fr} was increased, as shown in Table 6.1. Considering a scenario where $M = 20$ sensors, the IE approach was followed and the sensing nodes were uniformly distributed, it can be seen that even for single step ahead prediction, when $k_{fr} = 1$, T_N had improved by 2.4 time samples compared with when SOF was not employed ($k_{fr} = 0$). However, when $k_{fr} = 10$, T_N had substantially improved to 21.2 time samples longer. For the Rayleigh distributed case an improvement of 54.8 time samples was observed (a combined power reduction of 5.48 W using the device described in [129]).

From the plot shown in Figure 6.5, where $M = 20$, it is evident that a linearly increasing relationship existed between T_N and k_{fr}. As expected, the IE approach performed slightly better than the λG approach. Both of these optimisation approaches performed better than when random scheduling (denoted RD) was employed. For example, using the λG and IE approaches, when $k_{fr} = 5$, lead to an approximate increase in T_N over random scheduling of 1.6

© University of Pretoria

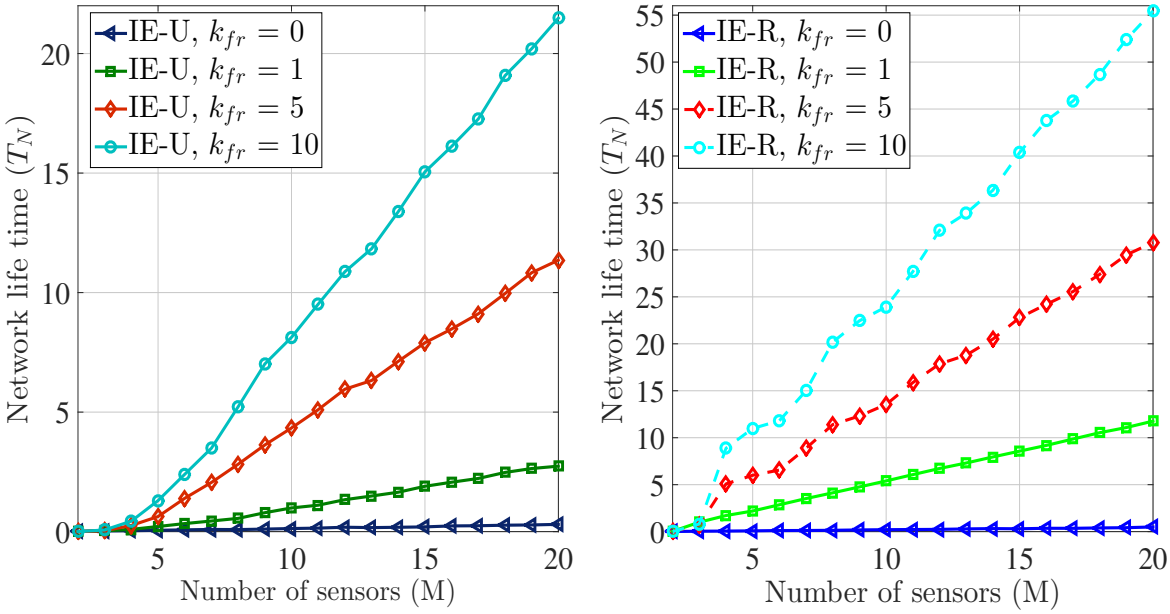

Figure 6.4: Simulated network lifetime T_N for various values of M and k_{fr}.

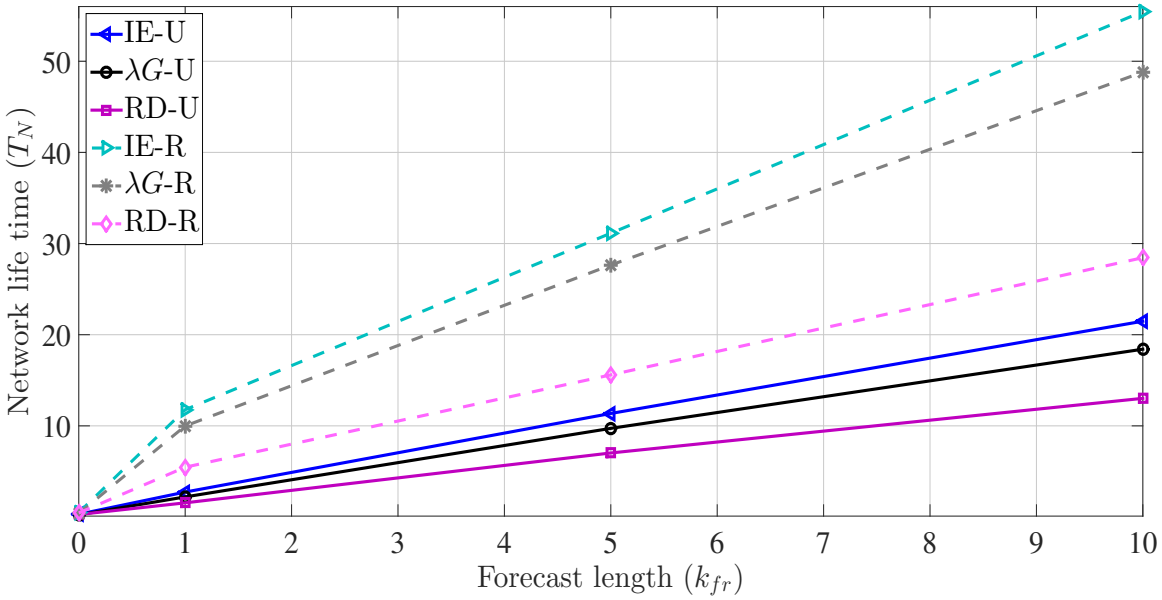

Figure 6.5: Simulated T_N for various values of k_{fr} when $M = 20$.

and 2.6 time samples respectively for the uniformly distributed case. For the Rayleigh distributed case, respective increases of approximately 26.9 and 20.4 time samples were observed. This improvement over random scheduling was also found to increase as k_{fr} was increased. This means that the sensor node network is able to remain operational for a longer period of time when SOF is employed and that increasing k_{fr} improves the benefit proportionally.

© University of Pretoria

However, in reality there would be practical limitations on how large k_{fr} could become before the decrease in SOF accuracy would lead to a violation of the constraints of Equation (6.2).

6.4.2.2 Algorithm complexity

The normalised average simulation time of each algorithm was measured and assumed to provide an indication of algorithm complexity. The normalised simulation times T_s for both distribution scenarios are presented, on a logarithmic scale, in Figure 6.6 and Figure 6.7. In Figure 6.6 an exponential increase in T_s was observed, as M was increased, for both distribution scenarios. A proportional relationship between T_s and T_N was also evident. This meant that T_s also increased as k_{fr} was increased, although, little difference was observed between the values obtained for T_s when $k_{fr} = 5$ and when $k_{fr} = 10$. In Fig 6.7, the IE and λG approaches were compared with random scheduling when SOF was employed for $M = 20$. The IE and random approaches clearly exhibited the highest complexity, with the IE approach having a T_s that was 20% shorter than random scheduling (under the uniform scenario with $k_{fr} = 10$). However, the λG approach was found to be significantly less complex than either of them with a T_s that was 99% shorter under the same conditions.

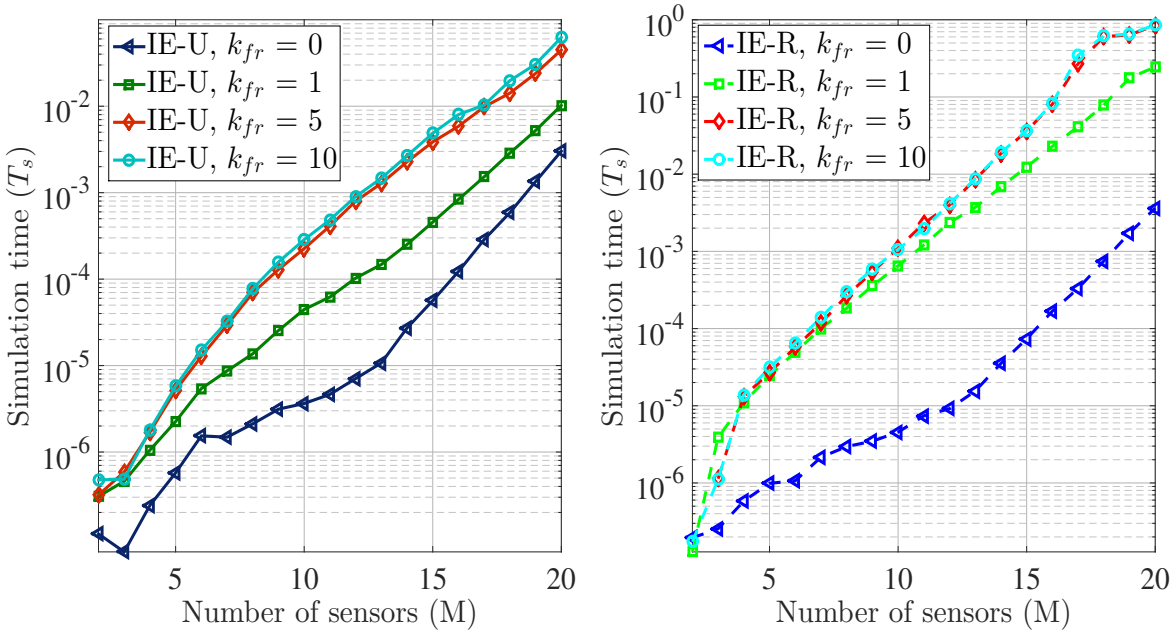

Figure 6.6: Simulations times T_s for various values of M and k_{fr}.

© University of Pretoria

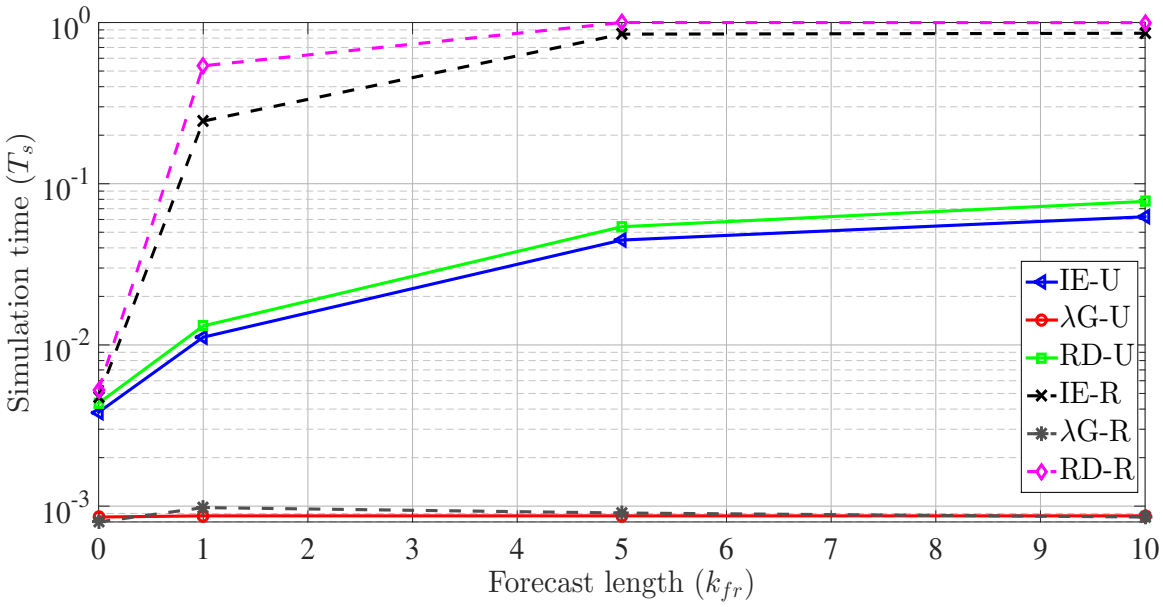

Figure 6.7: Simulated T_s for various values of k_{fr} when $M = 20$.

6.4.2.3 Node distribution

Results obtained under the two different sensor node distributions, when $M = 20$, are summarised in Table 6.2 (IE approach) and Table 6.3 (λG approach) respectively. The absolute percentage difference between the results obtained under the different distributions has also been included for both T_N (%$|\boldsymbol{\Delta T_N}|$) and T_s (%$|\boldsymbol{\Delta T_s}|$).

Under both distribution scenarios, T_N as well as T_s were found to be much higher under the Rayleigh distributed scenario (%$|\boldsymbol{\Delta T_N}|\approx$62% and %$|\boldsymbol{\Delta T_s}|\approx$95% longer when $k_{fr} = 10$).

Table 6.2: Network lifetime and complexity for different sensor node distributions for the IE approach when $M = 20$.

k_{fr}	$T_{N,U}$	$T_{N,R}$	%$\|\Delta T_N\|$	$T_{s,U}$	$T_{s,R}$	%$\|\Delta T_s\|$
0	0.304	0.498	*38.96*	0.0038	0.0048	*19.908*
1	2.738	11.77	*76.74*	0.0111	0.2446	*95.431*
5	11.36	30.79	*63.11*	0.0447	0.8470	*94.720*
10	21.48	55.34	*61.26*	0.0624	0.8578	*92.730*

© University of Pretoria

UNIVERSITEIT VAN PRETORIA
UNIVERSITY OF PRETORIA
YUNIBESITHI YA PRETORIA

Table 6.3: Network lifetime and complexity for different sensor node distributions for the λG approach when $M = 20$.

k_{fr}	$T_{N,U}$	$T_{N,R}$	$\%\lvert\Delta T_N\rvert$	$T_{s,U}$	$T_{s,R}$	$\%\lvert\Delta T_s\rvert$
0	0.242	0.386	*37.31*	0.00086	0.0008	*7.273*
1	2.207	9.987	*77.90*	0.00087	0.0010	*11.11*
5	9.725	27.64	*64.82*	0.00087	0.0009	*4.000*
10	18.41	48.81	*62.28*	0.00087	0.0009	*1.695*

This was because P_d and P_f were concentrated closer to the cooperation thresholds, which meant that a larger number of nodes met the cooperation criteria.

Under both scenarios, it was found that T_s for the IE approach was much longer than for the λG approach although the λG approach still achieved acceptable results (consistent with the findings of [64]). It was also evident that T_s grew exponentially as k_{fr} was increased for the IE approach, but remained relatively constant for the λG approach. For energy efficient SS the λG approach should thus be combined with SOF, where k_{fr} is large but within the constraints of Equation (6.2).

6.4.2.4 Cooperative detection and false alarm threshold

The T_N for different values of $\overline{Q}_d$ and $\overline{Q}_f$ is illustrated in Figure 6.8. Firstly, a fixed value of $\overline{Q}_f = 0.1$ was set and T_N observed for a range of $\overline{Q}_d$ values, shown on the left hand side of the figure. It was evident that there was a linear decrease in T_N as $\overline{Q}_d$ was increased. Secondly, a fixed value of $\overline{Q}_d = 0.9$ was set and T_N observed for a range of $\overline{Q}_f$ values, shown on the right hand side of the figure. In this case an increase in T_N was observed as $\overline{Q}_f$ was increased.

From these graphs it can be seen that T_N generally decreases, and that the EE benefit of employing SOF also decreases, as the detection and false alarm thresholds become more stringent. For example, consider the plot on the left hand side of Figure 6.8. For the IE algorithm when $\overline{Q}_d = 0.6$, T_N is 23.2 time samples longer when $K_{fr} = 10$ than when $K_{fr} = 1$. However, T_N is only 7.4 times samples longer when $\overline{Q}_d = 0.9$.

© University of Pretoria

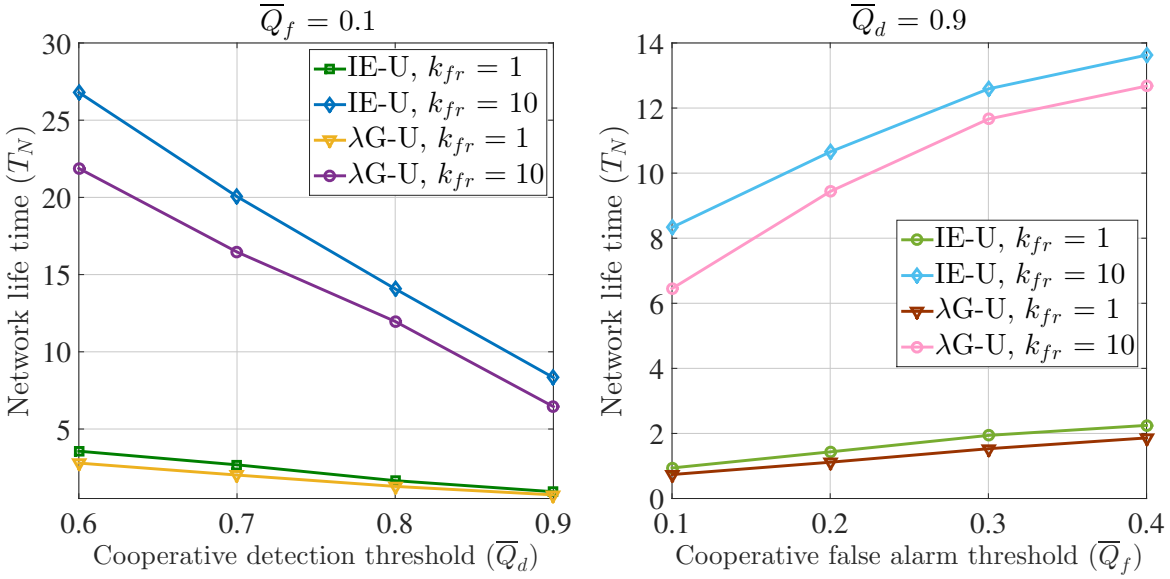

Figure 6.8: Simulated T_N for various values of $\overline{Q}_d$ and $\overline{Q}_f$ (uniform distribution with $k_{fr} \in \{0, 10\}$).

6.5 CONCLUSION

Accurate SS is a critical function of CRNs that allows the network to operate in an efficient and unobtrusive manner. As discussed in Chapter 2 and Chapter 5, there is a clear benefit to CRNs when SUs cooperate with each other to perform SS and SOF. Unfortunately, SS places additional power demands on the power consumption of the cooperating sensing devices. If these devices are energy constrained, this can have negative consequences for the lifetime of the cooperating network of SUs. In this chapter, the combination of SOF and optimal sensor node scheduling was proposed as a way to reduce the power demands placed on sensing devices by limiting the overall number of SS operations required by each sensing node. Simulation results indicated that the combination of reasonably accurate SOF and optimal scheduling lead to significant improvements in the collective lifetime of the sensor node network. A positive linear relationship between network lifetime and forecast length was evident. The extent of the benefit that SOF provided was also found to be influenced by the statistical distribution of the participating sensor nodes as well as the stringency of the cooperative detection and false alarm thresholds. The integration of SOF and optimal sensor node scheduling was thus found to be of great advantage to the combined lifetime of the sensor node network.

© University of Pretoria

CHAPTER 7

CONCLUSIONS AND FUTURE RESEARCH

7.1 SUMMARY OF WORK

The work described in this thesis may be summarised as follows:

- **Background on improving spectral efficiency**
  Background information, in the form of a comprehensive literature review that covered a number technologies and techniques that could be used to improve spectral efficiency, was presented in Chapter 2. Technologies such as fifth generation networking, TVWS and GLSDBs, as well various South African regulatory aspects, were discussed. A spectrally efficient technology, known as cognitive radio, was then introduced followed by a discussion on some of the important functions associated with this technology. Spectrum sensing, where information is gathered about the radio environment, was identified as one the most critical of these functions. Various spectrum sensing techniques were presented and the concept of cooperative sensing was discussed. A discussion of some of the techniques that could be used to model spectrum usage behaviour was also included.

- **Characterisation of spectrum occupancy in the South African context**
  In Chapter 3, the findings of an extensive spectrum occupancy measurement campaign were presented. The chapter began with a discussion on how to calculate spectrum occupancy and a novel noise threshold detection technique was presented. The details of a number of spectrum measurement campaigns, carried out at various locations in South Africa's Gauteng province, including the Hatfield campus of the

© University of Pretoria

University of Pretoria and Pinmill Farm in Johannesburg, were discussed. The bands measured covered the spectra associated with TV broadcasting and mobile cellular communication. It was found that a number of spectral opportunities currently exist in the TV broadcast bands that could be exploited by TVWS devices and other dynamic spectrum access based technologies. Conversely, the mobile cellular bands were found to be very well utilised and in same instances completely saturated, particularly in the bands around 900 MHz. This suggests that mobile operators in South Africa are currently in need of additional spectrum resources, a need that will most likely continue to increase in the future (as discussed in Section 1.1).

- **Primary user traffic prediction**

  Prediction of primary user traffic, by a single secondary user, was investigated in Chapter 4. Different types of theoretical primary user traffic patterns were classified and a low-complexity prediction method, called the occupancy window method, was proposed. The performance of this method was compared with various other techniques in the literature, both in terms of prediction accuracy and algorithm complexity, as well as for different types of traffic conditions. Under certain traffic conditions, the occupancy window method was found to have either comparable or better prediction performance than the other methods, but with much lower computational complexity. There were, however, a number of traffic conditions where the occupancy window method was found to have poorer prediction performance than the other methods, but always with a much lower degree of complexity.

- **Improving traffic prediction through cooperation**

  In Chapter 5 the traffic prediction concept was expanded upon to include the use of cooperation amongst secondary users. A simulation scenario was created where both the benefits as well as the costs of cooperative prediction could be investigated. The performance of the cooperative prediction scheme was investigated for a range of single user prediction algorithm accuracies and under various noisy channel conditions. For the scenarios investigated, it was found that cooperation always lead to improvements in prediction accuracy, particularly as the number of cooperating SUs was increased. An optimal cooperative forecasting problem was also formulated and a heuristic proposed for solving it, which was shown to further improve prediction accuracy. Pre

© University of Pretoria

UNIVERSITEIT VAN PRETORIA
UNIVERSITY OF PRETORIA
YUNIBESITHI YA PRETORIA

and post-fusion cooperation scenarios were compared and a higher degree of prediction accuracy was observed for the former approach than for the latter. The improved prediction performance of the pre-fusion approach did, however, come at a cost of increased computational complexity, proportional to the number of cooperating sensor nodes.

- **Forecasting for energy efficient cooperative spectrum sensing**
  In Chapter 6 the concepts of primary user traffic prediction, and secondary user co-operation, were applied to an energy consumption problem for a network of cooperating secondary sensing nodes. The benefit of employing prediction was applied to an optimal scheduling problem for sensor node activation as a way to reduce the power demands placed on sensing devices, by limiting the overall number of spectrum sensing operations required of each sensing node. It was found that prediction, or spectral opportunity forecasting, combined with optimal scheduling helped to significantly prolong the life-time of a cooperative cognitive radio based sensor node network. A positive linear relationship was found between network lifetime and forecast length. The extent of this benefit was found to be influenced by the statistical distribution of the participating sensor nodes as well as the chosen cooperative detection and false alarm thresholds.

7.2 FUTURE RESEARCH

Extensions to this research may include the following:

- **Diversified spectral occupation measurements**
  The work presented in Chapter 3 could be extended by conducting spectrum occupancy measurement campaigns for a much wider and more diverse range of geographical locations, within the same city and also between different cities within South Africa. A comparison between measurements covering different population densities may also be useful, e.g, spectral occupation in rural areas could be compared to that of urban or suburban areas.

- **Statistical predictions and geo-location spectrum databases**
  A further extension to Chapter 3 may include an extensive investigation to compare

© University of Pretoria

UNIVERSITEIT VAN PRETORIA
UNIVERSITY OF PRETORIA
YUNIBESITHI YA PRETORIA

the effectiveness of statistical prediction methods with that of geo-location spectrum databases for dynamic spectrum access in the TV broadcast bands. A investigation into a hybrid approach to this problem might also prove to be useful.

- **Optimal forecasting algorithm**

  A more advanced and complete optimal forecasting algorithm, than the one presented in Chapter 5, could be developed. In this case the algorithm could draw on a broader range of the factors influencing the accuracy of traffic prediction, e.g. knowledge about the suitability of certain models to different traffic patterns and conditions could be combined with knowledge about the historical correctness of different algorithms at a particular geographical location. This approach might include an investigation into the practical suitability of different algorithms to typical traffic patterns that may occur in wireless communication networks, e.g. voice, video, file transfer or general web browser traffic. An adaptive hybrid approach to the problem is suggested.

- **Energy efficiency**

  Further investigation into how to make cognitive radio networks more energy efficient is warranted, where the focus of the optimal forecasting algorithm could also be shifted away from prediction accuracy towards optimal prediction as a tool for improved energy efficiency.

- **Application of measured data to simulation driven models**

  The simulation driven models presented in Chapters 4, 5 and 6 could be further investigated by testing them against the measured data collected in Chapter 3. Classification of the traffic patterns inherent to the measured data could form part of this investigation.

- **Hardware test-bed implementation**

  A possible next step would be to incorporate the concepts discussed in this thesis into a cognitive radio network hardware test bed, so as to investigate the performance of these techniques in the context of a more complete cognitive radio system and also to garner a better understanding of the practicality of some of the theoretical concepts presented in this thesis.

© University of Pretoria

REFERENCES

[1] ITU-R, "Assessment of the global mobile broadband deployments and forecasts for international mobile telecommunications," Geneva, Switzerland, Tech. Rep. M.2243, 2012.

[2] "Spectrum policy task force report," Federal Communications Commission, Tech. Rep. ET Docket 02-155, Nov. 2002.

[3] "Mobile broadband: The benefits of additional spectrum," Staff Technical Paper, Federal Communications Commission, Oct. 2010.

[4] "Cisco visual networking index: Global mobile data traffic forecast update, 2011–2016," White Paper, Cisco Systems, Feb. 2012.

[5] ITU-R, "Future spectrum requirements estimate for terrestrial IMT," Geneva, Switzerland, Tech. Rep. M.2290-0, 2014.

[6] C. Shannon, "The zero error capacity of a noisy channel," *IRE Trans. Inform. Th.*, vol. 2, no. 3, pp. 8–19, Sept. 1956.

[7] 3GPP, "Feasibility study for further advancements for E-UTRA (LTE-Advanced)," Tech. Rep. 36.912, Sept. 2014.

[8] J. Mitola III and G. Q. Maguire Jr., "Cognitive radio: Making software radios more personal," *IEEE Pers. Commun.*, vol. 6, no. 4, pp. 13–18, Aug. 1999.

[9] S. Haykin, "Cognitive radio: Brain-empowered wireless communications," *IEEE J. Sel. Areas Commun.*, vol. 23, no. 2, pp. 201–220, Feb. 2005.

© University of Pretoria

[10] I. F. Akyildiz, W.-Y. Lee, M. C. Vuran, and S. Mohanty, "NeXt generation/dynamic spectrum access/cognitive radio wireless networks: A survey," *Comput. Netw.*, vol. 50, no. 13, pp. 2127–2159, Sept. 2006.

[11] M. Mueck and W. Jiang and G. Sun and H. Cao and E. Dutkiewicz and S. Choi, "Novel spectrum usage paradigms for 5G," IEEE Technical Committee Cognitive Networks Special Interest Group Cognitive Radio in 5G, Tech. Rep., Nov. 2014.

[12] S. D. Barnes, "Cognitive radio performance optimisation through spectrum availability prediction," Master's thesis, University of Pretoria, 2012.

[13] S. M. Wentworth, *Fundamentals of electromagnetics with engineering applications.* Hoboken, NJ: John Wiley & Sons, Inc., 2005, iSBN 0-471-26355-9.

[14] ETSI, "Reconfigurable Radio Systems (RRS); System requirements for operation of Mobile Broadband Systems in the 2300 MHz - 2400 MHz band under Licensed Shared Access (LSA) regime," Tech. Rep. TS 103 154, Oct. 2014.

[15] M. Palola, M. Matinmikko, J. Prokkola, M. Mustonen, M. Heikkila, T. Kippola, S. Yrjola, V. Hartikainen, L. Tudose, A. Kivinen, J. Paavola, and K. Heiska, "Live field trial of licensed shared access (LSA) concept using LTE network in 2.3 GHz band," in *Proc. IEEE Int. Symp. Dynamic Spectr. Access Netw.*, McLean, VA, 2014, pp. 38–47.

[16] M. M. Buddhikot, "Understanding dynamic spectrum access: Models, taxonomy and challenges," in *Proc. 2nd IEEE Int. Symp. New Frontiers Dynamic Spectr. Access Netw.*, Dublin, Ireland, 2007, pp. 649–663.

[17] *IEEE Standard definitions and concepts for dynamic spectrum access: terminology relating to emerging wireless networks, system functionality, and spectrum management*, IEEE Standard 1900.1, 2008.

[18] 3GPP, "Evolved universal terrestrial radio access (E-UTRA); carrier aggregation; base station (BS) radio transmission and reception," Tech. Rep. 36.808, Jul. 2013.

[19] K. Hong, S. Sengupta, and R. Chandramouli, "SpiderRadio: A cognitive radio implementation using IEEE 802.11 components"," *IEEE Trans. Mobile. Comput.*, vol. 12,

© University of Pretoria

no. 11, pp. 2105–2118, Nov. 2013.

[20] A. Asadi, Q. Wang, and V. Mancuso, "A survey on device-to-device communication in cellular networks," *IEEE Commun. Surveys Tuts.*, vol. PP, no. 99, 2014.

[21] Z. Pi and F. Khan, "An introduction to millimeter-wave mobile broadband systems," *IEEE Commun. Mag*, vol. 49, no. 6, pp. 101–107, Jun. 2011.

[22] T. Rappaport, S. Sun, R. Mayzus, H. Zhao, Y. Azar, K. Wang, G. Wong, J. Schulz, M. Samimi, and F. Gutierrez, "Millimeter wave mobile communications for 5G cellular: It will work!" *IEEE Access*, vol. 1, pp. 335–349, May 2013.

[23] S. Rangan, T. Rappaport, and E. Erkip, "Millimeter-wave cellular wireless networks: Potentials and challenges," *Proc. IEEE*, vol. 102, no. 3, pp. 366–385, Mar. 2014.

[24] J. Hoydis, S. T. Brink, and M. Debbah, "Massive MIMO in the UL/DL of cellular networks: How many antennas do we need?"," *IEEE J. Sel. Areas Commun.*, vol. 31, no. 2, pp. 160–171, Feb. 2013.

[25] S. D. Barnes, S. Joshi, B. T. Maharaj, and A. S. Alfa, "Massive MIMO and femto cells for energy efficient cognitive radio networks," in *Proc. Int. Conf. Cognitive Radio Oriented Wireless Netw.*, Doha, Qatar, 2015, pp. 1–12.

[26] S. Rajagopal, S. Abu-Surra, Z. Pi, and F. Khan, "Antenna array design for multi-Gbps mmwave mobile broadband communication," in *IEEE Global Telecommun. Conf.*, Houston, TX, 2011, pp. 1–6.

[27] M. J. Marcus, "Unlicensed cognitive sharing of TV spectrum: The controversy at the Federal Communications Commission," *IEEE Commun. Mag.*, vol. 43, no. 5, pp. 24–25, May 2005.

[28] D. Gurney, G. Buchwald, L. Ecklund, S. L. Kuffner, and J. Grosspietsch, "Geo-Location database techniques for incumbent protection in the TV white space," in *Proc. 3rd IEEE Symp. New Frontiers Dynamic Spectr. Access Netw.*, Chicago, IL, 2008, pp. 1–9.

[29] "Google spectrum database," Feb. 2015. [Online]. Available: ht-

© University of Pretoria

tps://www.google.com/get/spectrumdatabase/

[30] CSIR, "CSIR TV white space database," Dec. 2014. [Online]. Available: http://whitespaces.meraka.org.za

[31] A. A. Lysko and M. T. Masonta and L. Mfupe and M. Mofolo, "Field measurements done on operational TVWS trial network in Tygerberg," CSIR - Meraka, Pretoria, South Africa, Tech. Rep., Oct. 2013.

[32] L. Mfupe, F. Mekuria, and M. Mzyece, "Geo-location white space spectrum databases: Models and design of South Africa's first dynamic spectrum access coexistence manager," *KSII Transactions on Internet and Information Systems*, vol. 8, no. 11, pp. 3810–3836, 2014.

[33] T. M. Taher, R. B. Bacchus, K. J. Zdunek, and D. A. Roberson, "Long-term spectral occupancy findings in Chicago," in *Proc. IEEE Int. Symp. Dynamic Spectr. Access Netw.*, Aachen, Germany, 2011, pp. 100–107.

[34] M. Matinmikko, M. Mustonen, M. Höyhtyä, T. Rauma, H. Sarvanko, and A. Mämmelä, "Distributed and directional spectrum occupancy measurements in the 2.4 GHz ISM band," in *Proc. Int. Symp. Wireless Commun. Syst.*, York, United Kingdom, 2010, pp. 976–980.

[35] M. A. McHenry, "NSF spectrum occupancy measurements project summary," Shared Spectrum Company, Tech. Rep., Aug. 2005.

[36] M. A. McHenry, D. McClokey, D. Roberson, and J. T. MacDonald, "Spectrum occupancy measurements Chicago Illinois," Shared Spectrum Company, Vienna, Virginia, Tech. Rep., Nov. 2005.

[37] M. A. McHenry, P. A. Tenhula, D. McCloskey, D. A. Roberson, and C. S. Hood, "Chicago spectrum occupancy measurements & analysis and a long-term studies proposal," in *Proc. Int. Workshop Technol. Policy Accessing Spectr.*, Boston, MA, 2006.

[38] R. I. C. Chiang, G. B. Rowe, and K. W. Sowerby, "A quantitative analysis of spectral occupancy measurements for cognitive radio," in *Proc. IEEE Veh. Technol. Conf.*,

© University of Pretoria

Dublin, Ireland, 2007, pp. 3016–3020.

[39] M. López-Benítez, F. Casadevall, A. Umbert, J. Pérez-Romero, R. Hachemani, J. Palicot, and C. Moy, "Spectral occupation measurements and blind standard recognition sensor for cognitive radio networks," in *Proc. Int. Conf. Cognitive Radio Oriented Wireless Netw. Commun.*, Hannover, Germany, 2009, pp. 1–9.

[40] M. Wellens, J. Wu, and P. Mähönen, "Evaluation of spectrum occupancy in indoor and outdoor scenario in the context of cognitive radio," in *Proc. 2nd Int. Conf. Cognitive Radio Oriented Wireless Netw. Commun.*, Orlando, FL, 2007, pp. 420–427.

[41] ——, "Lessons learned from an extensive occupancy measurement campaign and stochastic duty cycle," *Mobile Netw. Appl.*, vol. 15, no. 3, pp. 461–474, Jun. 2010.

[42] M. Wellens, A. de Baynast, and P. Mähönen, "Performance of dynamic spectrum access based on spectrum occupancy statistics," *IET Commun.*, vol. 2, no. 6, pp. 772–782, Jul. 2008.

[43] T. Erpek, K. Steadman, and D. Jones, "Spectrum occupancy measurements: Dublin, Ireland, April 16-18, 2007," Shared Spectrum Company, Tech. Rep., Apr. 2007.

[44] "National radio frequency plan," *Government Gazette, Republic of South Africa*, vol. 541, no. 33409, Jul. 2010.

[45] "Technical considerations regarding harmonisation options for the Digital Dividend: A preliminary assessment of the feasibility of fitting new/future applications/services into non-harmonised spectrum of the digital dividend (namely the so-called "white spaces" between allotments)," Jun. 2008.

[46] O. Blomberg, "Conceptions of cognition for cognitive engineering," *Int. J. Aviation Psychology*, vol. 21, no. 1, pp. 85–104, Jan. 2011.

[47] J. Mitola III, "Software radios: Survey, critical evaluation and future directions," *IEEE Aerosp. Electron. Syst. Mag.*, vol. 8, no. 4, pp. 25–36, Apr. 1993.

[48] ITU-R, "Definitions of software defined radio (SDR) and cognitive radio system (CRS),"

© University of Pretoria

Tech. Rep. SM.2152, Sept. 2009.

[49] E. Arun, V. R. Catherine, and Harisree, "Relay based cooperation for cognitive radio networks," *Int. J. Syst. Signal Control Eng. Appl.*, vol. 4, no. 1, pp. 1–9, 2011.

[50] T. Yücek and H. Arslan, "A survey of spectrum sensing algorithms for cognitive radio applications," *IEEE Commun. Surveys Tuts.*, vol. 11, no. 1, pp. 116–130, 2009.

[51] J. Ma and Y. Li, "Soft combination and detection for cooperative spectrum sensing in cognitive radio networks," in *Proc. IEEE Global Telecommun. Conf.*, Washington, DC, 2007, pp. 3139–3143.

[52] J. G. Proakis and M. Salehi, *Digital communications*, 5th ed. Singapore: McGraw Hill, 2008.

[53] R. Tandra and A. Sahai, "Fundamental limits on detection in low SNR under noise uncertainty," in *Proc. Int. Conf. Wireless Netw. Commun. Mobile Comput.*, Maui, HI, 2005, pp. 464–469.

[54] S. Xu, Z. Zhao, and J. Shang, "Spectrum sensing based on cyclostationarity," in *Proc. 2008 Workshop Power Electron. Intell. Transp. Syst.*, Guangzhou, China, 2008, pp. 171–174.

[55] Y. Lin, C. He, L. Jiang, and D. He, "A cyclostationary-based spectrum sensing method using stochastic resonance in cognitive radio," in *Proc. IEEE Int. Conf. Commun. Workshops*, Cape Town, South Africa, 2010, pp. 1–5.

[56] J. Lundén, V. Koivunen, A. Huttunen, and H. V. Poor, "Spectrum sensing in cognitive radios based on multiple cyclic frequencies," in *Proc. 2nd Int. Conf. Cognitive Radio Oriented Wireless Netw. Commun.*, Orlando, FL, 2007, pp. 37–43.

[57] K. Kim, I. A. Akbar, K. K. Bae, J.-S. Um, C. M. Spooner, and J. H. Reed, "Cyclostationary approaches to signal detection and classification in cognitive radio," in *Proc. 2nd IEEE Int. Symp. New Frontiers Dynamic Spectr. Access Netw.*, Dublin, Ireland, 2007, pp. 212–215.

© University of Pretoria

[58] H. Urkowitz, "Energy detection of unknown deterministic signals," in *Proceedings of the IEEE*, vol. 55, no. 4, April 1967, pp. 523–531.

[59] S. Tang and B. L. Mark, "An adaptive spectrum detection mechanism for cognitive radio networks in dynamic traffic environments," in *Proc. IEEE Global Telecommun. Conf.*, New Orleans, LA, 2008, pp. 3009–3013.

[60] G. Atia, S. Aeron, E. Ermis, and V. Saligrama, "On throughput maximization and interference avoidance in cognitive radios," in *Proc. 5th IEEE Consum. Commun. Netw. Conf.*, Las Vegas, NV, 2008, pp. 963–967.

[61] J. Unnikrishnan and V. Veeravalli, "Cooperative sensing for primary detection in cognitive radio," *IEEE J. Sel. Topics Signal Process.*, vol. 2, no. 1, pp. 18–27, Feb. 2008.

[62] W. Zhang and K. B. Letaief, "Cooperative spectrum sensing with transmit and relay diversity in cognitive radio networks," *IEEE Trans. Wireless Commun.*, vol. 7, no. 12, pp. 4761–4766, Dec. 2008.

[63] A. Ghasemi and E. Sousa, "Opportunistic spectrum access in fading channels through collaborative sensing," *J. Commun.*, vol. 2, no. 2, pp. 71–82, Mar. 2007.

[64] R. Deng, J. Chen, C. Yuen, P. Cheng, and Y. Sun, "Energy-efficient cooperative spectrum sensing by optimal scheduling in sensor-aided cognitive radio networks," *IEEE Trans. Veh. Technol.*, vol. 61, no. 12, pp. 716–725, Feb. 2012.

[65] I. F. Akyildiz, B. F. Lo, and R. Balakrishnan, "Cooperative spectrum sensing in cognitive radio networks: A survey," *Physical Commun.*, vol. 4, no. 1, pp. 40–62, Mar. 2011.

[66] R. B. D. Cabric, S. Mishra, "Implementation issues in spectrum sensing for cognitive radios," in *Proc. Asilomar Conf. Signals, Systems and Comput.*, 2004, pp. 772–776.

[67] J. Ma, G. Zhao, and Y. Li, "Soft combination and detection for cooperative spectrum sensing in cognitive radio networks," *IEEE Trans. Wireless Commun.*, vol. 7, no. 11, pp. 4502–4507, Nov. 2008.

© University of Pretoria

[68] W. Han, J. Li, Z. Li, J. Si, and Y. Zhang, "Efficient soft decision fusion rule in cooperative spectrum sensing," *IEEE Trans. Signal Process.*, vol. 61, no. 8, pp. 1931–1943, Apr. 2013.

[69] B. F. Lo and I. F. Akyildiz, "Reinforcement learning for cooperative sensing gain in cognitive radio ad hoc networks," *Wireless Commun. Netw.*, vol. 19, no. 6, pp. 1237–1250, Aug. 2013.

[70] Z. Chen and R. C. Qiu, "Cooperative spectrum sensing using Q-Learning with experimental validation," in *Proc. IEEE SoutheastCon*, Nashville, TN, 2011, pp. 405–408.

[71] S. Chaudhari, J. Lundén, V. Koivunen, and H. V. Poor, "Cooperative sensing with imperfect reporting channels: Hard decisions or soft decisions?" *IEEE Trans. Signal Process.*, vol. 60, no. 1, pp. 18–28, Jan. 2012.

[72] S. Chaudhari, J. Lundén, and V. Koivunen, "On the BEP walls for soft decision based cooperative sensing in cognitive radios," in *Proc. IEEE Int. Conf. Commun.*, Budapest, Hungary, 2013, pp. 1220–1225.

[73] D. Duan and L. Yang, "Cooperative spectrum sensing with ternary local decisions," *IEEE Commun. Lett.*, vol. 16, no. 9, pp. 1512 – 1515, Sep. 2012.

[74] E. Peh, Y.-C. Liang, Y. L. Guan, and Y. Zeng, "Optimization of cooperative sensing in cognitive radio networks: A sensing-throughput tradeoff view," *IEEE Trans. Vehicular Technol.*, vol. 58, no. 9, pp. 5294–5299, Nov. 2009.

[75] N. Zhao, F. R. Yu, H. Sun, and A. Nallanathan, "Energy-efficient cooperative spectrum sensing schemes for cognitive radio networks," *Eurasip J. Wireless Commun. Netw.*, vol. 1, no. 120, pp. 1–13, May 2013.

[76] Y. Zhang, Z. Chen, F. Gao, and X. Zhang, "Cooperative spectrum sensing based on spatially-correlated Rayleigh shadowing," in *Proc. IEEE Int. Conf. Commun. China*, Beijing, China, 2012, pp. 312–316.

[77] A. W. Min and K. G. Shin, "Impact of mobility on spectrum sensing in cognitive radio networks," in *Proc. ACM Workshop Cognitive Radio Netw.*, Beijing, China, 2009, pp.

© University of Pretoria

13–18.

[78] W. Wang, L. Chen, K. G. Shin, L., and Duan, "Thwarting intelligent malicious behaviors in cooperative spectrum sensing," *IEEE Trans. Mobile Comput.*, vol. PP, no. 99, pp. 1–14, 2015.

[79] L. Yang, L. Cao, and H. Zheng, "Proactive channel access in dynamic spectrum networks," *Physical Commun.*, vol. 1, no. 2, pp. 103–111, Jun. 2008.

[80] S. D. Barnes and B. T. Maharaj, "Prediction based channel allocation performance for cognitive radio," *AEU - Int. J. Electronics Commun.*, vol. 68, no. 4, pp. 336–345, Apr. 2014.

[81] C. Xu, Y. Li, Y. Yang, and Y. Xian, "A novel spectrum prediction algorithm for cognitive radio system based on chaotic neural network," *J. Comput. Inf. Syst.*, vol. 9, no. 1, pp. 313–320, Jan. 2013.

[82] V. K. Tumuluru, P. Wang, and D. Niyato, "A neural network based spectrum prediction scheme for cognitive radio," in *Proc. IEEE Int. Conf. Commun.*, Cape Town, South Africa, 2010, pp. 1–5.

[83] ——, "Channel status prediction for cognitive radio networks," *Wireless Commun. Mobile Comput.*, vol. 12, no. 10, pp. 862–874, July. 2012.

[84] C.-J. Yu, Y.-Y. He, and T.-F. Quan, "Frequency spectrum prediction method based on EMD and SVR," in *Proc. IEEE 8th Int. Conf. Intell. Syst. Des. Appl.*, Kaohsiung, Taiwan, 2008, pp. 39–44.

[85] C. Ghosh, C. Cordeiro, D. P. Agrawal, and M. B. Rao, "Markov chain existence and hidden markov models in spectrum sensing," in *Proc. 7th Annu. IEEE Int. Conf. Pervasive Comput. Commun.*, Galveston, TX, 2009, pp. 1–6.

[86] T. W. Rondeau, C. J. Rieser, T. M. Gallagher, and C. W. Bostian, "Online modeling of wireless channels with hidden Markov models and channel impulse responses for cognitive radios," in *Proc. IEEE MTT-S Int. Microw. Symp. Dig.*, Fort Worth, TX, 2004, pp. 739–742.

© University of Pretoria

[87] S. Geirhofer, L. Tong, and B. M. Sadler, "A measurement-based model for dynamic spectrum access in WLAN channels," in *Proc. IEEE Military Commun. Conf.*, Washington, DC, 2007, pp. 1–7.

[88] H. Zhao, T. Luo, and G. Yue, "Multi-channel myopic sensing for opportunistic spectrum access using channel correlation," in *Proc. IEEE Int. Symp. Pers. Indoor Mobile Radio Commun.*, Tokyo, Japan, 2009, pp. 696–700.

[89] Y. Yao, Z. Feng, W. Li, and Y. Qian, "Dynamic spectrum access with QoS guarantee for wireless networks: A Markov approach," in *Proc. IEEE Global Telecommun. Conf.*, Miami, FL, 2010, pp. 1–5.

[90] Z. Chen and R. C. Qiu, "Prediction of channel state for cognitive radio using higher-order hidden Markov model," in *Proc. IEEE SoutheastCon*, Charlotte-Concord, NC, 2010, pp. 276–282.

[91] K. W. Choi and E. Hossain, "Estimation of primary user parameters in cognitive radio systems via hidden markov model," *IEEE Trans. Signal Process.*, vol. 61, no. 3, pp. 782–795, Feb. 2013.

[92] Z. Wen, C. Fan, X. Zhang, Y. Wu, J. Zou, and J. Liu, "A learning spectrum hole prediction model for cognitive radio systems," in *in Proc. 10th IEEE Int. Conf. Comput. Inf. Technol.*, Bradford, United Kingdom, 2010, pp. 2089–2093.

[93] D. Treeumnuk and D. C. Popescu, "Using hidden Markov models to enable performance awareness and noise variance estimation for energy detection in cognitive radio," in *Proc. 46th Annual Conf. Inf. Sci. Syst.*, Princeton, NJ, 2012, pp. 1–5.

[94] M. I. AlKadi, M. B. I. Reaz, M. Alauddin, and M. Ali, "Evolution of electroencephalogram signal analysis techniques during anaesthesia," *Sensors*, vol. 13, no. 5, pp. 6605–6635, May 2013.

[95] A. J. Smola and B. Schölkopf, "A tutorial on support vector regression," *Stat. Comput.*, vol. 14, no. 3, pp. 199–222, Aug. 2004.

[96] S. M. Clarke, J. H. Griebsch, and T. W. Simpson, "Analysis of support vector regression

© University of Pretoria

for approximation of complex engineering analyses," *J. Mech. Des.*, vol. 127, no. 6, pp. 1077–1087, Aug. 2004.

[97] R. Nakanishi, M. Ohta, and M. Taromaru, "Spectrum sensing and channel utilization prediction by Nth-order Markov chain model," in *Proc. IEEE Wireless Commun. Netw. Conf.*, New Orleans, LA, 2015, pp. 206–211.

[98] G. Haßlinger and O. Hohlfeld, "The Gilbert-Elliott model for packet loss in real time services on the internet," in *Proc. 14th GI/ITG Conf. Meas. Modelling Evaluation Comput. Commun. Syst.*, Dortmund, Germany, 2008, pp. 1–15.

[99] G. S. Uyanik, B. Canberk, and S. Oktug, "Predictive spectrum decision mechanisms in cognitive radio networks," in *Proc. IEEE Global Telecommun. Conf.*, Anaheim, CA, 2012, pp. 943–947.

[100] B. Canberk, I. F. Akyildiz, and S. Oktug, "Primary user activity modeling using first-difference filter clustering and correlation in cognitive radio networks," *IEEE/ACM Trans. Netw.*, vol. 19, no. 1, pp. 170–183, Feb. 2011.

[101] S. Yarkan and H. Arslan, "Binary time series approach to spectrum prediction for cognitive radio," in *Proc. IEEE Veh. Technol. Conf.*, Baltimore, MD, 2007, pp. 1563–1567.

[102] Z. Wen, T. Luo, W. Xiang, S. Majhi, and Y. Ma, "Autoregressive spectrum hole prediction model for cognitive radio systems," in *Proc. IEEE Int. Conf. Commun.*, Beijing, China, 2008, pp. 154–157.

[103] Z. Lin, X. Jiang, and L. Huang, "A energy prediction based spectrum sensing approach for cognitive radio networks," in *Proc. Wireless Commun. Netw. Mobile Comput. Conf.*, Beijing, China, 2009, pp. 1–4.

[104] A. M. Adas, "Using adaptive linear prediction to support real-time VBR video under RCBR network service model," *IEEE/ACM Trans. Netw.*, vol. 6, no. 5, pp. 635–644, Oct. 1998.

[105] W.-K. Kuo and S.-Y. Lien, "Dynamic resource allocation for supporting real-time mul-

© University of Pretoria

timedia applications in IEEE 802.15.3 WPANs," *IET Commun.*, vol. 3, no. 1, pp. 1–9, Jan. 2009.

[106] P. Kulkarni, T. Lewis, and Z. Fan, "Simple traffic prediction mechanism and its applications in wireless networks," *Wireless Pers. Commun.*, vol. 59, no. 2, pp. 261–274, Jul. 2011.

[107] D. Chunli, D. Yuning, and W. Li, "Autoregressive channel prediction model for cognitive radio," in *Proc. 5th Int. Conf. Wireless Commun. Netw. Mobile Comput.*, Beijing, China, 2009, pp. 1–4.

[108] M. H. Hayes, *Statistical digital signal processing and modeling.* New York: John Wiley & Sons, 1996.

[109] Y. Song and J. Xie, "ProSpect: A proactive spectrum handoff framework for cognitive radio ad hoc networks without common control channel," *IEEE Trans. Mobile Comput.*, vol. 11, no. 7, pp. 1127–1139, Jul. 2012.

[110] C. Ghosh, S. Pagadarai, D. P. Agrawal, and A. M. Wyglinski, "A framework for statistical wireless spectrum occupancy modeling," *IEEE Trans. Wireless Commun.*, vol. 9, no. 1, pp. 38–44, Jan. 2010.

[111] Z. Chen, N. Guo, Z. Hu, and R. C. Qiu, "Experimental validation of channel state prediction considering delays in practical cognitive radio," *IEEE Trans. Veh. Technol.*, vol. 60, no. 4, pp. 1314–1325, May. 2011.

[112] X. Xing, T. Jing, W. Cheng, Y. Huo, X. Cheng, and T. Znati, "Cooperative spectrum prediction in multi-PU multi-SU cognitive radio networks," *Mobile Netw. Appl.*, vol. 19, no. 4, pp. 502–511, Aug. 2014.

[113] ITU, "Final acts of the regional radiocommunication conference for planning of the digital terrestrial broadcasting service in parts of regions 1 and 3, in the frequency bands 174-230 MHz and 470-862 MHz," Geneva, Switzerland, Tech. Rep., Jun. 2006.

[114] S. D. Barnes, P. A. Jansen van Vuuren, and B. T. Maharaj, "Spectrum occupancy investigation: Measurements in South Africa," *Measurement*, vol. 46, no. 9, pp. 3098–

© University of Pretoria

3112, Nov. 2013.

[115] S. D. Barnes and B. T. Maharaj, "A comparison of spectrum occupancy in the South African 900 MHz GSM cellular bands," in *Proc. IEEE AFRICON Conf.*, Port Louis, Mauritius, 2013, pp. 1–5.

[116] S. D. Barnes, P. Botha, and B. T. Maharaj, "Spectral occupation of TV broadcast bands: Measurement and analysis," *Measurement*, vol. 93, pp. 272–277, Nov. 2016.

[117] D. Datla, A. M. Wyglinski, and G. J. Minden, "A spectrum surveying framework for dynamic spectrum access networks," *IEEE Trans. Veh. Technol.*, vol. 58, no. 8, pp. 4158–4168, Oct. 2009.

[118] Google, "University of Pretoria," Mar. 2015. [Online]. Available: https://goo.gl/maps/1Nrj4

[119] ——, "Pinmill Farm," Aug. 2012. [Online]. Available: http://goo.gl/maps/J7rEl

[120] ——, "Midrand and Centurion," Mar. 2015. [Online]. Available: https://goo.gl/maps/C36YY

[121] ——, "City of Tshwane," Mar. 2015. [Online]. Available: https://goo.gl/maps/yM1k6

[122] ICASA, "Draft terrestrial broadcasting frequency plan 2013," *Government Gazette: Republic of South Africa*, vol. 574, no. 36321, pp. 3–163, Apr. 2013.

[123] S. D. Barnes and B. T. Maharaj, "An occupancy window approach to primary user traffic modelling for cognitive radio," in *Proc. SATNAC*, Stellenbosch, South Africa, 2013, pp. 395–399.

[124] S. D. Barnes, B. T. Maharaj, and A. S. Alfa, "Cooperative prediction in cognitive radio networks." *Wireless Pers. Commun.*, vol. 89, no. 4, pp. 1177–1202, Aug. 2016.

[125] M. Höyhtyä, S. Pollin, and A. Mämmelä, "Performance improvement with predictive channel selection for cognitive radios," in *Proc. 1st Int. Workshop Cognitive Radio Adv. Spectr. Manage.*, Aalborg, Denmark, 2008, pp. 1–5.

© University of Pretoria

[126] C.-S. Yang, L.-Y. Chuang, Y.-J. Chen, and C.-H. Yang, "Feature selection using memetic algorithms," in *Proc. Int. Conf. Convergence Hybrid Inf. Technol.*, Busan, South Korea, 2008, pp. 416–423.

[127] S. D. Barnes and B. T. Maharaj, "Collaborative spectral opportunity forecasting for cognitive radio," in *Proc. IEEE AFRICON Conf.*, Addis Ababa, Ethiopia, 2015, pp. 1–6.

[128] S. Atapattu, C. Tellambura, and H. Jiang, "Energy detection based cooperative spectrum sensing in cognitive radio networks," *IEEE Trans. Wireless Commun.*, vol. 10, no. 4, pp. 1232–1241, Apr. 2011.

[129] V. Krishnamurthy, M. Maskery, and G. Yin, "Decentralized adaptive filtering algorithms for sensor activation in an unattended ground sensor network," *IEEE Trans. Signal Process.*, vol. 56, no. 12, pp. 6086–6101, Dec. 2008.

[130] I. F. Akyildiz, W. Su, Y. Sankarasubramaniam, and E. Cayirci, "A survey on sensor networks," *IEEE Commun. Mag.*, vol. 40, no. 8, pp. 102–105, Aug. 2002.

[131] X. Xiaorong, H. Aiping, and B. Jianrong, "Energy efficiency analysis of cooperative sensing and sharing in cognitive radio networks," in *Proc. IEEE 11th Int. Symp. Commun. Information Technol.*, Hangzhou, China, 2011, pp. 422–427.

[132] Z. Zhou, S. Zhou, S. Cui, and J.-H. Cui, "Energy-efficient cooperative communication in a clustered wireless sensor network ," *IEEE Trans. Veh. Technol.*, vol. 57, no. 6, pp. 3618–3628, Nov. 2008.

[133] S. D. Barnes, B. T. Maharaj, and A. S. Alfa, "Spectrum opportunity forecasting for energy efficient sensing in cognitive radio networks," in *Proc. Int. Symp. Telecommun. Technol.*, Langkawi, Malaysia, 2014, pp. 128–132.

[134] "IEEE Standard for local and metropolitan area networks - Specific requirements," *IEEE Std. 802.22-2011*, pp. i–659, 2011.

© University of Pretoria

APPENDIX A

DERIVATION OF THE MAXIMUM NORMAL FIT METHOD

A.1 INTRODUCTION

In this appendix the expression for the noise threshold λ_i is derived.

A.2 NOISE THRESHOLD CALCULATION

Lemma A.2.1 *Let the signal detection threshold λ_i be given by the following expression,*

$$\lambda_i = \frac{\mu_s\sigma_n^2 \pm \sigma_n\sigma_s\sqrt{2\ln\left(\frac{\sigma_n}{\sigma_s}\right)(\sigma_n^2-\sigma_s^2)+\mu_s^2}}{\sigma_n^2-\sigma_s^2} \tag{A.1}$$

where μ_s and σ_s^2 are the mean and variance of the information carrying component of a received signal respectively and σ_n^2 is the variance of the noise component.

Proof Let the probability density functions of the information and noise components be,

$$f_N(x) = \frac{1}{\sigma_n\sqrt{2\pi}}\exp\frac{(x-\mu_n)^2}{2\sigma_n^2} \tag{A.2}$$

and

$$f_S(x) = \frac{1}{\sigma_s\sqrt{2\pi}}\exp\frac{(x-\mu_s)^2}{2\sigma_s^2} \tag{A.3}$$

respectively.

To solve for x, let $f_N(x) = f_S(x)$ such that,

$$\frac{1}{\sigma_n\sqrt{2\pi}}\exp\frac{(x-\mu_n)^2}{2\sigma_n^2} = \frac{1}{\sigma_s\sqrt{2\pi}}\exp\frac{(x-\mu_s)^2}{2\sigma_s^2} \tag{A.4}$$

© University of Pretoria

UNIVERSITEIT VAN PRETORIA
UNIVERSITY OF PRETORIA
YUNIBESITHI YA PRETORIA

This expression can be simplified and written in the form of a second order polynomial, $ax^2 + bx + c = 0$, where the coefficient are given as,

$$a = x^2(\sigma_n^2 - \sigma_s^2) \tag{A.5}$$

$$b = 2x(\sigma_s^2\mu_n - \sigma_n^2\mu_s) \tag{A.6}$$

$$c = \sigma_n^2\mu_s^2 - \sigma_s^2\mu_n^2 - 2\sigma_n^2\sigma_s^2 \ln\left(\frac{\sigma_n}{\sigma_s}\right) \tag{A.7}$$

If $\lambda_i = x$, is the solution for Equation (A.4), then,

$$\lambda_i = \frac{\mu_s\sigma_n^2 - \mu_n\sigma_s^2 \pm \sigma_n\sigma_s\sqrt{2\ln\left(\frac{\sigma_n}{\sigma_s}\right)(\sigma_n^2 - \sigma_s^2) + \mu_n^2 + \mu_s^2 - 2\mu_n\mu_s}}{\sigma_n^2 - \sigma_s^2} \tag{A.8}$$

But, under the assumption that $f_N = \mathcal{N}(0, \sigma_n^2)$, $\mu_n = 0$ must be substituted into Eq. (A.8) to give the following expression,

$$\lambda_i = \frac{\mu_s\sigma_n^2 \pm \sigma_n\sigma_s\sqrt{2\ln\left(\frac{\sigma_n}{\sigma_s}\right)(\sigma_n^2 - \sigma_s^2) + \mu_s^2}}{\sigma_n^2 - \sigma_s^2} \tag{A.9}$$

© University of Pretoria

APPENDIX B

TSHWANE METROPOLITAN AREA TELEVISION CHANNEL ASSIGNMENTS

B.1 INTRODUCTION

Television channels assigned to the Tshwane metropolitan area are listed in Table B.1 for the very-high frequency (VHF) bands and in Table B.2 for the ultra-high frequency (UHF) bands, together with the broadcast site from which transmissions are made for each channel [122]. The broadcast sites are: Gelukskroon Pretoria (GPT), Pretoria North (PN), Sunnyside (SD), Menlo Park (MP) and the council for scientific and industrial research (CSIR).

B.2 VERY-HIGH FREQUENCY CHANNEL ASSIGNMENTS

Table B.1: VHF channel assignments for the Tshwane metropolitan area.

Channel	Frequency	Site	Station
5	183.25	GPT	SABC2
8	207.25	GPT	SABC1
11	231.25	GPT	SABC3

© University of Pretoria

UNIVERSITEIT VAN PRETORIA
UNIVERSITY OF PRETORIA
YUNIBESITHI YA PRETORIA

B.3 ULTRA-HIGH FREQUENCY CHANNEL ASSIGNMENTS

Table B.2: UHF channel assignment for the Tshwane metropolitan area.

Channel	Frequency	Site	Station
21	471.25	GPT	MNET
25	503.25	GPT	CSN
27	519.25	SD	TSHW
29	535.25	GPT	ETV
33	567.25	GPT, PN, SD, MP	DVB-T2
35	583.25	GPT, PN, SD, MP, CSIR	DVB-H
37	599.25	PN	ETV
38	607.25	SD	ETV
40	623.25	PN	SABC2
44	655.25	MP	CSN
46	671.25	SD	CSN
48	687.25	MP	ETV
50	703.25	PN	MNET
52	719.25	PN	SABC1
53	727.25	MP	SABC2
54	735.25	GPT, PN, SD, MP	DVB-T2
55	743.25	SD	SABC2
56	751.25	PN	CSN
57	759.25	MP	SABC1
58	767.25	GPT, PN, SD, MP	DVB-T2
59	775.25	SD	SABC3
61	791.25	MP	MNET
63	807.25	SD	SABC1
65	823.25	MP	SABC3
67	839.25	SD	MNET

© University of Pretoria